Forschungszentrum Karlsruhe
in der Helmholtz-Gemeinschaft

Wissenschaftliche Berichte
FZKA 7024

KAPOOL Experiments on Melt-through of a Metal Plate by an Overlying Melt Pool

B. Eppinger, T. Cron, G. Fieg, G. Merkel, S. Schmidt-Stiefel, W. Tromm T. Wenz, J. Grune, G. Stern

Institut für Kern- und Energietechnik Programm Nukleare Sicherheitsforschung

August 2004

Forschungszentrum Karlsruhe
in der Helmholtz-Gemeinschaft

Wissenschaftliche Berichte

FZKA 7024

KAPOOL experiments on melt-through of a metal plate by an overlying melt pool

B. Eppinger, T. Cron, G. Fieg, G. Merkel, S. Schmidt-Stiefel, W. Tromm
T. Wenz, J. Grune*, G. Stern*

Institut für Kern- und Energietechnik
Programm Nukleare Sicherheitsforschung

*Firma Pro Science, Ettlingen

Forschungszentrum Karlsruhe GmbH, Karlsruhe
2004

Impressum der Print-Ausgabe:

Als Manuskript gedruckt

Forschungszentrum Karlsruhe GmbH
Postfach 3640, 76021 Karlsruhe

Mitglied der Hermann von Helmholtz-Gemeinschaft
Deutscher Forschungszentren (HGF)

ISSN 0947-8620

urn:nbn:de:0005-070244

Abstract

In the event of a hypothetical severe accident in a Light Water Reactor (LWR) it is possible that the core melts and relocates to the lower head of the reactor pressure vessel (RPV). If the severe accident management measures are not successful, the RPV can fail and the core melt is discharged onto the basement of the containment. To prevent a significant release of radioactivity to the environment due to the melt-through of the basement, LWR's might incorporate the ability to retain and cool the core melt on the basement of the containment (core catcher concept).
Before the melt arrives on the cooling device on the basement, the melt has to penetrate the reactor cavity. The reactor cavity may be equipped with a metallic plate at its bottom, covered by a layer of sacrificial concrete, to collect the melt over a certain time period. To achieve a complete and homogeneous spreading of the melt over the total area of the cooling device a fast and sufficiently wide melt-through of the metallic plate is required.
To investigate the important processes concerning the melt-through of a metallic plate by a simulated core melt, a series of transient KAPOOL experiments has been performed in the years 1998 to 2000. The corium melt in the KAPOOL tests is simulated by an alumina/iron melt, produced by a thermite reaction. Therefore it was possible to investigate the interaction of both parts of the corium melt (metallic and oxidic) with a metal plate.
The experiments show that metallic melts in contact with a steel plate that simulates the melt gate between the reactor cavity and the core catcher compartment lead to fast melting of the steel plate (**KAPOOL 9**). Oxide melts in contact with a steel or an aluminium plate lead to oxide crust formation at the steel or aluminium interface, and subsequent formation of gaps between the crust and the metal plate. In case of a steel plate no ablation of the plate by the oxide melt could be observed (**KAPOOL 11** and **12**). Due to the lower melting temperature of the aluminium one could detect and analyse failure modes of the plate due to high thermal loadings (**KAPOOL 13** and **15 to 17**).

In addition to the experiments, heat transfer calculations with the HEATING5 code have been performed. The results of the calculations helped to reproduce the experimental results and to identify the important processes concerning the melt-through of a metal plate.

A drawback of the KAPOOL tests is the transient character: Volumetric heat production in the melt was not possible to simulate the nuclear decay heat. In the case of real corium melts with decay heat a later thermal erosion of a melt gate made of steel would be expected in contrary to the outcomes of the tests KAPOOL 11 and 12.
From the results of the KAPOOL tests 15 to 17 it is advantageous to use aluminium as the material for the bottom of the reactor cavity, as for this material the tests have proved a sufficient fast and large opening of the plate. A very important advantage of using aluminium is the high thermal conductivity of the material, which supports a fast opening of the gate over a large area. When steel should be used as material for the melt gate, further investigations deem necessary to prove a sufficiently large opening of this gate by an oxide melt.

KAPOOL Experimente zum Durchschmelzen einer Metallplatte durch eine aufliegende Schmelze

Zusammenfassung

Im Falle eines hypothetischen schweren Unfalls in einem Leichtwasserreaktor (LWR) ist es möglich, dass der Kern schmilzt und sich in die Bodenkalotte des Reaktordruckbehälters verlagert. Wenn die Maßnahmen zum Unfallmanagement nicht wirken bzw. ausfallen, kann der Reaktordruckbehälter versagen und die Kernschmelze gelangt auf das Fundament des Reaktors. Um eine Freisetzung von Radioaktivität infolge einer Durchdringung des Fundamentes an die Umgebung zu verhindern, können Reaktoren die Möglichkeit vorsehen, die Kernschmelze auf dem Fundament des Sicherheitsbehälters zurückzuhalten und zu kühlen (Kernfängerkonzept).
Bevor die Kernschmelze auf die Kühleinrichtung auf dem Fundament gelangt, muss sie die Reaktorgrube durchdringen. Die Reaktorgrube kann am Boden mit einer Metallplatte abgeschlossen sein. Diese Metallplatte ist mit einer Opferbetonschicht bedeckt, um die Schmelze über eine gewisse Zeitspanne in der Reaktorgrube zu halten. Um eine komplette und homogene Ausbreitung der Schmelze über die gesamte Fläche der Kühleinrichtung zu erreichen, muss die Metallplatte möglichst schnell über eine ausreichende Öffnung durchschmolzen werden.
Um die wichtigen Vorgänge beim Durchschmelzen von metallischen Platten durch eine simulierte Kernschmelze zu untersuchen, wurde in den Jahren 1998 bis 2000 eine Serie von KAPOOL Experimenten durchgeführt. Als Simulationsschmelze für die Kernschmelze wurde eine Schmelze aus Eisen und Aluminiumoxid verwendet, die durch eine Thermitreaktion erzeugt wurde. Dadurch war es möglich, die Wechselwirkung beider Teile einer Kernschmelze (metallisch und oxidisch) mit einer Metallplatte zu untersuchen.
Die Ergebnisse der Versuche zeigen, dass metallische Schmelzen in Kontakt mit einer Stahlplatte, die das Schmelzentor zwischen Reaktorgrube und Kühleinrichtung simuliert, zu einem schnellen Aufschmelzen der Stahlplatte führen (**KAPOOL 9**). Oxidische Schmelzen in Kontakt mit einer Stahl- oder einer Aluminiumplatte führen zu einer Krustenbildung des Oxids auf dem Stahl oder dem Aluminium und zu einer nachfolgenden Spaltbildung zwischen der Kruste und der Platte. Im Falle der Stahlplatte konnte kein Aufschmelzen der Platte durch die Oxidschmelze erreicht werden (**KAPOOL 11** und **12**). Aufgrund der niedrigeren Schmelztemperatur des Aluminiums konnten Versagensmodi der Platte untersucht und analysiert werden (**KAPOOL 13** und **15-17**).
Zusätzlich zu den Experimenten wurden begleitende Wärmeübergangsrechnungen mit dem Rechencode HEATING5 durchgeführt. Die Ergebnisse der Rechnungen halfen dabei, die experimentellen Ergebnisse nachzuvollziehen und wichtige Prozesse beim Durchschmelzen einer Metallplatte zu identifizieren.
Ein Nachteil der KAPOOL Experimente ist deren transienter Charakter: Volumetrische Wärmeerzeugung in der Schmelze war nicht möglich. Im Gegensatz zu den Ergebnissen der Experimente KAPOOL 11 und 12 würde man bei realen Kernschmelzen mit Nachzerfallswärme eine spätere thermische Erosion der Stahlplatte erwarten.
Unter Berücksichtigung der Ergebnisse der Experimente KAPOOL 15 bis 17 ist es vorteilhaft, Aluminium als Material für den Boden der Reaktorgrube zu verwenden, da die Experimente für dieses Material ein ausreichend schnelles und großflächiges Öffnen der Platte gezeigt haben. Ein sehr wichtiger Vorteil des Aluminiums liegt in seiner hohen Wärmeleitfähigkeit, welche ein schnelles Öffnen des Schmelzentors über eine große Fläche unterstützt. Wenn eine Stahlplatte als Schmelzentor verwendet werden soll, sollten weitere Untersuchungen erfolgen, um ein ausreichend großes Aufschmelzen der Platte durch die Oxidschmelze nachzuweisen.

CONTENTS

LIST OF TABLES

LIST OF FIGURES

1 Introduction

1.1 Background

In the case of a very unlikely core melt down accident with failure of the reactor pressure vessel (RPV), melt-through of the basement and significant release of radioactivity to the environment should be prevented. Therefore Light Water Reactors (LWR) might incorporate the ability to retain and cool the core melt on the basement of the containment (core catcher concept).
To achieve melt cooling on the basement of the containment by whatever specific cooling concept, it is advantageous to promote melt spreading by fast melt release from the reactor cavity, [1]-[4]. This requires a safe and sufficiently large opening of the reactor cavity that may be equipped with a metallic plate (melt gate) at its bottom, covered by a layer of sacrificial concrete. Through this combination, collecting of the melt in the reactor cavity over a certain time period and its subsequent fast release to the basement after melt-through of the melt gate, are the goals to be achieved.

In a more general sense, the problem of metal attack by an overlying corium pool can occur at various stages of a severe accident, in-vessel and ex-vessel, for which a better understanding is required.
The present investigations shall highlight the important processes under the aspect of achieving a fast and sufficiently wide melt-through of a metal plate that may initially be covered by a sacrificial concrete layer.

1.2 Objectives of the test series

In the KAPOOL tests various important processes in the reactor cavity are investigated. The first KAPOOL experiments have investigated the melt-concrete interaction in the reactor cavity, [5]-[8]. The KAPOOL tests, which are presented in this report and which were performed in the years 1998 - 2000, study the melt-through of a metallic plate and the subsequent release of the melt through this metallic plate.

The main objectives of the experiments are:

- Investigation of the interaction of a metallic melt with the melt gate made of steel (**KAPOOL 9**)
- Investigation of the interaction of an oxidic melt with the melt gate made of steel (**KAPOOL 11** and **12**)
- Investigation of the interaction of an oxidic melt with the melt gate made of aluminium (**KAPOOL 13** and **KAPOOOL 15** to **17**)

All these tests use a high temperature melt and are strongly transient because there is no simulation of the decay heat in the simulated core melt. This limitation poses certain requirements to the experiments to identify the important heat transfer and melting processes in the short term range. In the case of real corium melts with decay heat production, long term processes could also play an important role.

2 Experimental Setup

2.1 Melt and Melt Generation

The corium melt as released from the RPV is composed of a metallic (steel, zirconium) and oxidic (UO_2, ZrO_2, FeO) phase. In the KAPOOL experiments these two phases are simulated by an iron/alumina melt produced by a thermite reaction.
The thermite reaction ($2\ Al + Fe_2O_3 \rightarrow Al_2O_3 + 2\ Fe$) produces about 50 wt% iron and 50 wt% oxidic melt. The reaction is strongly exothermic and the maximum temperature of the melt is up to 2400 °C.
The solidus-liquidus range of a realistic corium melt in the reactor cavity after erosion of sacrificial concrete is relatively large. To simulate as close as possible this characteristic property, 8 wt% of SiO_2 has been added to the alumina melt in the experiments KAPOOL 9 and 11.
Beginning with KAPOOL 12, SiO_2 has been replaced by a certain amount of calcium oxide to lower the liquidus and solidus temperature of the oxide melt. The initial temperatures in the experiments are similar to the temperatures of the core melt in the reactor situation after erosion of the sacrificial concrete of the reactor cavity bottom.

2.2 KAPOOL test facility

In Figure 1, the schematic of the KAPOOL test facility is shown on the basis of the setup for the test KAPOOL 13. The setup for the different tests can slightly differ from each other, but the main components are shown in Figure 1. A photo of the test facility is shown in Figure 2.
The KAPOOL test facility consists of a reaction crucible, in which the melt is produced by the thermite reaction (except for the test KAPOOL 9). Due to different densities (iron melt at 6500 kg/m^3 and oxide melt close to 3000 kg/m^3) the iron melt segregates at the bottom of the reaction crucible and is therefore the first component, which is released from the crucible. For the tests, where only the oxidic part of the thermite melt is used, the iron melt is separated and is discharged into a special container. The oxide melt is then poured into the KAPOOL test container where the interaction between the melt and the metallic plate starts. Via a mirror the bottom of the KAPOOL container and so the metallic plate can be observed.

2.3 Instrumentation

2.3.1 Thermocouples

K-type thermocouples (NiCr-Ni) have been installed in the metallic plate at different heights and lateral positions to detect the transient temperature front. These thermocouples are of the sheathed type with an outer stainless steel sheath of 1 mm diameter.
To detect the temperature of the melt and its decrease during the test period, high-temperature thermocouples (W-Re thermocouples) are immersed into the melt one after the other. The life-time of the thermocouples is restricted and therefore a series of up to 10 thermocouples is prepared.

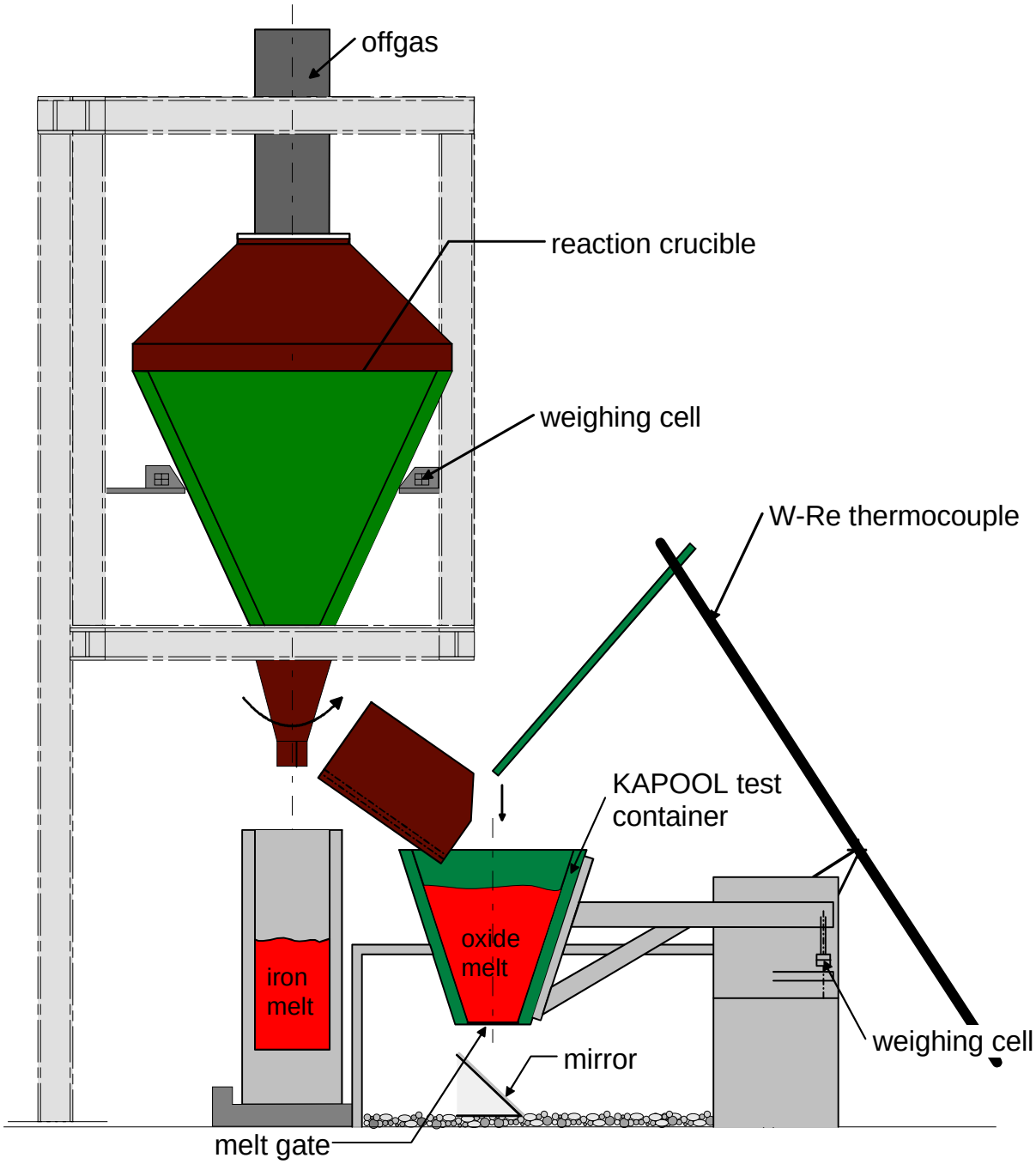

Figure 1: Schematic of the KAPOOL test facility (KAPOOL 13)

2.3.2 Weighing cells

In all tests the KAPOOL container and, when necessary, the reaction crucible are equipped with weighing cells to record the mass flows. Hence the exact amount of oxidic melt in the KAPOOL container at the beginning of the test and the mass losses during the test due to thermocouple immersion into the melt or by outflow of the melt can be determined.

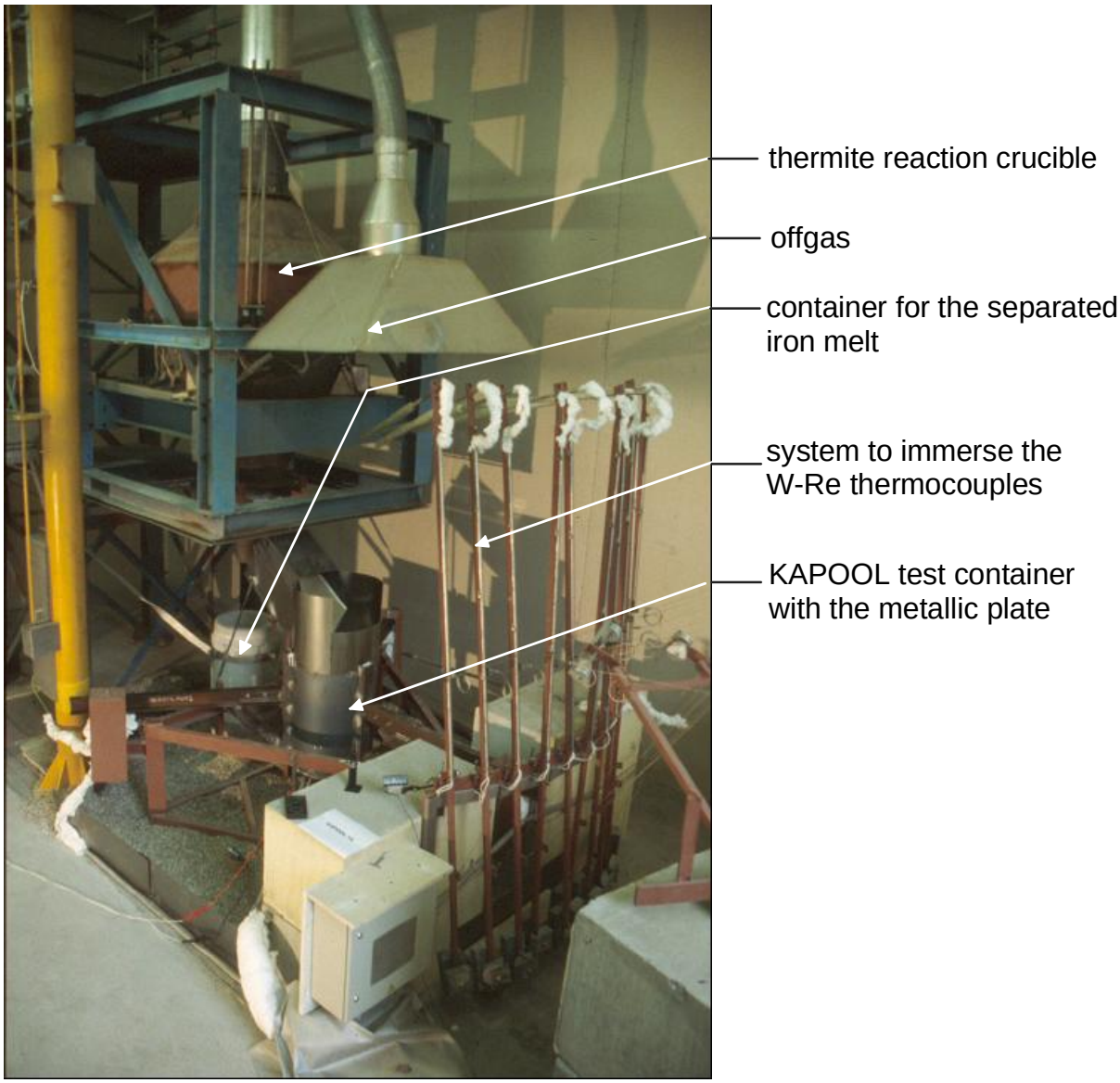

Figure 2: Photo of the LIVE test facility (KAPOOL 15)

2.3.3 Video cameras

Video cameras were installed at different locations to record the conduct of the test. Via a mirror also the bottom of the steel plate could be observed. An additional video camera is set and focused to record the melt jet after melt-through of the metallic plate. The installation of this camera also allows the measurement of the increasing jet diameter.

3 Theoretical investigations of the KAPOOL experiments

For the theoretical support of the KAPOOL experiments the HEATING5 code has been used [9]. The HEATING5 code is designed to solve steady-state and/or transient heat conduction problems in one-, two-, or three-dimensional Cartesian or cylindrical coordinates or one-dimensional spherical coordinates.
To make calculations with the HEATING5 code the problem must be geometrically described and several input data must be created. First, the configuration of the problem is approximated by dividing it into different regions, depending on e.g. the shape, material structure or other deviations from the general geometry. A region may contain at most one material, and a gap region does not contain any material. The second requirement for describing the overall configuration is to construct a set of lattice lines perpendicular to each axis and extending the entire length of the remaining coordinates. The lattice lines are points, lines or planes for a one-, two-, or three-dimensional problem, respectively.
In accordance with the geometrical description, further input data must be created. These include e.g. the number of different materials with the corresponding material properties. The material properties like thermal conductivity, density and specific heat can be temperature-dependent or even time-dependent. The boundary conditions of the regions in the calculations can be adiabatic, isothermal or radiation with the appropriate emissivities.
Unfortunately, for most of the analysed cases the temperature-dependent material properties are not known and therefore the transient character of a calculation cannot be exactly reproduced.
Another problem of the HEATING5 calculations is the restriction to heat conduction. In some KAPOOL experiments also heat convection processes play an important role, so that the calculation gives only tentative results.
The HEATING5 calculations, which were performed for some KAPOOL experiments, are described and presented in detail in the chapters of the respective experiments.

4 Interaction of an iron melt with a steel plate (KAPOOL 9)

The objective of this test was the interaction between the iron fraction of the thermite melt and a steel plate. It was assumed that the metallic part of the corium melt (steel, zirconium) is situated below the oxidic phase in the reactor cavity. Molten corium-sacrificial concrete interaction (MCCI) takes place before the corium melt comes into contact with the steel plate between the reactor cavity and the basement of the containment.

4.1 Setup of the test KAPOOL 9

The initial conditions in this test accounted for the possibly inhomogeneous concrete erosion: There was a 10 mm concrete layer (siliceous concrete) on top of the steel plate, except for a small hole in the center. It was assumed that the iron melt had already eroded a certain height of sacrificial concrete and due to some inhomogeneous erosion, comes first into contact with the steel plate at the center. The free surface in the center was 20 mm in diameter. Therefore, the initial situation in KAPOOL 9 simulates the fact, that concrete erosion is not homogeneous across the full surface and differences up to ± 10 mm have been found in former tests [6]. To avoid an early spalling of the concrete after contact with the hot melt, the concrete layer was anchored with the steel plate.
Figure 3 shows the nearly cylindrical test container. The thickness of the bottom steel plate (structural steel) was 40 mm. Its internal wetted diameter was 260 mm, and the external diameter 400 mm. The thickness of the conical lateral ceramic insulation was 70 mm.

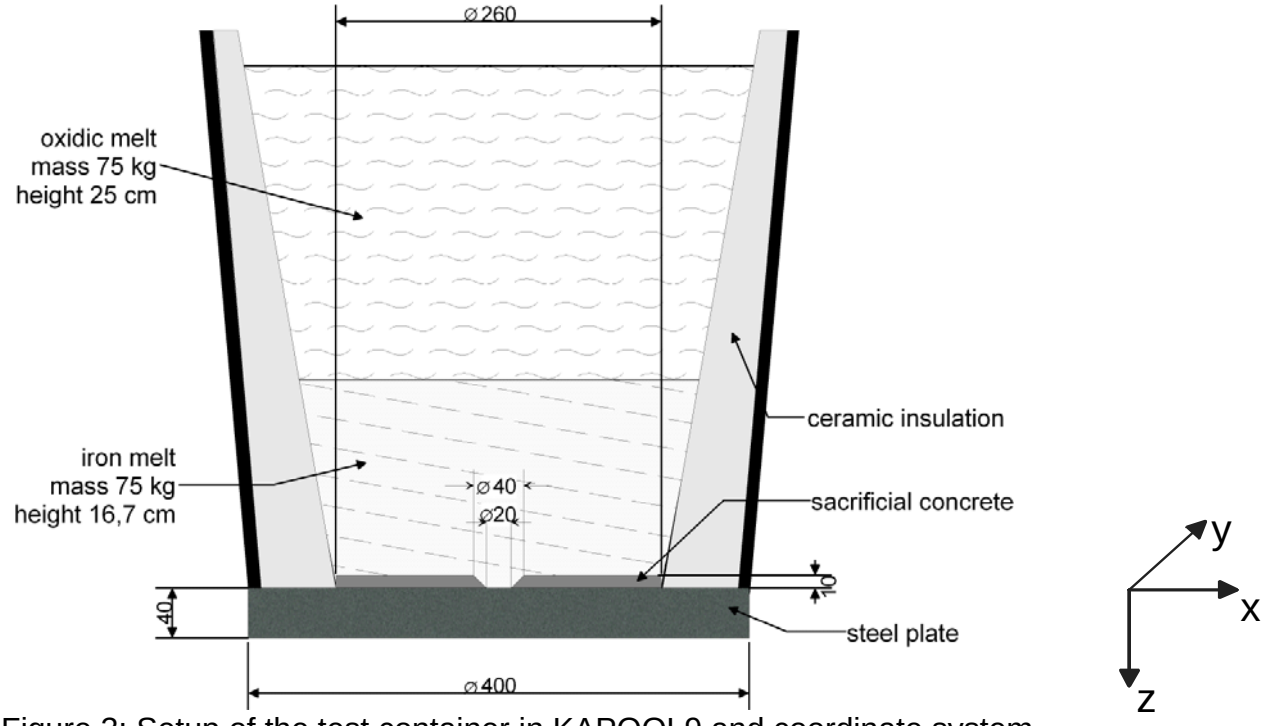

Figure 3: Setup of the test container in KAPOOL9 and coordinate system

29 K-type thermocouples have been installed inside the steel plate. Table 1 (see chapter 4.2.2) lists the individual positions of all thermocouples. One thermocouple (#1) was positioned at the center 1 mm atop the surface to detect the arrival of the

iron melt. Thermocouples in the center of the plate are positioned at vertical locations at z = 5, 10, 15, 20, 25, 30, 35 and 40 mm from the top surface. Additionally, in each direction of the four axes (+x, -x, +y, -y), five thermocouples are positioned in the midplane (z = 20 mm) at lateral distances 20 mm from each other.
For the KAPOOL 9 experiment, a simplified test procedure was applied: The thermite powder was directly ignited in the KAPOOL test container. The iron and the oxide melt separated immediately and the oxide melt did not intervene with the steel plate. 150 kg of thermite powder have been used to produce about 75 kg of iron and 75 kg of oxide melt. The calculated height of the iron melt in the KAPOOL test container at the end of the reaction time was 167 mm; the total height including the oxide melt was 417 mm. Time 0 s is defined by the ignition of the thermite powder.

4.2 Experimental Results

4.2.1 Iron Melt temperature

The iron melt temperature was measured during the conduct of the test by immersing W-Re thermocouples into the iron melt pool, which is situated below the oxide melt. The recording of the first thermocouple shows that the asymptotic temperature of the thermocouple was not yet reached before the thermocouple failed, Figure 4. The initial temperature was about 2200 °C and decreased to about 1900 °C after 65 s.

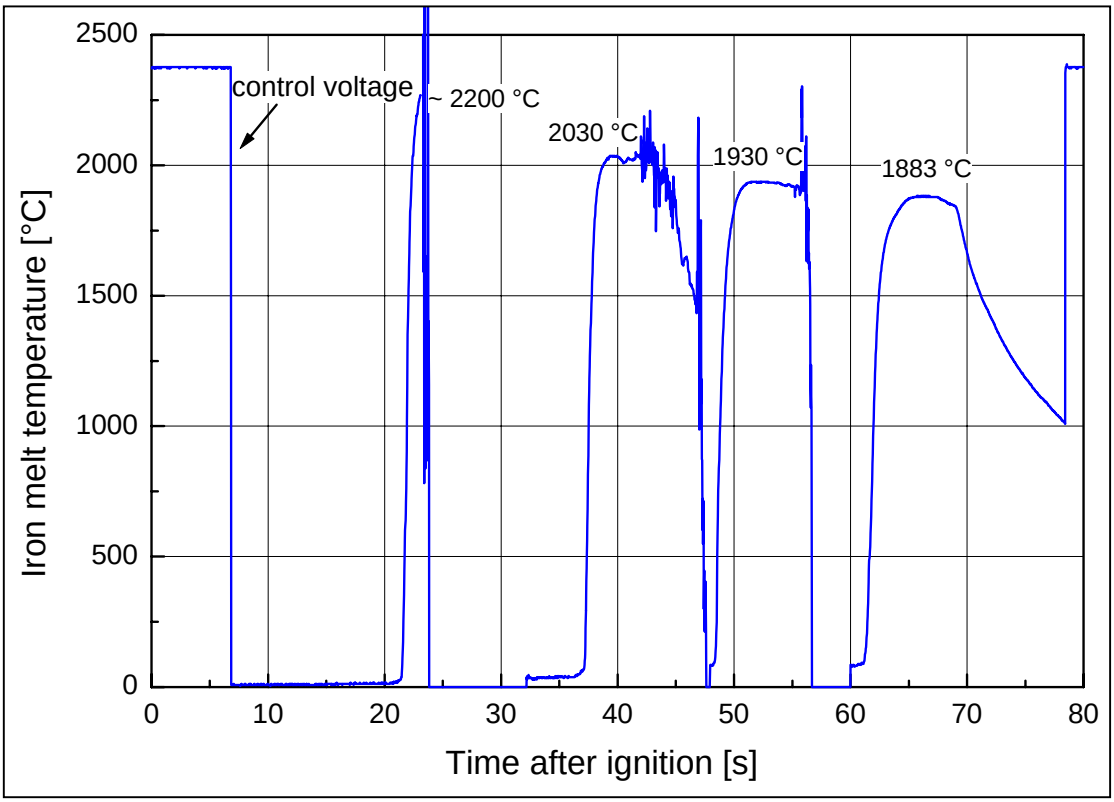

Figure 4: Measured temperatures in the iron melt pool in KAPOOL 9

The thermocouple readings clearly show the decrease of the temperature of the iron melt, which is mainly due to concrete erosion and heat-up and melting of the steel plate. Heat losses to the ceramic insulation and radiation from the oxide melt surface have a smaller influence on the steel temperature.

4.2.2 Temperature readings of NiCr -Ni thermocouples in the steel plate

13.7 s after ignition of the thermite powder the top thermocouple #1 in the center about one millimetre above the steel plate surface registered the arrival of the melt, detected by the failure of the thermocouple at about 1300 °C.
Table 1 lists the failure times for all thermocouples in the steel plate. As the failure times of the thermocouples correspond to a temperature of about 1300 °C, the 1300 °C temperature front in the centerline of the plate can be deduced from these recordings, Figure 5.

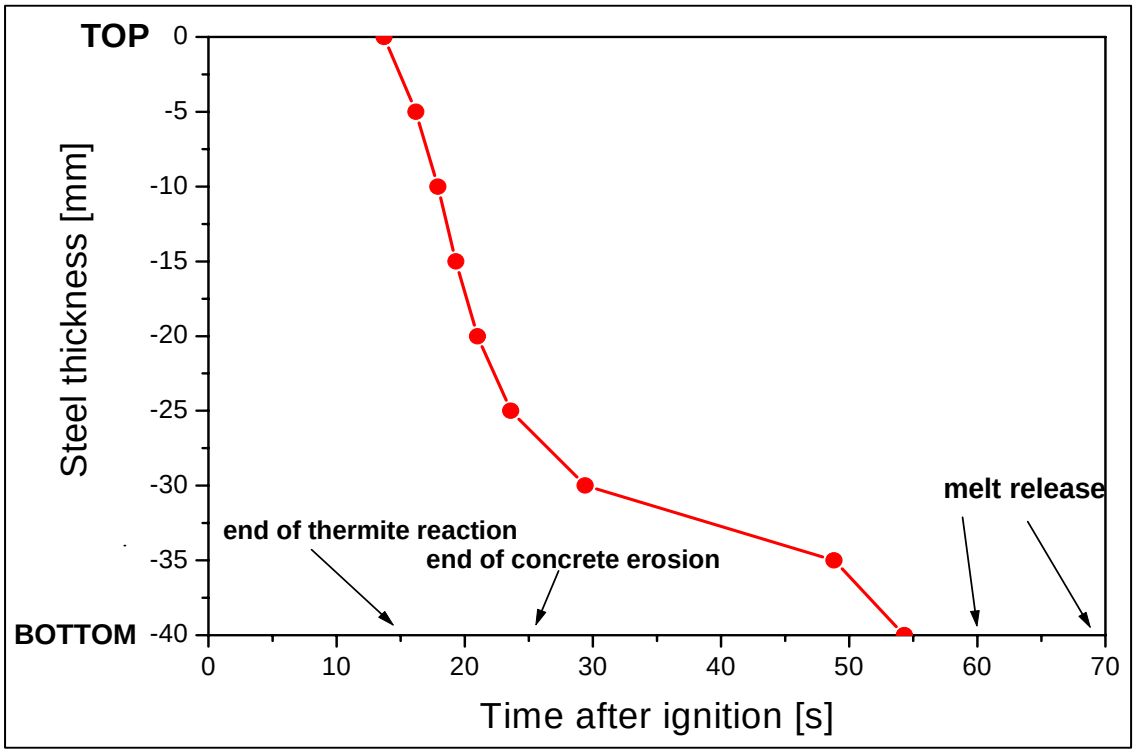

Figure 5: Axial 1300 °C temperature front in the centerline of the steel plate

The concrete erosion starts also at 13.7 s. Former MCCI concrete erosion tests [5] showed an erosion time for the 10 mm concrete layer of 10 s for a melt temperature of about 2200 °C. This means that for about 10 s, the attack of the steel plate by the iron melt occurs only in the free center. Thereafter the iron melt is supposed to be in direct contact with the whole surface of the steel plate.
The recordings of the type K thermocouples in the centerline, Figure 5, show that the 1300 °C front proceeded rather fast into the plate during this period. The melting point of the steel plate is about 1400 °C, close to the thermocouple failure. Within the 10 s, where the melt had only been in contact with the steel plate at its center, the melt has penetrated about 25 mm of the steel plate.
The initial velocity of the melting front is very high with about 3 mm/s and can only be understood by the intense convection processes due to the concrete erosion, which transports always hot iron melt to the melting interface. The resulting convective heat transfer is of course substantially higher than pure heat conduction.
From Figure 5 it is also possible to calculate erosion rates of the steel plate and to estimate heat transfer coefficients, Appendix A. The determined heat transfer coefficients for the steel plate erosion during the period of concrete erosion are relatively high with a maximum value of about 25 kW/m^{2}K, more than a factor of 8 higher than the heat transfer coefficients to an eroded concrete surface [8]. Therefore the as-

sumption of a very high heat transfer enhanced by released gases from concrete erosion, which transport hot iron melt to the melting interface of the steel plate, is correct. The lower heat transfer to a decomposing concrete surface is explained by gas bubbles at the surface, which can form a (local) gas film on top of the concrete surface.

Table 1: Positions of K-type thermocouples in the steel plate and failure times

T/C #	Position x [mm]	Position y [mm]	Vertical position z [mm]	Failure time[1] [s]
1	5	5	-1 (above steel plate)	13.7
2	0	5	5	16.2
3	-5	5	10	17.9
4	5	0	15	19.3
5	0	0	20	21.0
6	-5	0	25	23.6
7	5	-5	30	29.4
8	0	-5	35	48.8
9	-5	-5	40	54,3
10	20	0	20	26.6
11	40	0	20	36.4
12	60	0	20	40.7
13	80	0	20	38.2
14	100	0	20	37.5
15	0	20	20	26.4
16	0	40	20	38.5
17	0	60	20	45.2
18	0	80	20	55.0
19	0	100	20	59.5
20	-20	0	20	25.1
21	-40	0	20	44.5
22	-60	0	20	53.9
23	-80	0	20	63.0
24	-100	0	20	-
25	0	-20	20	24.3
26	0	-40	20	40.7
27	0	-60	20	57.7
28	0	-80	20	59.3
29	0	-100	20	53.2

[1]corresponds to a temperature of about 1300 °C

Later, the axial erosion front slowed down from initially 3 mm/s to 0.26 mm/s, due to the end of the vigorous convection after all concrete is eroded.
A first, very thin melt jet penetrating the steel plate has been recorded with a video camera 61 s after ignition, which is 47 s after begin of the interaction between the iron melt and the steel plate. The diameter of the jet steadily increases and reaches a final value of 109 mm between 65 and 66 s.
Of special interest is the lateral extension of the melting zone in the steel plate. Towards the end of concrete erosion, close to 25 s, the 1300 °C front in the midplane (z = 20 mm) has proceeded in lateral direction only to a radius of about 20 mm.

Figure 6 shows the time dependent lateral temperature front progression in the midplane. An isolated area of early concrete erosion is found along the positive x-axis near a radius of 80 mm: there the 1300 °C temperature front was detected at earlier times than at smaller radii. Figure 7 shows the lateral progression of the 1300 °C front in the 20 mm midplane of the steel plate in the form of a contour plot for different progression times. The symmetric progression in the beginning (up to about 30 s) starts to become more asymmetric due to the inhomogeneous concrete erosion.

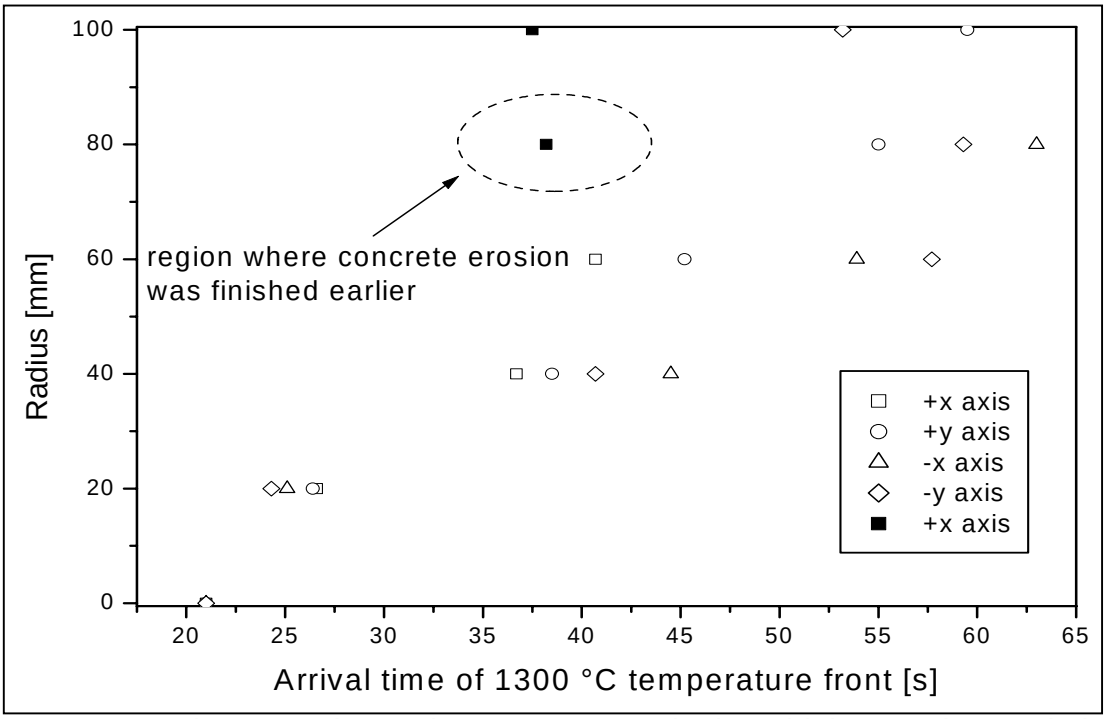

Figure 6: Lateral progression of the 1300 °C front in the midplane of the steel plate

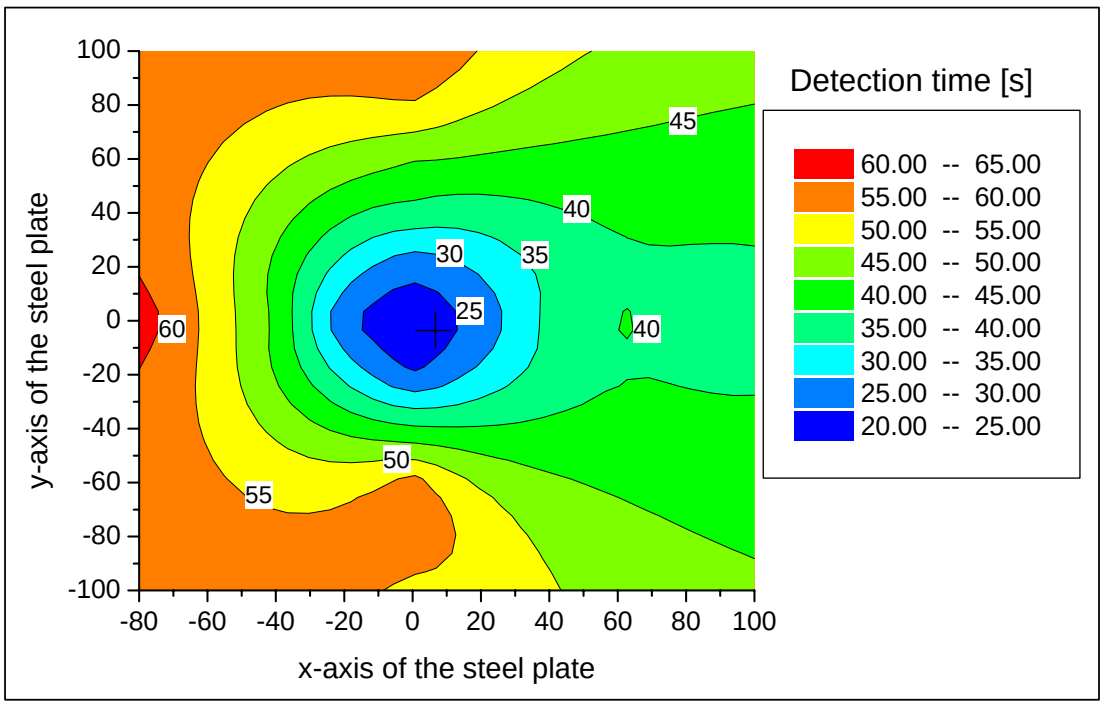

Figure 7: Contour plot of the lateral progression of the 1300 °C temperature front in the midplane of the steel plate. Contour parameter is the arrival time.

A contour map of the progressing 1300 °C front below the 20 mm midplane has been produced from thermocouple readings, Figure 8. Here, a vertical cut through the plate along the positive x-axis is shown which confirms, that due to the inhomogeneous concrete erosion, the temperature front inside the steel plate is not fully symmetric to the centerline of the plate. This figure clearly shows the fast downward melting and the widening of the melted zone, which is responsible for the fast increase of the jet diameter.

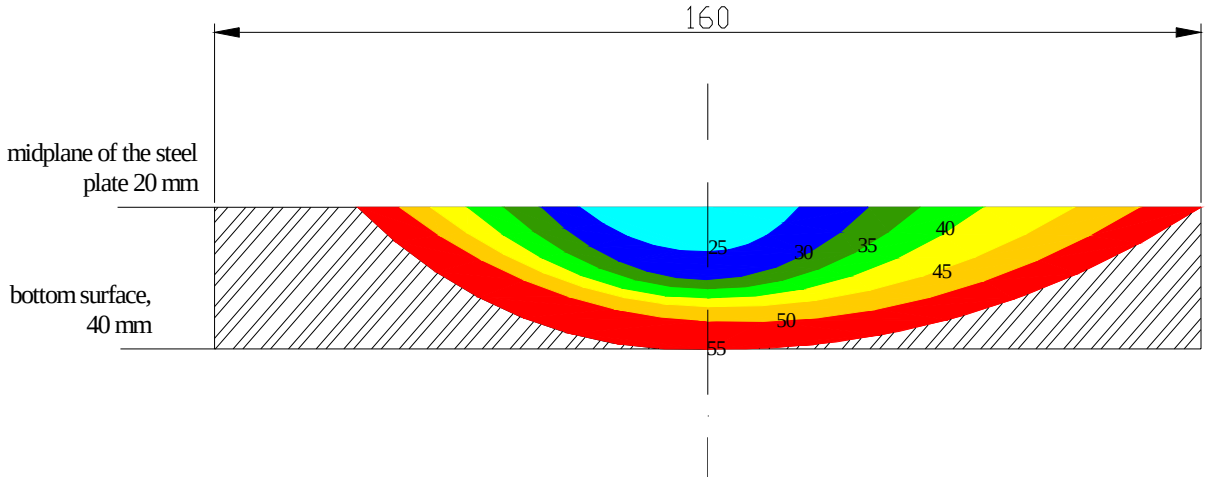

Figure 8: Contour map along x-axis of the 1300 °C temperature front in the steel plate below the 20 mm midplane. Contour parameters are the times after ignition in seconds.

4.2.3 Mass loss of the KAPOOL container

Three weighing cells recorded the transient mass loss of the KAPOOL container, Figure 9, which occurs between 60 and 67 s after ignition.

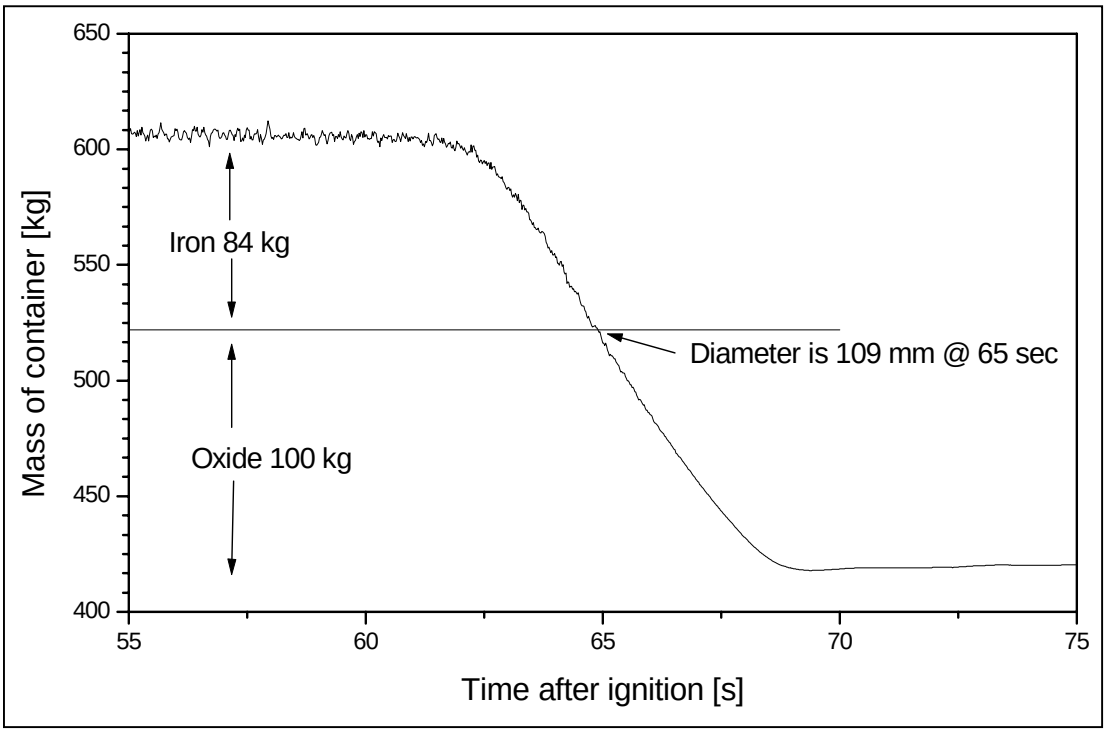

Figure 9: Transient recording of the container mass by load cells in KAPOOL 9

The total mass release was 184 kg. At 65 s, which coincides with the time when the jet diameter reached its final value of 109 mm, the mass loss through the ablated hole in the plate was 84 kg. Video recordings show that at this time the surface structure of the jet changes, the flow switched from iron to oxide melt. For a mass balance the amount of eroded steel of the plate (11.7 kg) has to be added to the 75 kg of iron melt, the result is a total metallic melt of 86.7 kg, close to the detected value of 84 kg. From these observations one can conclude that the steel plate ablation was only due to the interaction with the iron melt. The following oxide melt did not erode the steel plate any further as evaluated from the detailed video analysis of the jet diameter.
A total amount of about 100 kg oxide melt has been released following the iron melt release, it is composed of 75 kg oxide melt of the thermite reaction, the residual mass of 25 kg is from concrete erosion and side wall erosion, which is consistent with the post test measurements of about 20 mm eroded wall material.

4.2.4 Post test analysis in KAPOOL 9

The residual form (from the side and from the top) of the steel plate after erosion is shown in Figure 10. The erosion of the steel extended to the outer diameter of the plate, thereby the erosion thickness is steadily decreasing from the center to the outermost radius.

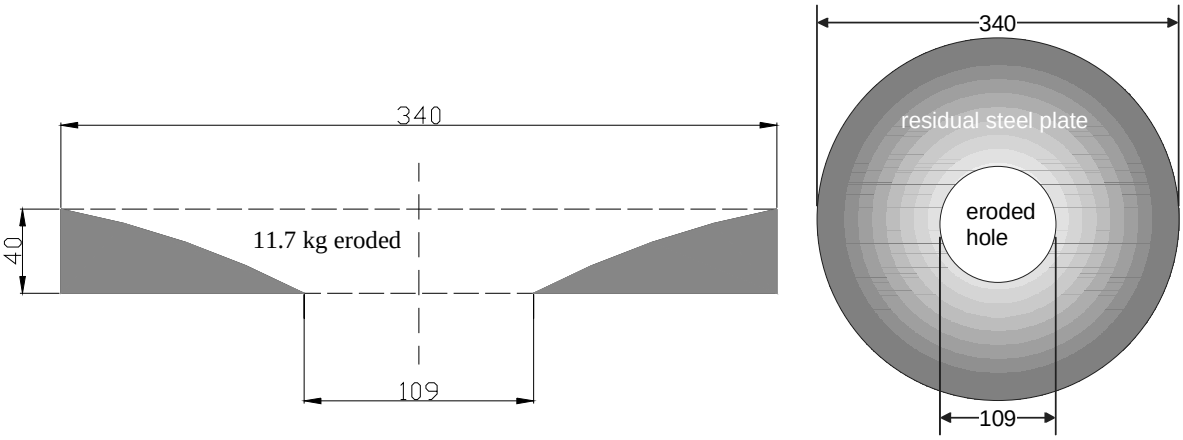

Figure 10: Form of the residual steel plate from the side and from the top after the test

From the final eroded front, Figure 10, one can conclude that the ablation of the steel plate during outflow of the melt is due to the pre-existing temperature profile, as plotted in Figure 8, and the convective heat transfer arising from the iron melt flowing at a relatively high velocity along the steel plate to the hole in the center.

4.3 Calculations with the HEATING5 code

The experiment KAPOOL 9 was recalculated with the HEATING5 code. The results and the analysis of the experiment in the previous chapters showed that the convection process of the melt due to the concrete erosion led to a high heat transfer from the melt to the steel plate. However, the HEATING5 code is restricted to solve heat conduction problems and not heat convection processes.
Nevertheless, to model the convection process of the melt following approach has been made: the heat conductivity of the iron melt has been multiplied by an empirical factor of 10 or 20, respectively. A further problem is the modelling of the ablation of the steel plate by the iron melt and consequently the modelling of the progress of the iron melt through the steel plate. To simulate these phenomena, further assumptions have been made: below the solidus temperature of the steel plate, the heat conductivity was set to its original value of λ = 43 W/mK. Above the solidus temperature in the liquid range, when the steel plate melts and the iron melt moves on into the plate, the heat conductivity λ of the molten part of the steel plate has been changed to the heat conductivity of the iron melt multiplied with the empirical factor. In Table 2 the material properties for the calculations are summarised. For the one-dimensional calculations, the initial melt temperature was set to 2000 °C and in the following two-dimensional calculations the initial melt temperature was increased to 2250 °C.

Table 2: Material properties for the HEATING5 calculations (KAPOOL 9)

	iron melt	**steel plate**
initial temperature T_0	2000 °C (2250 °C)[1]	20 °C
solidus temperature T_s [°C] [2]	1536 °C (1450 °C)	1450 °C
heat conductivity λ	43 W/mK[3]	43 W/mK
density ρ	$\rho(T) = 7030-0.88(T-T_s)$ kg/m^3	7900 kg/m^3
specific heat c_p	823 J/kgK	452 J/kgK
emissivity ε	0.35	0.35
latent heat	277000 J/kg	277000 J/kg
height of the iron melt	163 mm	
thickness of the steel plate		40 mm

[1]for the 2-dim calculations the melt temperature was set to 2250 °C
[2]to facilitate evaluation, both solidus temperature data have been set to 1450 °C
[3]increased by a factor of 10 or 20 to account for convection

4.3.1 One-dimensional calculations

The 1-dim calculations involve only the steel plate and the iron melt. The sacrificial concrete layer between the iron melt and the steel plate has been neglected. The initial stage of this calculation coincides with the moment when the iron melt is in first contact with the center of the steel plate in the experiment.
The modelling includes two regions, the iron melt and the steel plate, Figure 11. The steel plate has been subdivided in 20 grid lines of constant 2 mm distance. The iron melt has also been subdivided in a grid with different distances between several nodes. Near the contact surface between the iron melt and the steel plate a fine 1 mm

mm grid with 10 nodes was modelled. Above were 20 nodes with a distance of 2 mm, then 22 nodes with a distance of 5 mm and, at the interface of the iron melt with the surrounding atmosphere, again 3 nodes with a distance of 1 mm. The whole modelling consists of a grid with 75 nodes.

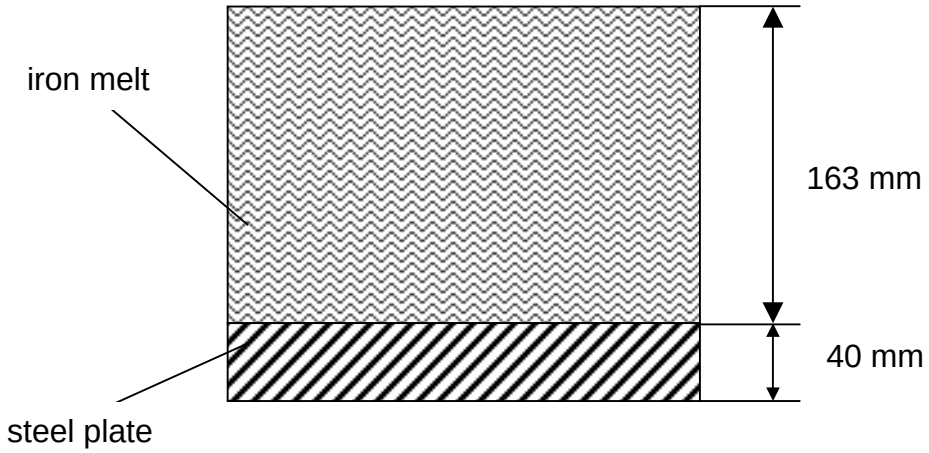

Figure 11: Modelling of the 1-dim calculations in KAPOOL 9

Two different calculations have been performed using different heat conductivities of the iron melt in the liquid phase: In the first calculation the heat conductivity has been multiplied by a factor of 10 to simulate the convection process of the iron melt. In the second calculation a higher convective heat transfer was assumed, here the heat conductivity was multiplied by a factor of 20.
Figure 12 shows the comparison between the experimental 1300 °C temperature fronts in the center of the steel plate with the calculated 1300 °C temperature fronts of the two calculations using two different heat conductivities for the iron melt. In the experiment the iron melt was in first contact with the steel plate about 14 s after ignition and at this point the ablation started, which is set to time zero in Figure 12. 40 s later the 1300 °C temperature front reached the bottom of the steel plate. A first, very thin melt jet penetrating the steel plate has been recorded with a video camera 61 s after ignition, which is 47 s after begin of the interaction between the iron melt and the steel plate.
In the first calculation with a multiplication factor of 10, the ablation process up to 2 mm is in good agreement with the experimental data. From there the calculated ablation process is proceeding much slower than detected in the experiment. The ablation process would be finished 85 s after first contact. This is twice as slow as in the experiment. In the second case (multiplication factor for the heat conductivity is 20) the ablation process up to 2 mm depth is identical with the first calculation. Then the ablation front is faster than in the first calculation but still slower than in the experiment. The ablation would be finished 53 s after first contact, compared to 40 s in the experiment.
These two calculations show clearly that it is very difficult to simulate the important phenomena during the conduct of the experiment in a 1-dim calculation with a code originally dedicated only to solve heat conduction problems. All approaches to simulate convection processes and the ablation of the steel plate do not fit with the reality. At the beginning of the calculation, the code calculates a contact temperature of the steel plate with the iron melt which is below the solidus temperature of the melt. This temperature increases rapidly, but throughout the whole calculation the temperature

of the melt at the contact surface is only 50 to 100 °C above the solidus temperature of the melt. Consequently, the temperature at the contact surface is lower than in the experiment, because in the experiment always hot iron melt is transported to the contact surface due to the convection process of the melt. This convection process is provoked by the concrete erosion and also by the immersion of the W-Re thermocouples. Due to these discrepancies between the experiment and the modelling, the calculations can describe the experiment only tentatively.

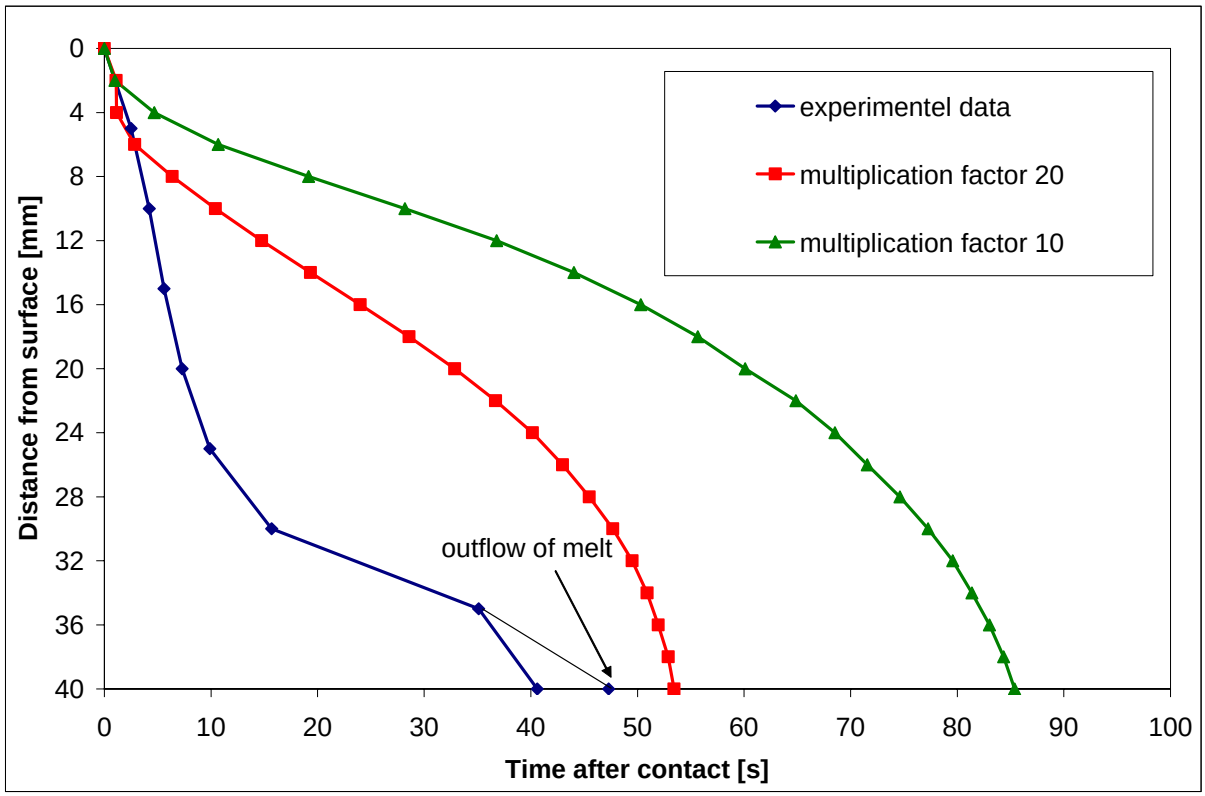

Figure 12: 1300 °C temperature fronts in the center of the steel plate in the experiment and in the calculations (time zero is the first contact of the iron melt with the plate)

4.3.2 Two-dimensional simulations

In order to model the experiment more realistically than in the 1-dimensional calculations, additionally 2-diminsional calculations with the HEATING5 code have been performed. In all 2-dimensional calculations the initial temperature of the iron melt was set to 2250 °C. Besides this, the same material properties have been used as in the one-dimensional calculations, Table 2.
Two different approaches have been made to take into consideration the existence of a temporary concrete layer: In a first calculation (step 1) the sacrificial concrete layer is taken into account for a given time period (which was about 10 s in the experiment). A second calculation (step 2), using the results of the first run as initial conditions, models the progress of the melt into the steel plate without sacrificial concrete. Two different calculation series (Series I and II) have been performed, in which different heat conductivities for the liquid iron melt and the melted steel plate have been used to account for the convection heat transfer.

4.3.2.1 Modelling of the 2-dimensional calculations

Modelling with sacrificial concrete (step 1)

The material properties of the sacrificial concrete are listed in Table 3. A center hole (30 mm diameter) in the concrete layer allows the iron melt to have contact with the steel plate, Figure 13. An average diameter of 30 mm for the center hole has been chosen instead of the original 20 mm in the experiment, because of its conical shape (40 mm top, 20 mm bottom), see Figure 3.

No melt/concrete interaction is taken into account in this model, the layer of concrete serves only as a thermal barrier for a given time period. The simulation includes 3 regions: the iron melt, the sacrificial concrete layer and the steel plate. The modelling was performed in r-z-geometry with a radius of 130 mm. In radial direction there were 12 nodes, 8 nodes at a distance of 3 mm, then 4 nodes at a distance of 26.5 mm in the outer region. In z-direction 25 nodes were modelled in the steel plate with a distance of 1.60 mm, 1 node for the 10 mm sacrificial concrete layer with a 30 mm gap in the center and 5 nodes for the iron melt with a distance of 32.6 mm. The whole modelling consists of a grid with 372 nodes.

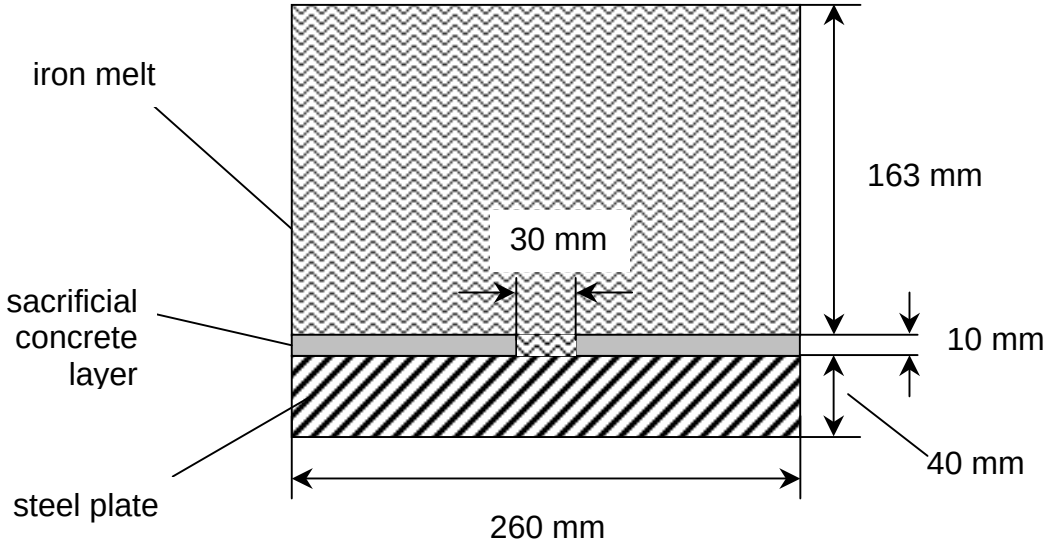

Figure 13: Modelling of the first step of the two-dimensional calculations

Table 3: Material properties of the sacrificial concrete

	sacrificial concrete
heat conductivity λ	3,5 W/mK
density ρ	2300 kg/m^3
specific heat c_p	1390 J/kgK
thickness of the sacrificial concrete layer	10 mm

Investigations in former experiments KAPOOL 1-5 [5] showed that a layer of 10 mm sacrificial concrete was eroded within 10 s (at iron melt temperatures of 2000°C) and so the computing time for the first step of the two-dimensional calculations has been fixed to 10 s.

Modelling without sacrificial concrete (step 2)

In the second part of the two-dimensional calculations it is assumed that the sacrificial concrete layer is already eroded. Therefore, the modelling includes only two regions, the partly melted steel plate and the iron melt, Figure 14. The conditions at the end of the calculation of the first step after 10 s were taken as the initial conditions for the second step. The parts of the steel plate, which were already molten at the end of the step 1 calculations were replaced by the hot iron melt, Figure 14. Also the bulk temperature of the iron melt was set to 2250 °C. This assumption was made due to the fact that always hot melt is in contact with the steel plate.

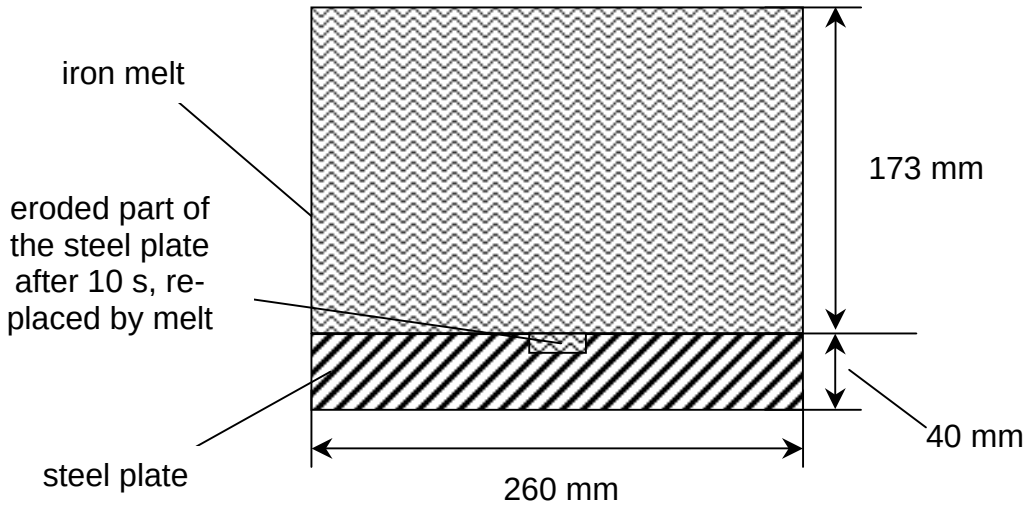

Figure 14: Modelling of the second step of the two-dimensional calculations

The subdivision of the grid in the second step of the simulation was practically identical with the first step except for the sacrificial concrete layer node, which was replaced by an additional node to model the iron melt. Furthermore, the melted part of the steel plate was modelled with the material propeties of the iron melt.

4.3.2.2 Results of the calculation Series I

In the Series I calculations the heat conductivity of the liquid iron melt has been multiplied with a factor of ten to account for convective heat transfer rather than conduction. The calculation of step 1 was performed for 10 s. Figure 15 shows the temperature distribution at the end of step 1 in vertical and radial direction up to a radius of 24 mm. At this time the 1300 °C temperature front reached a depth of about 6 mm in the center of the steel plate and a radius of 15 mm. In contrary, experimental data show that at this time the 1300 °C temperature front proceeded already more than halfway through the plate in vertical direction.

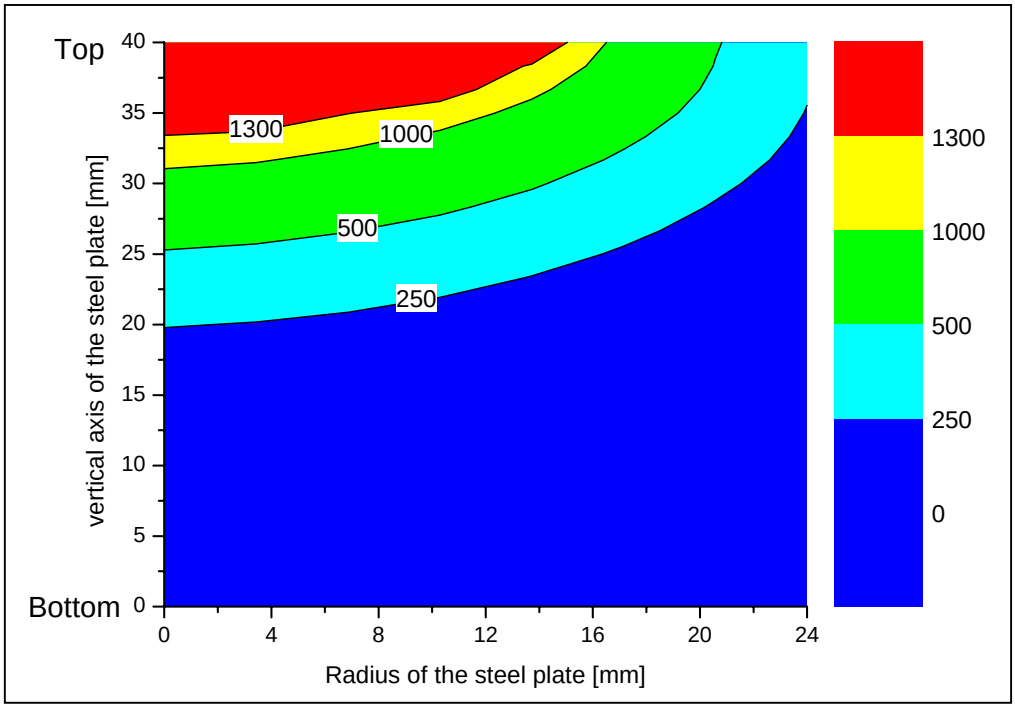

Figure 15: Temperature distribution at the end of the first step of the Series I calculation after 10 s

The result of the first step after 10 s is then the initial input for the second step of the Series I calculation. The melted part of the steel plate was replaced by iron melt and the temperature of the iron melt is increased to the initial temperature 2250 °C to model that always hot melt is in contact with the steel plate. The initial conditions for the second step of the calculation differ already from the experimental one, so it is clear that the result of the second step will even deviate more from the experimental results. Figure 16 to Figure 18 show the temperature distributions of the second step of the calculation at 20, 30 and 50 seconds in axial and radial directions up to a radius of 24 mm. They show also the corresponding results for the outer radial region ranging from radii 50.5 mm to 130 mm. The 1300 °C front progressed to a depth of 10 mm after 20 s, 15 mm after 30 s and 22 mm after 50 s, rather slow compared to the experimental results. In the experiment, at 40 s the 1300 °C temperature front already reached the bottom of the steel plate. As can be seen, the 1300 °C temperature front is homogeneously distributed over the total radius of 130 mm of the steel plate, but the vertical erosion progress is still too small compared to the experimental result. In this Series I calculation the 1300 °C temperature front reached the bottom of the steel plate after about 80 s, twice as slow as in the experiment.

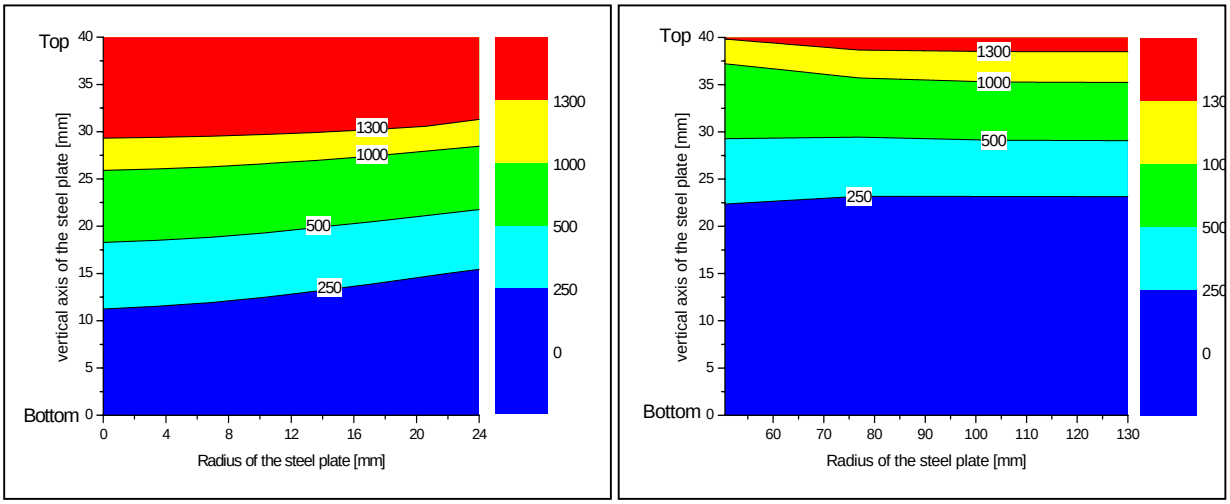

Figure 16: Temperature distribution after 20 s for an inner radius of 24 mm and an outer radial region from radii 50.5 to 130 mm

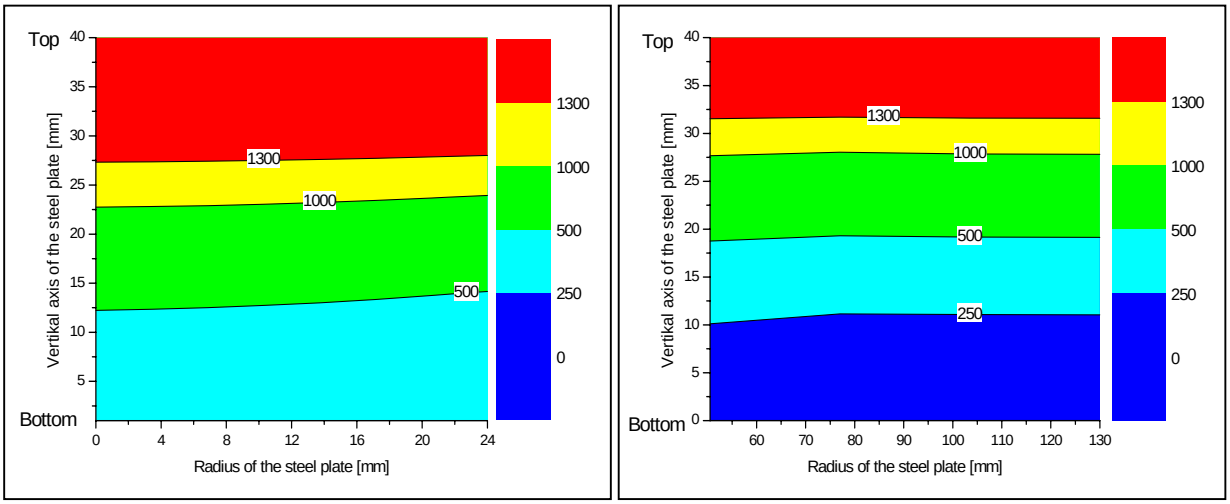

Figure 17: Temperature distribution after 30 s for an inner radius of 24 mm and an outer radial region from radii 50.5 to 130 mm

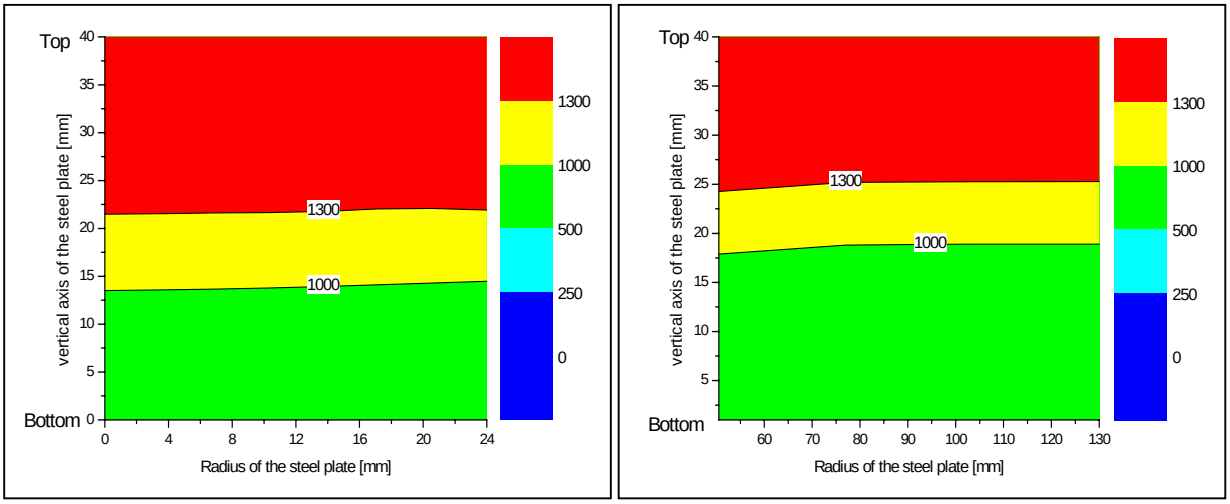

Figure 18: Temperature distribution after 50 s for an inner radius of 24 mm and an outer radial region from radii 50.5 to 130 mm

4.3.2.3 Results of the calculation Series II

In spite of a more realistic modelling of the experiment KAPOOL 9 in the two-dimensional Series I calculation, the results still differ considerable from experimental findings. The reason for these discrepancies is very likely due to the choice of an iron melt heat conductivity multiplied by a factor of ten to simulate the heat transfer by convection. It is clear that this approach can only be an approximation of the convective heat transfer, but it is the only way to realise such calculations with the HEATING5 code.

Before the calculation Series II has been performed, the effect of heat conductivity (which simulates the amount of convective heat transport) has been investigated. For theses investigations the two-dimensional model, which includes the 10 mm concrete layer, Figure 13, has been used for all time steps and not only for 10 seconds as in the Series I calculation. In several calculations the heat conductivity multiplication factor has been varied until the time interval for the vertical temperature front to proceed through the steel plate was closest to the experimental data. This has been achieved with a multiplication factor of 42, about four times higher than the value of 10 which was used in the Series I calculation. Due to the fact that the concrete layer was existent all over the time of the calculations except for the center hole, the calculated radial temperature front progression cannot be compared with the experimental data.

With this multiplication factor of 42 for the effective heat conductivity of the iron melt, a final HEATING5 calculation series (Series II) has been performed, now again applying the Series I method. The first part of the simulation with the two-dimensional model including the concrete layer was used for 10 s. The conditions at the end of the first part after 10 s were taken as initial conditions for the second part of the calculation without concrete. For these final calculations (Series II) temperature dependent material properties for heat conductivity and specific heat of the steel plate have been used, Table 4 [10].

Table 4: Temperature dependent specific heat and heat conductivity of steel

Temperature [K]	**specific heat [J/kgK]**	**Temperature [K]**	**heat conductivity [W/mK]**
300	436	400	50,33
400	500	500	47,7
500	545	600	44,5
600	582	700	41
700	627	800	37,33
800	700	900	33,5
900	800	1000-1723	30
1000	982	above 1723	1806*)
1032	1745		
1088-1723	755		

*) heat conductivity multiplied with the factor 42

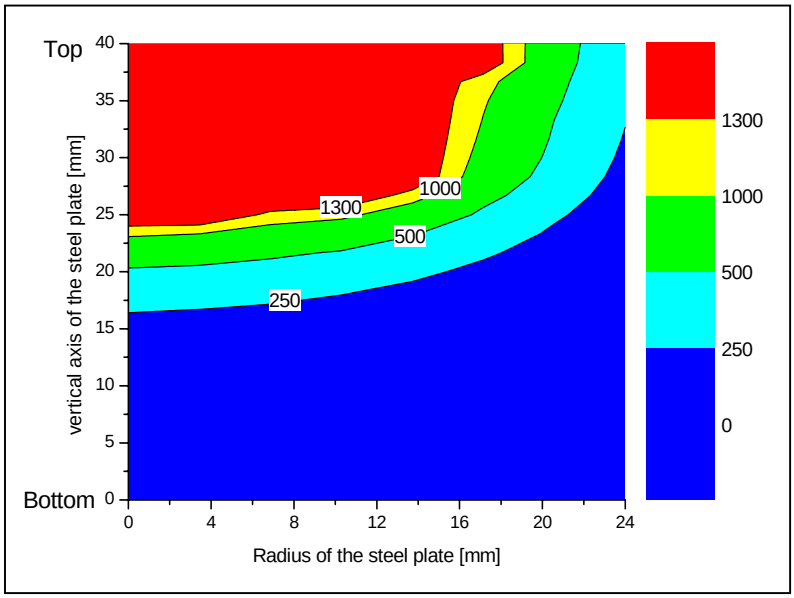

Figure 19: Temperature distribution at the end of the first step of the Series II calculation after 10 s

Figure 19 shows the temperature distribution after 10 seconds in vertical and radial directions up to a radius of 24 mm.
At the end of the first part of the calculation the 1300 °C temperature front reached a depth of about 16 mm in the center of the steel plate and a radius of 18 mm. In the experiment the 1300 °C temperature front proceeded already more than halfway through the plate in vertical direction. But in comparison with the first step of the Series I calculations the experiment is better described for the first 10 seconds. The result of the first step of the Series II calculation is the initial input for the second step of the simulation. As in the Series I calculations, the melted part of the steel plate was replaced by iron melt and the temperature of the iron melt is again increased to the initial temperature 2250 °C to model that always hot melt is in contact with the steel plate.
Figure 20 to Figure 23 show the temperature distributions of the second step at 20, 30, 40 and 50 seconds in axial and radial directions up to a radius of 24 mm. They show also the corresponding results for the outer radial region ranging from radii 50.5 mm to 130 mm. The 1300 °C front progresses to a depth of 24 mm after 20 s, 26 mm after 30 s and 32.5 mm after 40 s. After 50 s the 1300 °C front has already reached the bottom of the steel plate for the inner radius of 24 mm. In the experiment the 1300 °C front reached the bottom at about 40 s. So the experiment can be described better with this Series II calculation as with the Series I calculation. With the high multiplication factor and the two different modelling of the 2-dim simulations, the homogenous distribution of the 1300 °C front over the total radius of 130 mm can be avoided.
In spite of the fine grid, which has been used in the Series II calculation, rather large instabilities are detected in the results, see the outer radial region in Figure 20. This is due to large temperature gradients in the range between 1000 °C and 1300 °C, Figure 19. The grid structure which has been used was still not fine enough to account for these large gradients.

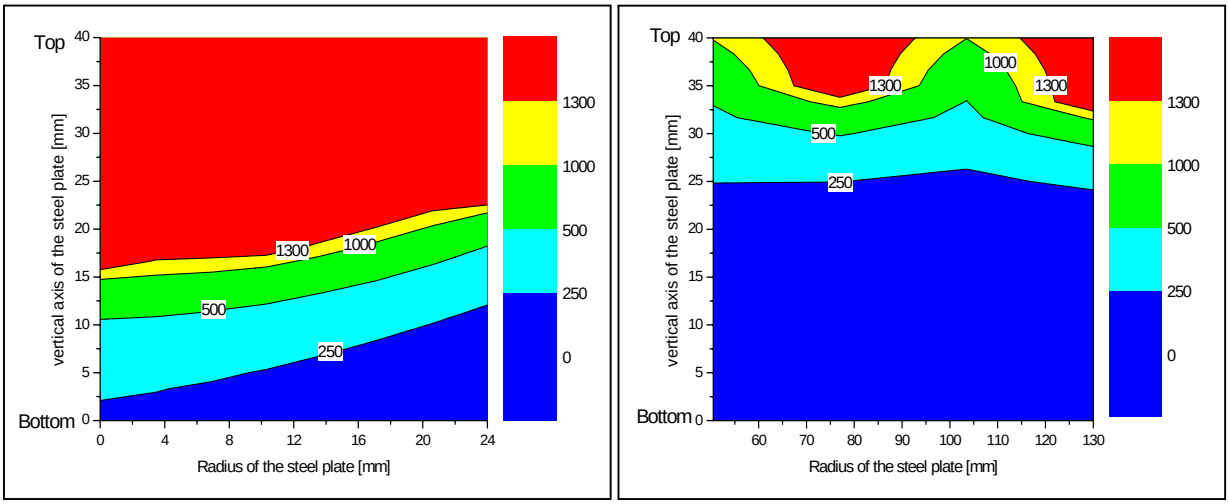

Figure 20: Temperature distribution after 20 s for an inner radius of 24 mm and an outer radial region from radii 50.5 to 130 mm

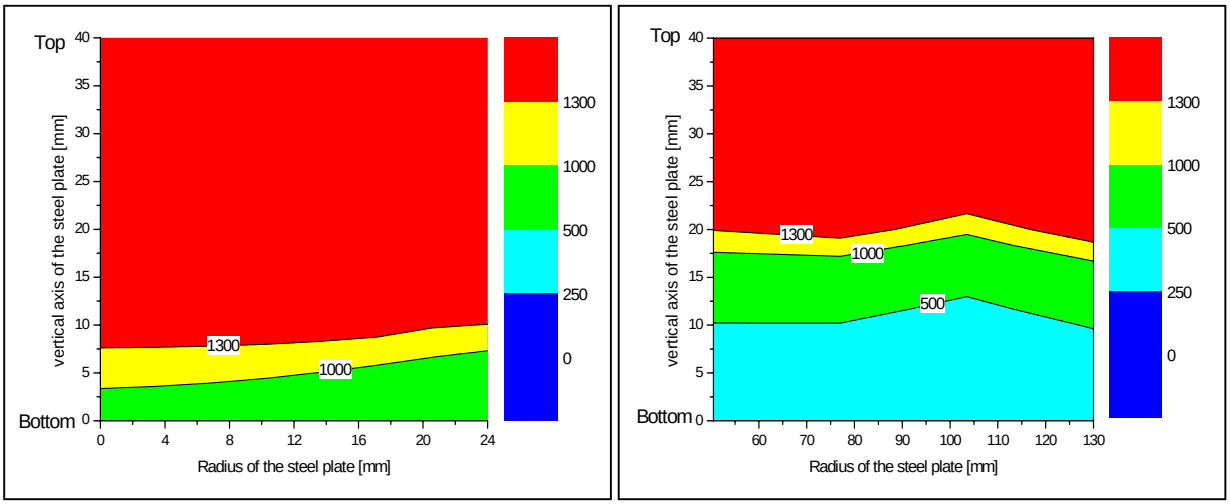

Figure 21: Temperature distribution after 30 s for an inner radius of 24 mm and an outer radial region from radii 50.5 to 130 mm

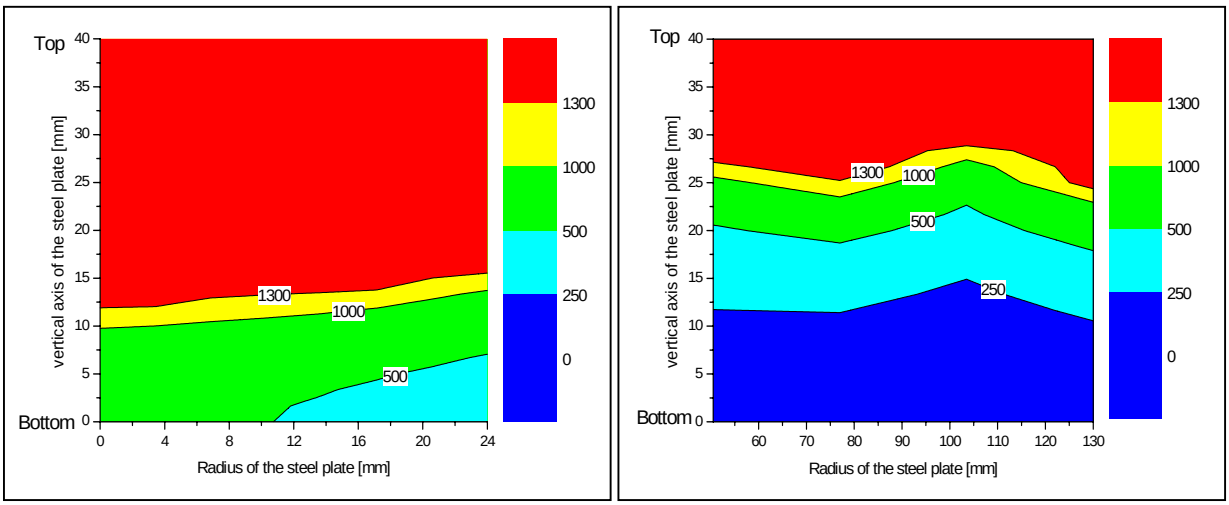

Figure 22: Temperature distribution after 40 s for an inner radius of 24 mm and an outer radial region from radii 50.5 to 130 mm

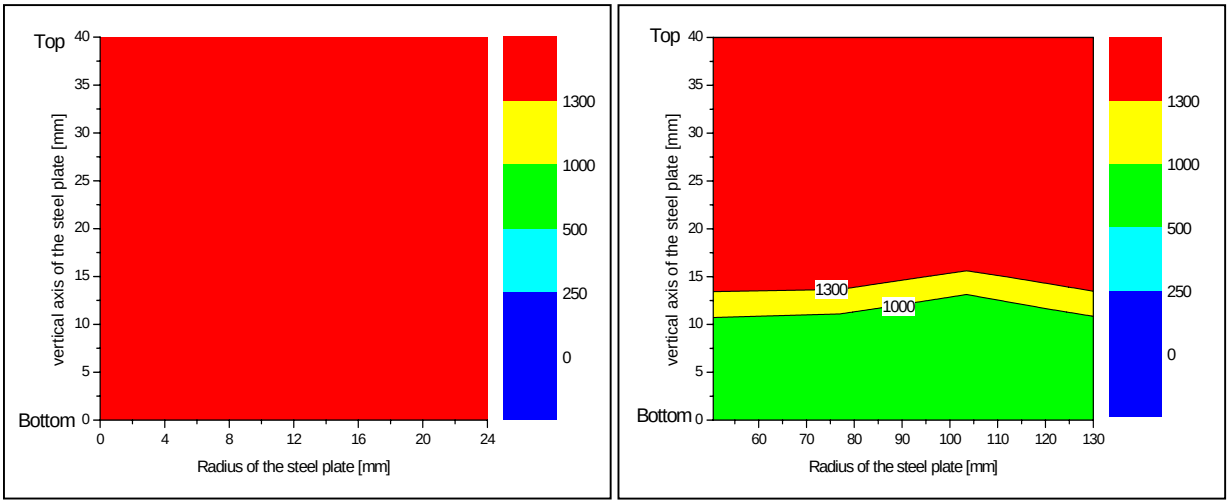

Figure 23: Temperature distribution after 50 s for an inner radius of 24 mm and an outer radial region from radii 50.5 to 130 mm

5 Interaction of an oxide melt with a steel plate (Experiments KAPOOL 11 and 12)

The objective of these two tests was the study of the interaction between the oxidic part of the thermite melt and a steel plate. To allow separation of the required oxide melt, the thermite powder was ignited in a separate reaction crucible. The melt release through a 20 mm nozzle started after full segregation of the two phases. The heavier metallic melt and a part of the oxidic melt were dumped into a separate tank, and then the oxide melt was redirected into the KAPOOL container, Figure 1.

5.1 The experiment KAPOOL 11

300 kg of thermite powder and 8 wt% SiO_2 have been ignited in the reaction crucible to produce about 150 kg iron and 150 kg oxide melt. The specific thermite mixture yields an oxide melt with 1925 °C as liquidus and 1570 °C as solidus temperature according to GEMINI calculations [11] and Data of Slag Atlas [12].

5.1.1 Setup of KAPOOL 11

The shape of the test container was quadratic with inner dimensions of 406 mm x 406 mm. The sidewalls and the bottom (except for the steel plate) were insulated with cordierite (ceramic) plates (total thickness 40 mm). The size of the steel plate was 220 mm x 220 mm and the thickness was 25 mm. A part of the steel plate was covered by cordierite plates; the free surface of the plate was 150 mm x 150 mm. The lower surface of the steel plate was not insulated. 16 K-type thermocouples have been installed inside the plate at different vertical and horizontal positions.

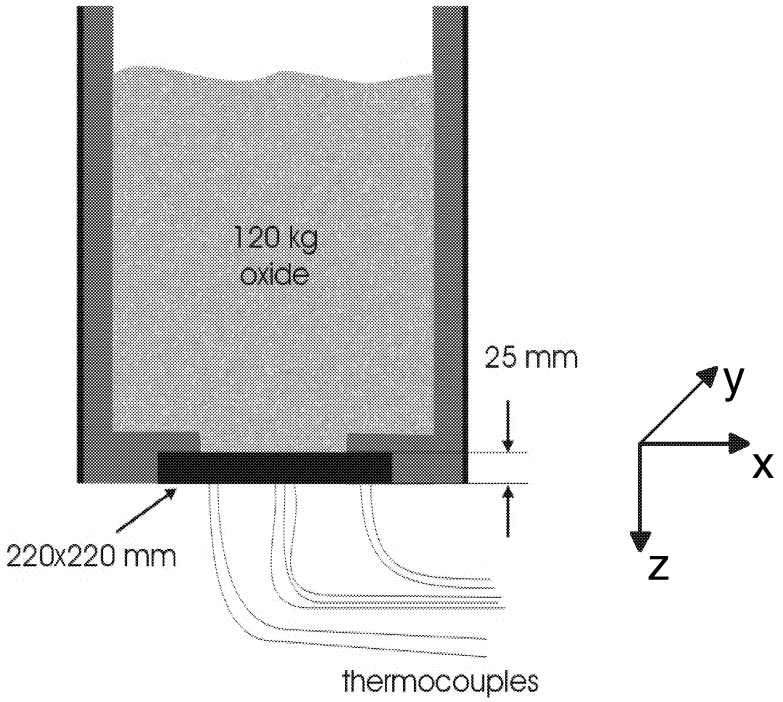

Figure 24: Setup of the test container in KAPOOL 11 and coordinate system

Table 5 lists the individual positions of all thermocouples. Five thermocouples (#1-5) were positioned 1 mm below the top steel surface, five in the midplane (12.5 mm below the top surface) and five at the bottom. Thermocouple #16 was positioned in the midplane outside the free plate surface.
Time 0 s is defined by the ignition of the thermite powder in the reaction crucible.

Table 5: Positions of NiCr-Ni thermocouples in the steel plate of KAPOOL 11

T/C #	Position x [mm]	Position y [mm]	Vertical position z [mm]
1	0	0	1
2	-46	-46	1
3	-46	46	1
4	46	46	1
5	46	-46	1
6	5	0	12.5
7	-42	-42	12.5
8	-42	42	12.5
9	42	42	12.5
10	42	-42	12.5
11	-5	0	24
12	-50	-50	24
13	-50	50	24
14	50	50	24
15	50	-50	24
16	80	0	12.5

5.1.2 Experimental Results of KAPOOL 11

5.1.2.1 Mass measurements in KAPOOL 11

The release of the melt from the reaction crucible started 19.6 s after ignition of the melt. Figure 25 shows the transient mass loss of the reaction crucible and the transient mass flow of oxide melt into the KAPOOL test container. The mass flow curve of the reaction crucible shows a distinct change at 35 s after ignition. At this time, the melt flow changes from iron to oxide melt. The redirection of the melt jet into the KAPOOL container was activated at 40 s, therefore all iron melt and some oxide melt was dumped into the separate tank and only oxide melt is flowing into the test container. The weighing cells of the test container recorded the first arrival of oxide melt at 41.6 s. In total about 120 kg of oxide melt were gathered in the test container, the calculated height of the melt was 250 mm (120 kg, 2900 kg/m^3). The mass loss of about 20 kg is due to intense interactions between the melt and the insulation of the W-Re thermocouple sheaths.

5.1.2.2 Oxide melt temperature in KAPOOL 11

Nine temperature measurements of the melt have been performed, Figure 26. The temperature of the melt pool was 1988 °C in the beginning and dropped to about 1900 °C at 130 s after ignition, which is near the liquidus temperature.

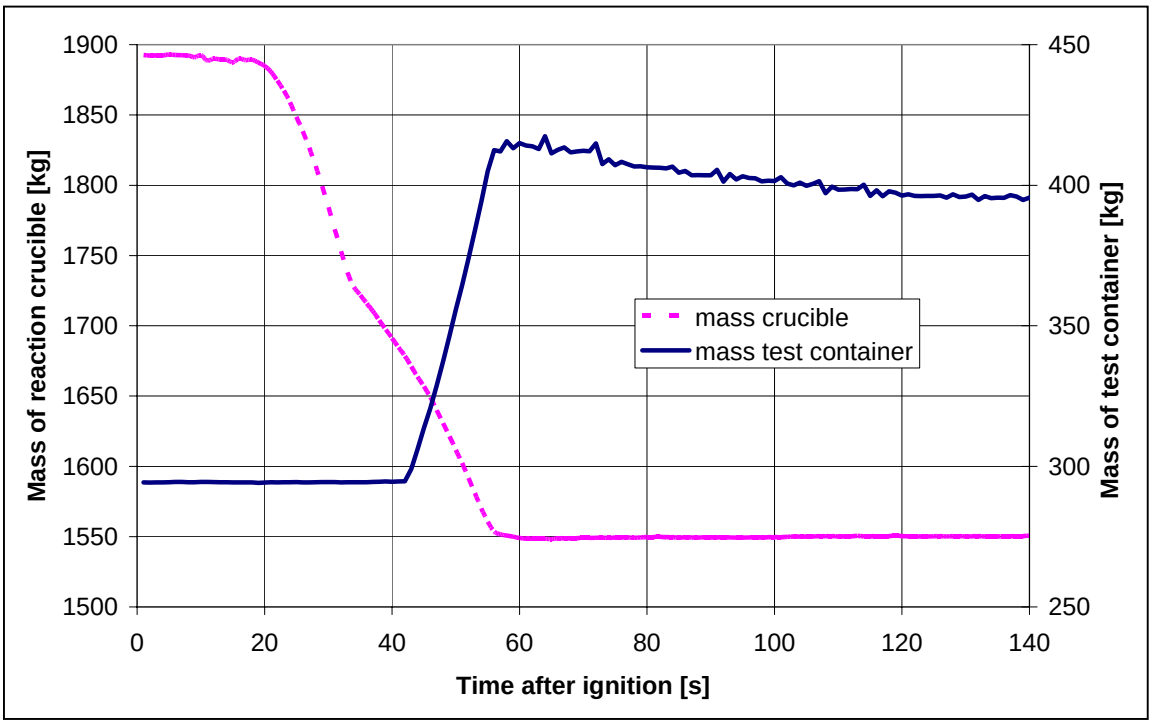

Figure 25: Mass of the reaction crucible and of the test container in KAPOOL 11

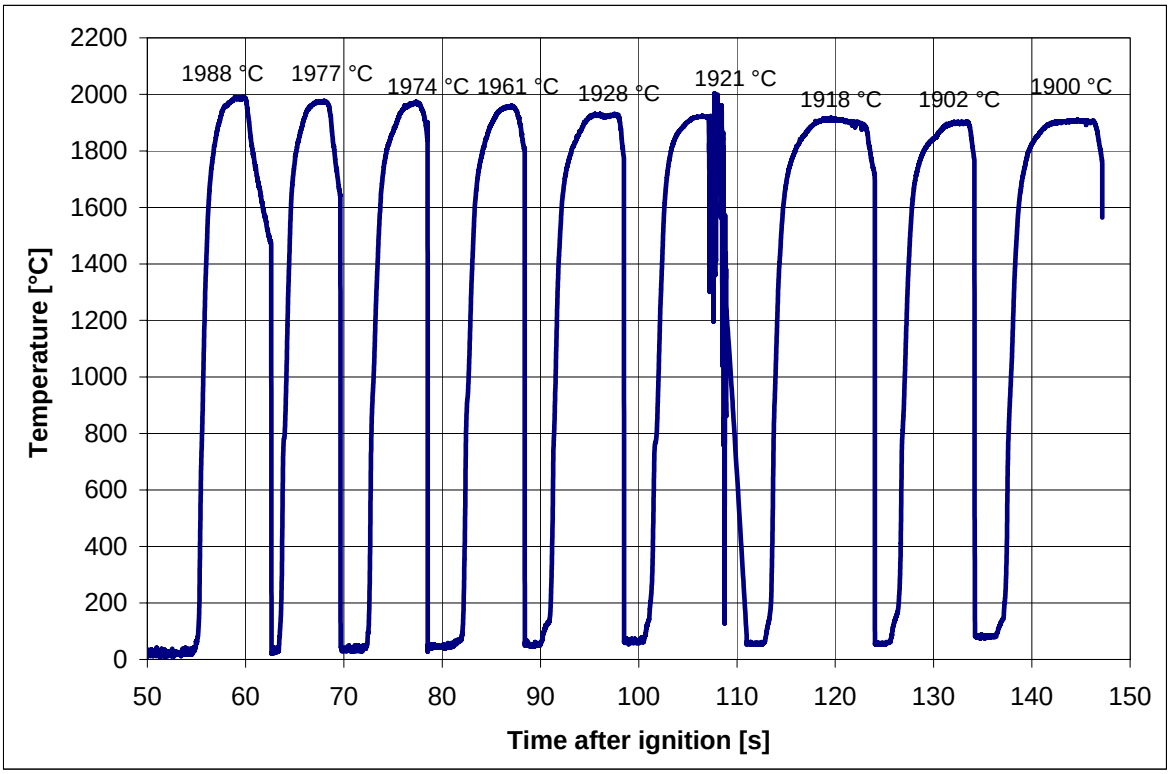

Figure 26: Measured temperature of the oxide melt in KAPOOL 11

5.1.2.3 Temperature readings of NiCr-Ni thermocouples in the steel plate

The temperatures in the center of the steel plate at different vertical positions are shown in Figure 27. The highest temperature of about 630 °C is recorded 1 mm below the top surface of the steel plate. The lateral positions recorded lower temperatures of about 400 to 500 °C which is due to the fact that only 46 % of the steel plate were exposed to the oxide melt, 54 % of the plate were covered with cordierite plates. The steel melting temperature of 1385 °C has not been reached and the steel plate did not fail.

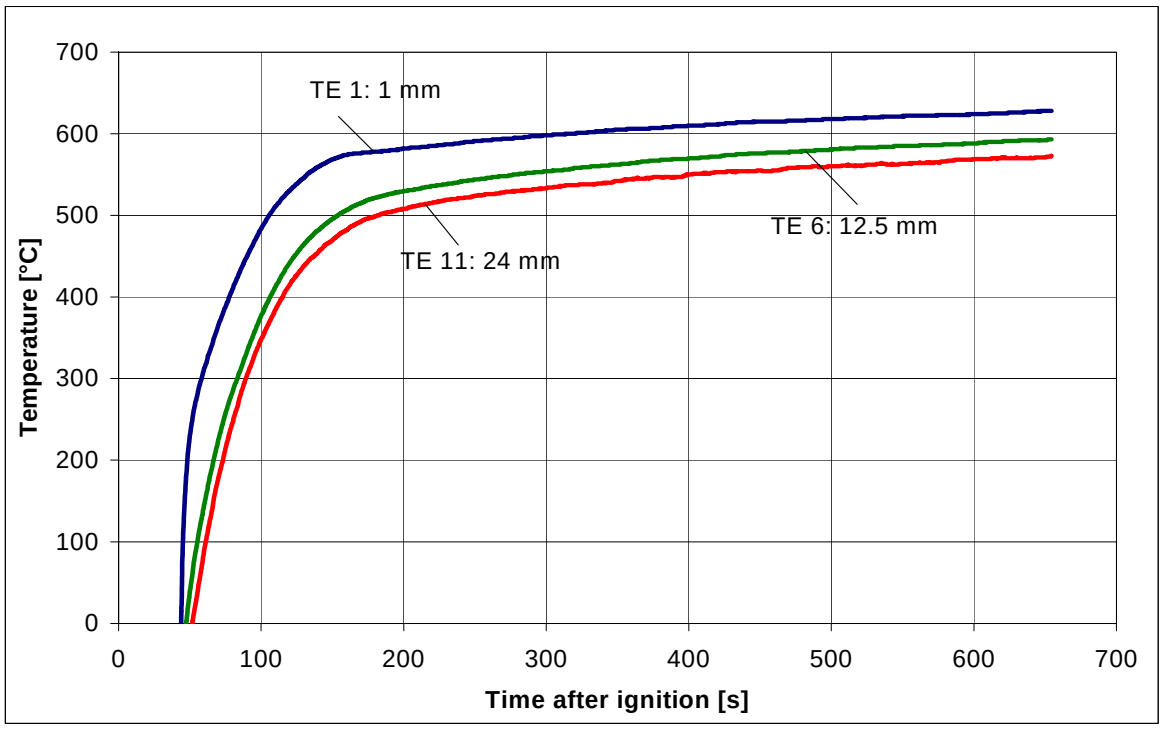

Figure 27: Transient temperature measurements in the center of the steel plate in KAPOOL 11

5.1.3 Post test examinations in KAPOOL 11

The steel plate in this test did not fail and even no ablation of the steel plate by the oxide melt was observed.
To understand these phenomena assuming unsteady heat conduction the interfacial temperature between the oxide melt and the steel plate was determined. In theory, when two semi-infinite bodies of different materials initially at constant but different temperatures are brought together, an interfacial temperature T_i can be calculated [13]:

$$T_i = \frac{\frac{b_1}{b_2} \cdot T_1 + T_2}{1 + \frac{b_1}{b_2}} \qquad \text{with:} \quad b = \frac{\lambda}{\sqrt{a}} = \sqrt{\lambda \cdot \rho \cdot c}$$

T_i: Interface or contact temperature [K]
T_1: Initial temperature of the steel plate [K]

T_2: Initial temperature of the oxide melt [K]
b: Thermal penetration coefficient [$Ws^{1/2}/Km^2$]
a: Thermal diffusivity [m^2/s]
ρ: Density [kg/m^3]
c: Specific heat [J/kgK]
λ: Thermal conductivity [W/mK]

Table 6: Material properties and calculation result

	Steel plate (St37)	**Oxide melt**
λ [W/mK]	~ 45	~5,4
ρ [kg/m^3]	7850	2917
c_p [J/kgK]	420	1400
T_1 [°C]	20	-
T_2 [°C]	-	1990
a [m^2/s]	$1{,}36*10^{-5}$	$1{,}32*10^{-6}$
b [$Ws^{1/2}/Km^2$]	12181	4696
T_i [°C]	**568**	

In Table 6 the material properties for the calculation and the result of the calculation is shown. The calculated initial contact or interfacial temperature is about 570 °C, much lower than the solidus temperature of the oxide melt. Therefore formation of an oxide crust is predicted by the calculation. The thermal contact of the crust to the steel plate may not be ideal, so thermal contact resistances may become important for the further heat transfer.
Even though the calculation is only valid for a short time range and additionally the oxide melt and the steel plate are no semi-infinite bodies as they are regarded in the calculation, the results of the calculation indicate, that the oxide melt forms initially a crust at the surface of the steel plate.
When the heat content of the melt would be high enough or the melt is volumetrically heated, this oxide crust could remelt. Then the heat transfer from the melt to the steel plate could be high enough to melt the steel plate. But in this test, the heat losses into the test container and the heat losses by radiation were to high and therefore no ablation of the steel plate could be observed, despite of an initial melt bulk temperature higher than the melting temperature of the steel plate.

The solidified oxide melt after the test is shown in Figure 28. The area where the oxide melt contacted the steel plate, is rather small compared to the total area of the melt surface, hence the geometrical dimensions were not favourable in this test.

Figure 28: Solidified oxide melt after the test in KAPOOL 11

5.2 The experiment KAPOOL 12

In this test 300 kg of thermite powder have been mixed with 90 kg calcia (CaO) to yield an oxide melt with lower liquidus and solidus temperatures as in KAPOOL 11. This mixture produces 150 kg iron and 240 kg of oxide melt. The liquidus and solidus temperatures are 1500 °C and 1395 °C, respectively [12]. The addition of calcia does not exclude early formation of an oxide crust, but should reduce its influence later in the test.

5.2.1 Setup of KAPOOL 12

In KAPOOL 12 the setup was different in comparison to KAPOOL 11. The container was of a conical shape with an inner diameter of 200 mm at the base, Figure 29. The angle of the conical insulated sidewall was 5° from the vertical. The total diameter of the steel plate was 300 mm. The inner part of diameter 200 mm, which was exposed to the melt, was 15 mm thick. At the rim, the steel plate was tapered off to reduce lateral heat losses, Figure 30. In contrast to KAPOOL 11 the bottom of the steel plate has been thermally insulated to reduce downward heat losses by radiation. Therefore a direct view of the bottom surface was not possible during this test.
21 K-type thermocouples have been installed inside the plate. Table 7 lists the individual positions of all thermocouples. Three thermocouples (#1,8,15) were positioned in the center of the plate at the top surface, in the midplane (7.5 mm) and at the bottom surface. Furthermore there were six additional lateral positions with three thermocouples at the same vertical positions at a radius of 50 and 75 mm.
Time 0 s is defined by the ignition of the thermite powder in the reaction crucible.

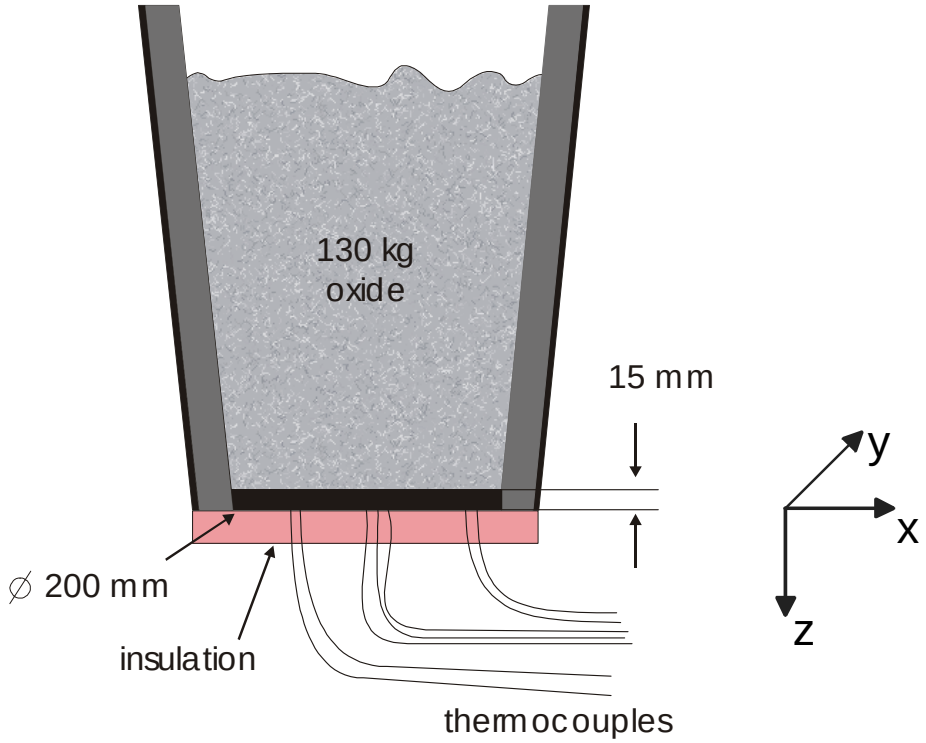

Figure 29: Setup of the test container in KAPOOL 12 and coordinate system

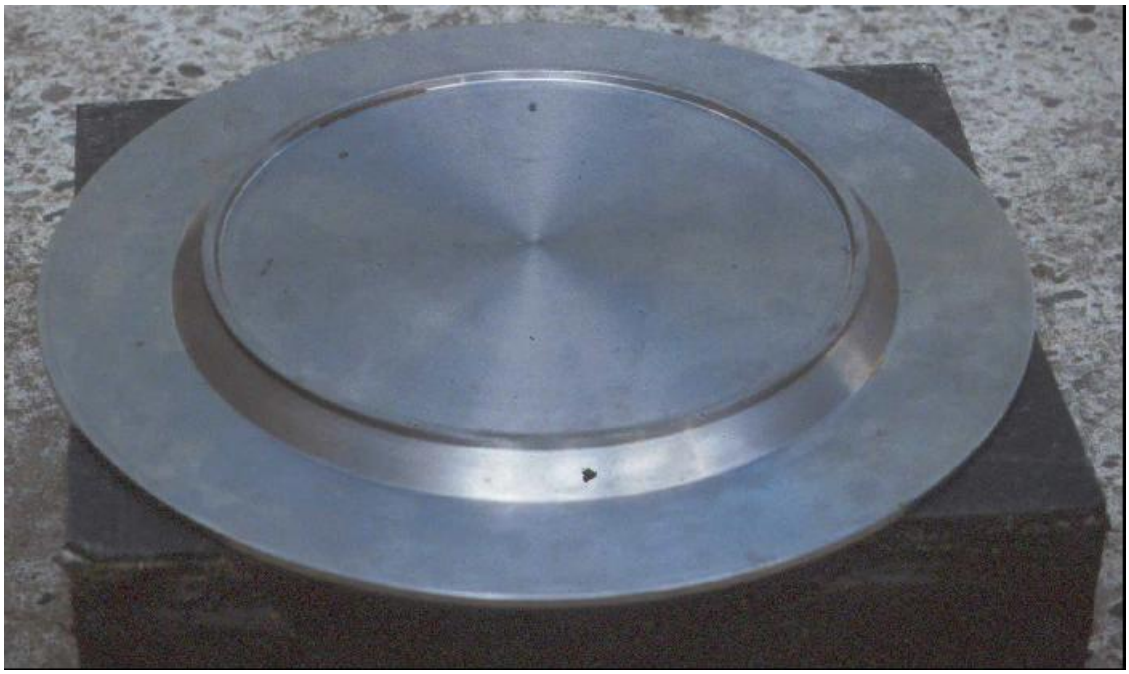

Figure 30: Steel plate for the test KAPOOL 12

Table 7: Positions of NiCr-Ni thermocouples in the steel plate of KAPOOL 12

T/C #	Position x [mm]	Position y [mm]	Vertical position z [mm]
1	0	0	0
2	-50	0	0
3	25	43.3	0
4	25	-43.3	0
5	-37.5	-65	0
6	-37.5	65	0
7	75	0	0
8	0	0	7.5
9	-50	0	7.5
10	25	43.3	7.5
11	25	-43.3	7.5
12	-37.5	-65	7.5
13	-37.5	65	7.5
14	75	0	7.5
15	0	0	15
16	-50	0	15
17	25	43.3	15
18	25	-43.3	15
19	-37.5	-65	15
20	-37.5	65	15
21	75	0	15

5.2.2 Conduct of KAPOOL 12

Some pictures describing the conduct of the test KAPOOL 12 are shown in Figure 31. In the first picture (top left) the release of the iron melt into the separate tank and in the second picture (top right) the release of the oxide melt into the test container is presented. In the third picture (down left) the first thermocouple to measure the melt temperature is immersed into the test container. The melt was filled close to the rim and the interaction between the shielding of the thermocouple and the melt was really intense. Therefore the melt is overflowing the test container and is destroying the mirror below the test container. In the last picture (down right) the situation is stable. Another thermocouple is immersed into the melt and the interaction of the melt with the steel plate continues.

Figure 31: Conduct of the test KAPOOL 12

5.2.3 Experimental Results of KAPOOL 12

5.2.3.1 Mass measurements in KAPOOL 12

Release of the melt through the nozzle started 36 s after ignition. Figure 32 shows the transient mass loss of the reaction crucible and the transient mass flow of oxide melt into the KAPOOL test container. The mass flow curve of the reaction crucible shows a distinct change at 54 s after ignition. At this time, the melt flow changes from iron to oxide melt. The redirection of the melt jet into the KAPOOL container is delayed and started four seconds later to ensure that no iron melt is poured into the container. The weighing cells of the test container recorded the first arrival of oxide melt at 60 s. About 135 kg of oxide melt were gathered in the KAPOOL container, it was filled close to the rim. This is why the mass losses have been relatively strong during immersion of the first W-Re thermocouples (about 40 kg).

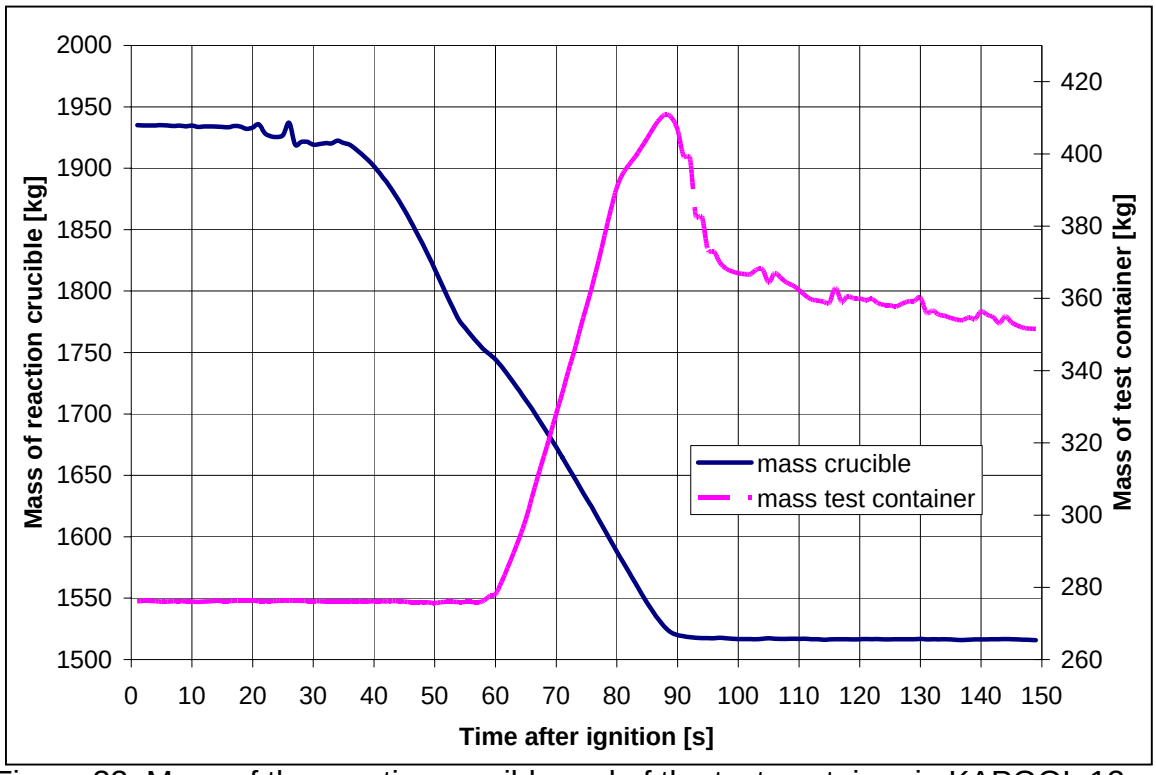

Figure 32: Mass of the reaction crucible and of the test container in KAPOOL 12

5.2.3.2 Oxide melt temperature in KAPOOL 12

Nine temperature measurements of the melt have been performed, Figure 33. The temperature of the melt fell from initially 1899 °C to 1624 °C within about 120 s. The initial temperature is 100 K below that of KAPOOL 11 which is due to the CaO addition to the thermite powder.

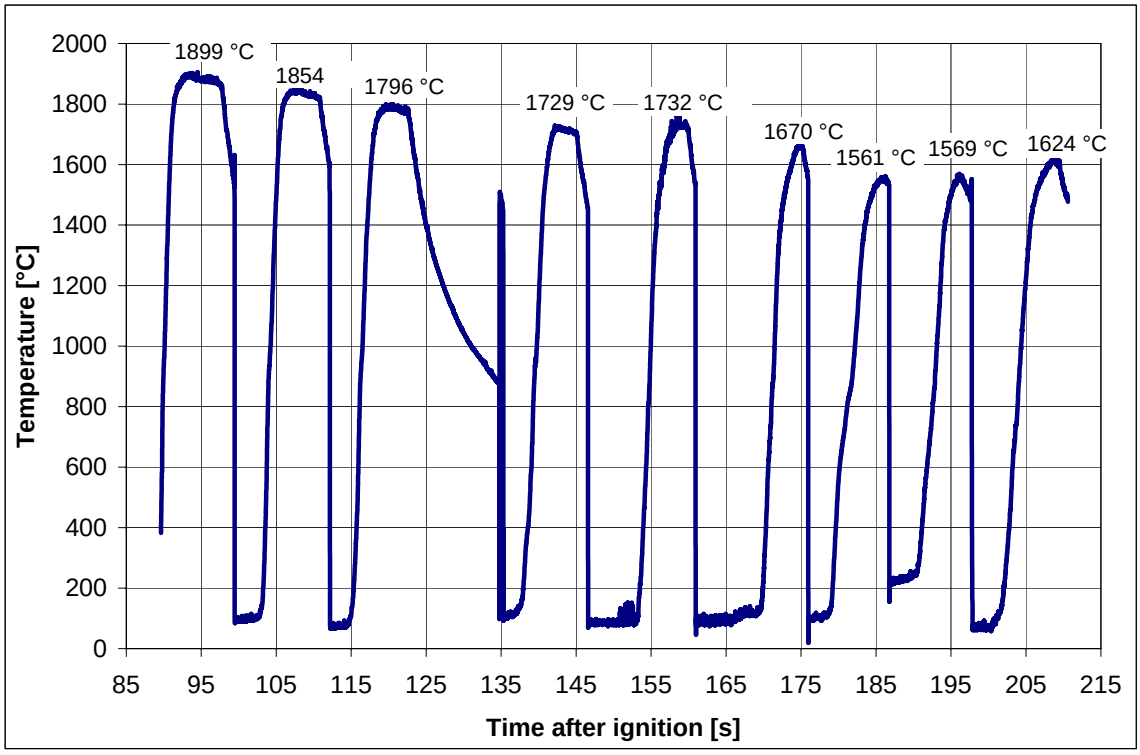

Figure 33: Measured temperature of the oxide melt in KAPOOL 12

The values for the last four measurements are scattering between 1550 and 1650 °C. The reason for this behaviour could be that the temperature of the melt was only slightly above the liquidus temperature and therefore the oxide melt formed a crust at the tip of the thermocouple and the accuracy of the measurement decreases.

5.2.3.3 Temperature readings of NiCr-Ni thermocouples in the steel plate

The transient temperature development in the center of the steel plate is shown in Figure 34.

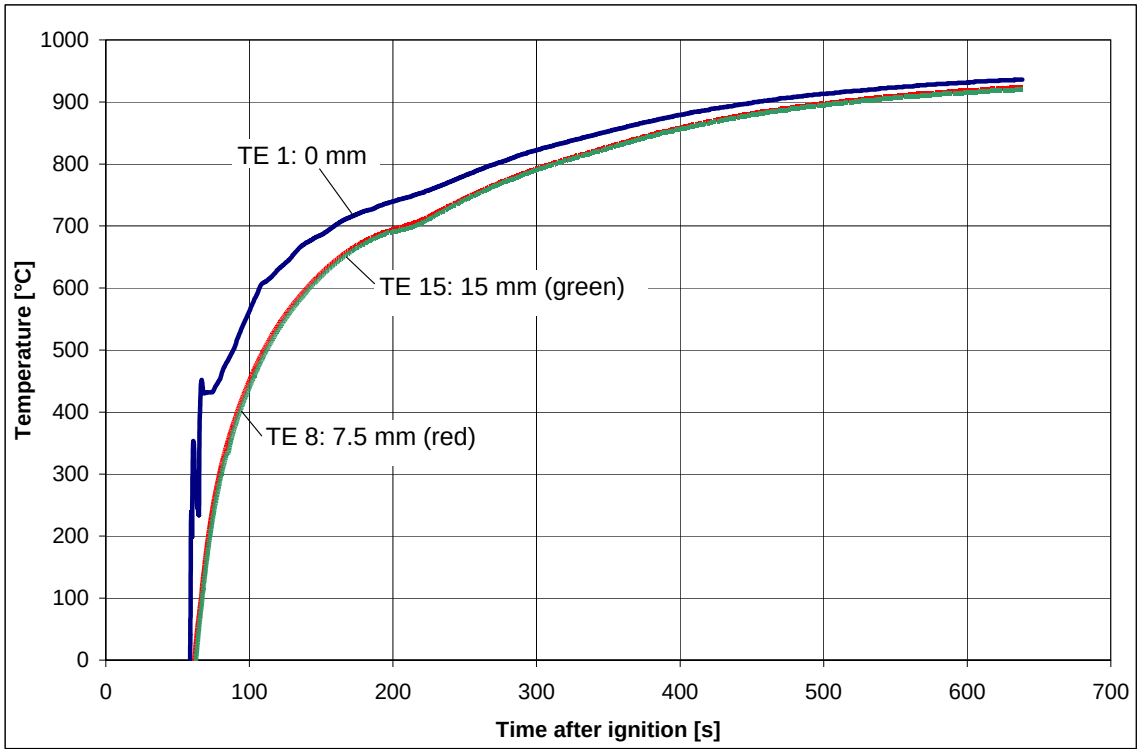

Figure 34: Transient temperature measurements in the center of the steel plate in KAPOOL 12

The thermocouple readings for the top surface temperature (thermocouple 1 in Figure 34) are characteristic for early crust formation: within a short time a fast temperature rise due to an initial contact between melt and plate, then a slowing down or even decrease of the surface temperature because immediately after contact a crust is formed. As in KAPOOL 11 also here the highest temperature values are found in the center of the steel plate, however, the differences to outer lateral positions are small as the entire upper steel plate surface has contact to the melt and the lower surface of the steel plate is insulated. A maximum asymptotic temperature of about 900 °C was reached in this test which is however 500 °C below the melting temperature of the steel plate.

5.2.4 Post test examinations in KAPOOL 12

Also in this test the steel plate did not fail and also even no ablation of the steel plate by the oxide melt was observed, similar to KAPOOL 11. The changes in the setup of the test did not lead to melting of the steel plate and the reached temperatures in the steel plate were only 300 °C higher than in KAPOOL 11.
As in the test KAPOOL 11 it is possible to calculate an initial contact temperature between the steel plate and the oxide melt. The material properties are the same as in

KAPOOL 11 (see chapter 5.1.3), only the oxide melt temperature is 100 °C lower. Therefore the calculated interfacial temperature is also lower as in KAPOOL 11 and is about 543 °C. For this reason the same phenomena as in KAPOOL 11 take place with an initial crust formation of the oxide melt at the surface of the steel plate which explains the early plateau of thermocouple 1 in Figure 34.
In Figure 35 the surface of the oxide melt at the interface to the steel plate after the test is shown. It can be assumed that the initially formed oxide crust is stable during the test and was not remelted.
The surface of this crust is rather rough and therefore the thermal contact between the melt and the plate was not given over the total surface. Heat transfer from the crust to the steel plate was partly conductive and partly by radiation.

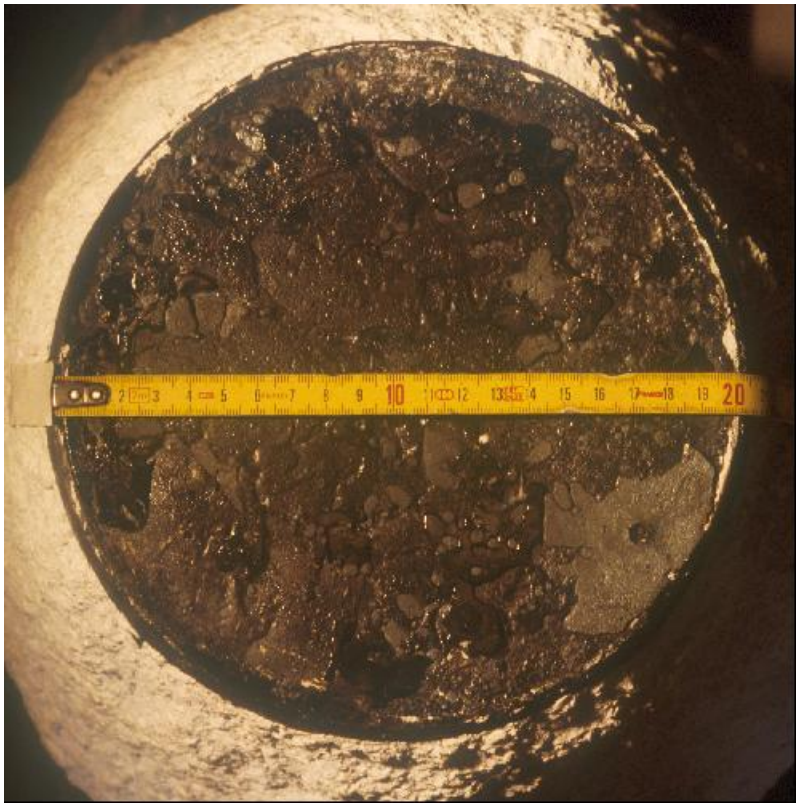

Figure 35: Lower surface of the oxide melt removed from the steel plate after the test

5.3 Calculations with the HEATING5 code

Different from the experiment KAPOOL 9, there was no concrete layer on top of the steel plate in the experiments KAPOOL 11 and 12. Therefore the heat transfer from the melt to the steel plate was not dominated by a strong convection process due to concrete erosion. But anyhow, due to the immersion of the W-Re thermocouples into the melt, there was a certain movement of the melt, which can influence the heat transfer from the melt to the steel plate.

5.3.1 Calculations for the KAPOOL 11 experiment

For the test KAPOOL 11 different 1-dimensional calculations with HEATING5 have been performed. The first two calculations have been performed with the oxide melt in contact with the steel plate and the following calculations have been performed with a gap between the oxide melt and the steel plate. The size of the gap was varied between 0.5 and 1 mm and the material of the gap was also varied. In some calculations, the gap was defined without a gas and therefore the heat transfer over the gap was due to radiation only. In another calculation, the gap was defined as a material region with the material properties of air. In this case, the heat transfer from the melt over the gap to the steel plate is only due to heat conduction. These different calculations correspond to the possibilities of the HEATING5 code.
The material properties of the oxide melt, the steel plate and air are summarised in Table 8. The density of air was used as a temperature dependent input, Table 9.

Table 8: Material properties for the HEATING5 calculations (KAPOOL 11)

	oxide melt	**steel plate**	**air**
initial temperature T_0	2000 °C	20 °C	
solidus temperature T_s	1751 °C	1450 °C	
heat conductivity λ	5.4 W/mK	45 W/mK	0.026 W/mK
density ρ	2917 kg/m^3	7900 kg/m^3	s. Table 9
specific heat c_p	1400 J/kgK	452 J/kgK	1005 J/kgK
emissivity ε	0.9	0.35/0.6	
latent heat	1068000 J/kg	277000 J/kg	
height	250 mm	25 mm	0.5/1 mm

Table 9: Temperature dependent density of air

Temperature [°C]	Density of air [kg/m^3]	Temperature [°C]	Density of air [kg/m^3]
0	1.275	400	0.517
25	1.168	500	0.4502
50	1.078	600	0.4502
75	1	700	0.3576
100	0.9329	800	0.3243
150	0.8226	900	0.2967
200	0.7356	1000	0.2734
300	0.6072		

5.3.1.1 Modelling of the calculations

The modelling of the calculations with the oxide melt and the steel plate in direct contact includes two regions, left part of Figure 36. The steel plate has been subdivided into 24 grid lines with a constant distance between each grid line. The oxide melt was also subdivided into a grid with different distances between the grid lines. Near the contact surface between the oxide melt and the steel plate a fine 0.2 mm grid with 24 nodes was modelled. Above were 22 nodes with a distance of 2 mm and then 20 nodes with a distance of 10 mm. The whole modelling consists of 91 nodes.

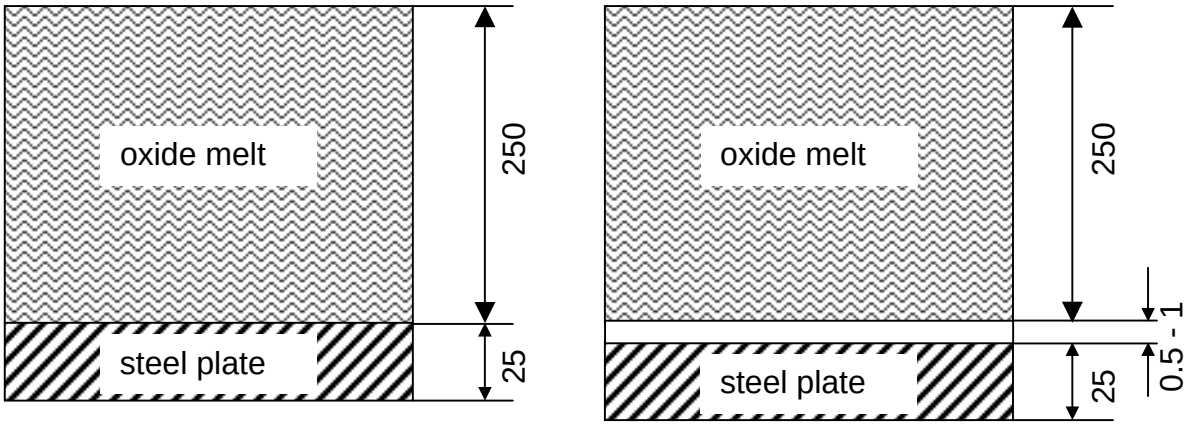

Figure 36: Modelling of the calculations of the KAPOOL 11 experiment

For the calculations with a gap between the oxide melt and the steel plate an additional node for this gap has been modelled. The boundary conditions at the top of the melt and at the bottom of the steel plate are that there is radiation to the environment with the appropriate emissivity, Table 8.

5.3.1.2 Results of the calculations

In Table 10 the different calculations for KAPOOL 11 are summarised. The first two calculations have been performed with the oxide melt and the steel plate in direct contact. The only difference in the calculations was, that the first calculation has been performed without the possibility of a phase change of the oxide melt and the steel plate (calculation 1) and the second calculation has been performed with the possibility of a phase change (calculation 2).

Table 10: Summary of the HEATING5 calculations for KAPOOL 11

calculation 1	Calculation with oxide melt and steel plate in direct contact without phase change of the materials
calculation 2	Calculation with oxide melt and steel plate in direct contact with phase change of the materials
calculation 3	Calculation with a gap of 0.5 mm between the oxide melt and the steel plate; radiation over the gap; ε=0.35 (steel), ε=0.9 (oxide)
calculation 4	Calculation with a gap of 1 mm between the oxide melt and the steel plate; radiation over the gap; ε=0.35 (steel), ε=0.9 (oxide)
calculation 5	Calculation with a gap of 1 mm between the oxide melt and the steel plate; radiation over the gap; ε=0.6 (steel), ε=0.9 (oxide)
calculation 6	Calculation with a gap of 1 mm between the oxide melt and the steel plate; the material of the gap is air, heat transfer over the gap by conduction only

In Figure 37 the temperature evolution in the steel plate 1 mm below the contact surface to the oxide melt has been plotted for the different calculations and for the thermocouple 1 from the experiment. The time 0 s in this figure relates to the arrival of melt in the test container, about 50 s after ignition.
The thermocouple 1 from the experiment shows an increase to about 600 °C in 200 s and then only a slow asymptotic increase to about 630 °C after 600 s. In the calculations 1 and 2, the temperatures are higher than in the experiment right from the beginning. The temperature in calculation 1 rises to about 950 °C after 200 s and then to about 1100 °C after 600 s. In calculation 2 the temperature is even higher than in calculation 1, because this calculation accounts for the released heat during the phase change of the oxide melt from liquid to solid.
In Figure 38 the calculated crust thicknesses of the oxide melt at the contact surface to the steel plate are presented. In calculation 1 the crust thickness after 600 s is about 45 mm and in calculation 2 the crust thickness after 600 s is about 25 mm. So, the crust in calculation 2 is smaller than in calculation 1, which corresponds to the higher temperature in calculation 2 due to the released heat during the phase change of the oxide melt.
In conclusion, the calculations 1 and 2 show, that the temperatures in the steel plate in the experiment should be higher when the oxide melt and the steel plate are in direct contact to each other. From these calculations it can concluded, that the oxide melt and the steel plate were not in good thermal contact during the experiment.

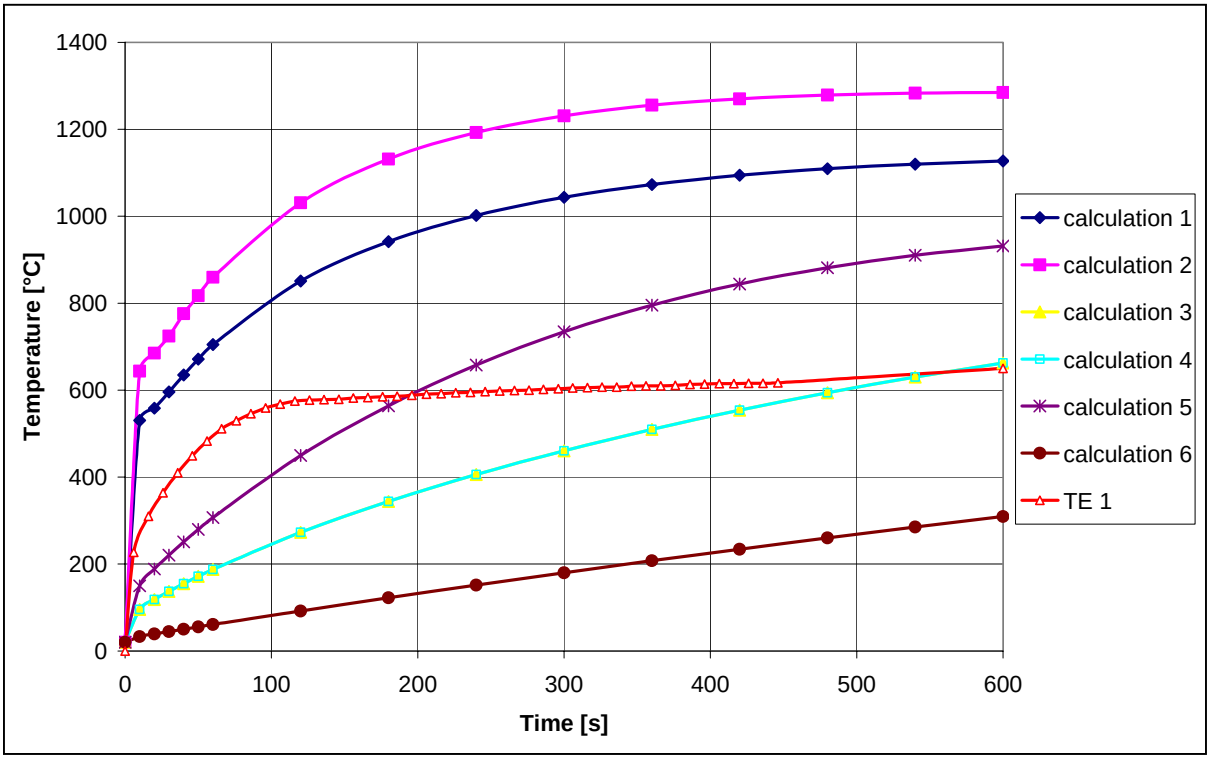

Figure 37: Temperature in the steel plate 1 mm below the contact surface of the oxide melt and the steel plate in the experiment and in the calculations

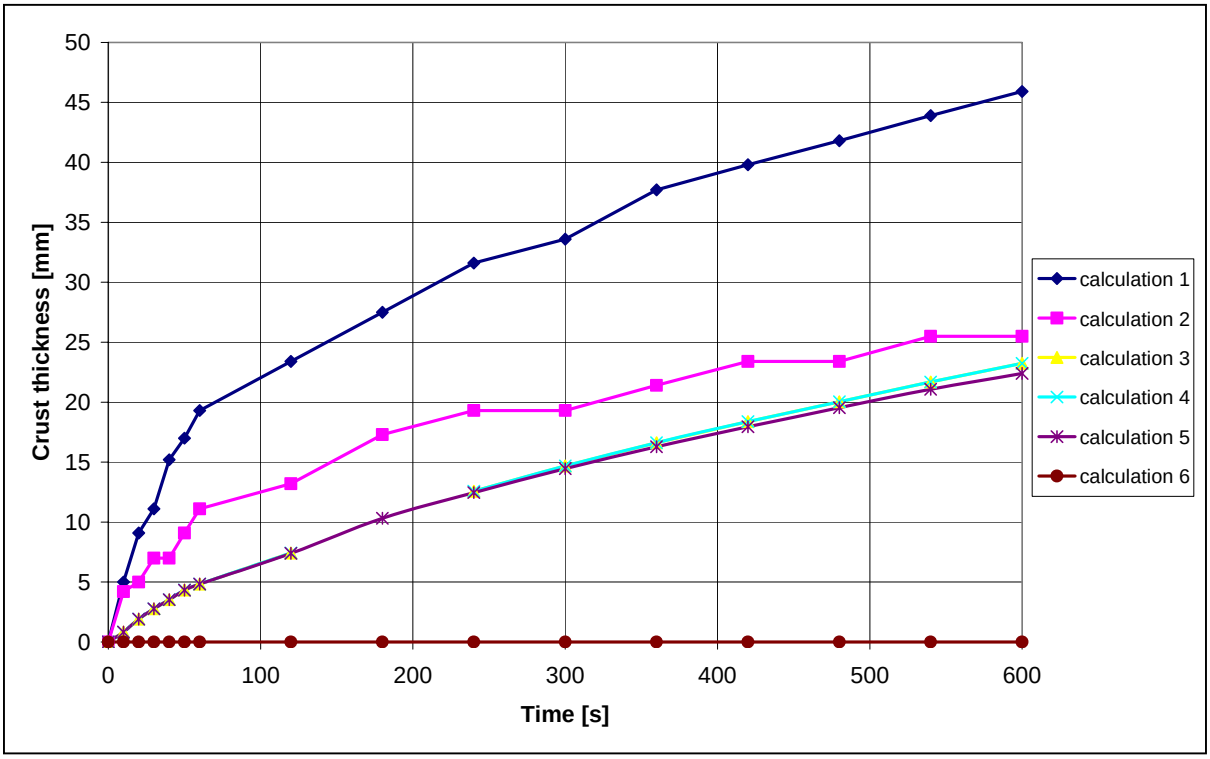

Figure 38: Crust thickness of the oxide melt at the contact surface to the steel plate in the different calculations

For this reason, calculations 3 to 6 assume a gap between the oxide melt and the steel plate. In reality, there was certainly no gap over the total contact surface of the melt to the steel plate, but it can be assumed that there were regions with gaps and regions with direct contact.
In calculation 3 there was a gap of 0.5 mm and in calculation 4 was a gap of 1 mm between the oxide melt and the steel plate. In both calculations there was only heat transfer due to radiation (emissivities see Table 8) over this gap and the gap was defined without a material. The temperature evolution in these two calculations is identical as radiation between parallel plates is independent of their distance, Figure 37. The calculated temperature increases slower than in the experiment, but after 600 s, the temperature rises above the temperature of the experiment. The crust thickness of the oxide melt above the gap is in both calculations about 25 mm after 600 s, Figure 38.
In calculation 5, the calculation 4 was repeated with the same conditions and parameters, except for the emissivitiy of the steel plate, which was increased from 0.35 to 0.6. Due to the higher emissivity, the heat transfer from the oxide melt to the steel plate over the gap was also increased and the temperature in the steel plate rises to about 930 °C after 600 s. Besides, the higher emissivity of the steel plate has no large influence on the crust thickness calculation.
In the last calculation, the 1 mm gap between the oxide melt and the steel plate was defined as a material region (air) and therefore the heat transfer was due to heat conduction only without radiation. In this calculation, the temperature in the steel plate rises very slowly and reaches only a temperature of about 300 °C after 600 s. In this calculation no crust is calculated with HEATING5.

5.3.2 Calculations for the KAPOOL 12 experiment

As in KAPOOL 11 different 1-dimensional HEATING5 calculations have been performed. The first calculations have been performed with the oxide melt and the steel plate in direct contact. Here, the boundary conditions at the bottom of the steel plate have been varied between radiation and no radiation. In the experiment, the bottom of the steel plate was insulated and therefore there was no heat transfer due to radiation to the environment. In the following calculations, a gap has been assumed between the oxide melt and the steel plate. In these calculations, the material of the gap (no material or air) and the boundary conditions at the bottom of the steel plate have been varied.
The material properties of the oxide melt and the steel plate are similar to those in KAPOOL 11, except for the solidus temperature of the oxide melt and the thickness of the steel plate. The solidus temperature of the oxide melt is lower as in KAPOOL 11 due to the addition of calcia to the melt. The material properties, which have been used in the calculations, are summarised in Table 11 and the material properties of air are the same as in KAPOOL 11, Table 11 and Table 9.

Table 11: Material properties for the HEATING5 calculations (KAPOOL 12)

	oxide melt	**steel plate**	**air**
initial temperature T_0	1900 °C	20 °C	
solidus temperature T_s	1395 °C	1450 °C	
heat conductivity λ	5.4 W/mK	45 W/mK	0.026 W/mK
density ρ	2917 kg/m^3	7900 kg/m^3	s. Table 9
specific heat c_p	1400 J/kgK	452 J/kgK	1005 J/kgK
emissivity ε	0.9	0.35	
latent heat	1068000 J/kg	277000 J/kg	
height	250 mm	15 mm	1 mm

5.3.2.1 Modelling of the calculations

The modelling of the calculations with the oxide melt in direct contact with the steel plate includes again 2 regions, left part of Figure 39. The steel plate has been subdivided into 15 grid lines with a constant distance of 1 mm between each grid line. The oxide melt was subdivided in a grid with different distances between the grid lines. Near the contact surface between the oxide melt and the steel plate a fine 0.2 mm grid with 25 nodes was modelled. Above, 22 nodes with a distance of 2 mm and then 20 nodes with a distance of 5 mm were modelled. The whole modelling consists of 84 nodes.

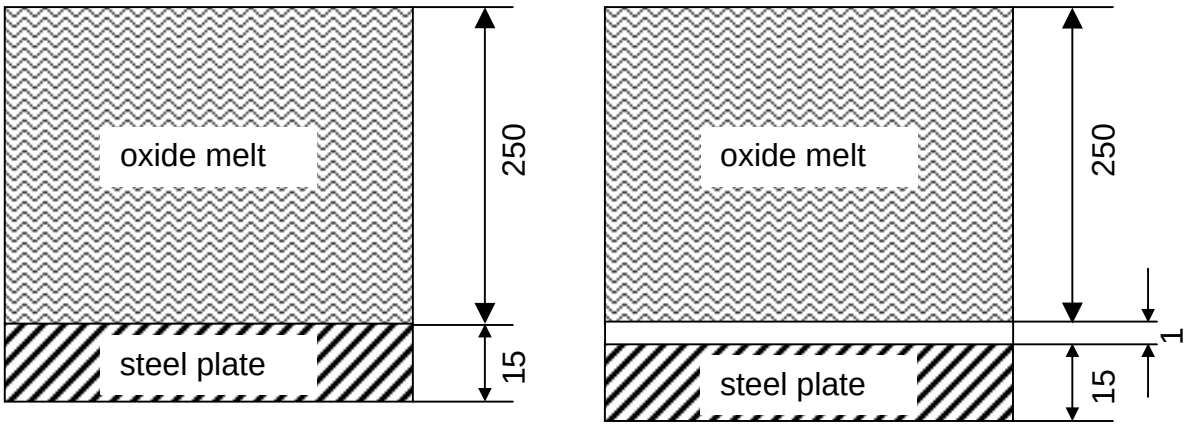

Figure 39: Modelling of the calculations of the KAPOOL 12 experiment

For the calculations with a gap between the oxide melt and the steel plate 5 additional nodes for this gap have been modelled.

5.3.2.2 Results of the calculations

In Table 12 the different calculations, which have been performed for the experiment KAPOOL 12, are summarised. The first two calculations (calculation 1 and 2) have been performed with the oxide melt and the steel plate in direct contact. The only difference in the calculations is, that in the second calculation the bottom of the steel plate is insulated and therefore there is no heat transfer due to radiation to the environment. In the experiment, the bottom of the steel plate was insulated, but both calculations have been performed to compare the effect of insulating the bottom of the steel plate.

Table 12: Summary of the HEATING5 calculations for KAPOOL 12

calculation 1	Calculation with oxide melt and steel plate in direct contact with phase change and radiation at the top of the melt and at the bottom of the steel plate
calculation 2	Calculation with oxide melt and steel plate in direct contact with phase change and radiation at the top of the melt and no radiation at the bottom of the steel plate
calculation 3	Calculation with a gap of 1 mm between the oxide melt and the steel plate; radiation over the gap; radiation at the top of the melt and at the bottom of the steel plate
calculation 4	Calculation with a gap of 1 mm between the oxide melt and the steel plate; radiation over the gap; radiation at the top of the melt and no radiation at the bottom of the steel plate
calculation 5	Calculation with a gap (air) of 1 mm between the oxide melt and the steel plate; heat conduction over the gap; radiation at the top of the melt and radiation at the bottom of the steel plate
calculation 6	Calculation with a gap (air) of 1 mm between the oxide melt and the steel plate; heat conduction over the gap; radiation at the top of the melt and no radiation at the bottom of the steel plate

In Figure 40 the temperature evolution at the top of the steel plate has been plotted for the different calculations and for the thermocouple 1 from the experiment. The time 0 s in this figure relates to the arrival of melt in the test container, which is about 60 s after ignition of the melt.
The thermocouple 1 from the experiment shows a temperature increase to about 930 °C after 580 s. In the calculation 1 and 2, the temperatures are higher than in the experiment. In calculation 1 with radiation at the bottom of the steel plate a maximum temperature of about 1230 °C after 600 s is reached and in calculation 2 with a insulated bottom of the steel plate, even 1400 °C are reached. So, the insulation of the bottom of the steel plate leads to a 170 °C higher temperature, but the melting temperature of the steel is not yet reached in the calculation. In Figure 41 the calculated crust thicknesses of the oxide melt at the contact surface to the steel plate are plotted. In calculation 1 the crust thickness rises continuously to about 9 mm after 600 s. The evolution of the crust thickness in calculation 2 up to 50 s is identical to that in calculation 1, but then the crust thickness decreases continuously to 0.1 mm after 600 s.
As in KAPOOL 11 the calculations 1 and 2 show that the temperatures in the steel plate in the experiment should be higher if the oxide melt and the steel plate are in direct contact to each other over the total contact surface.

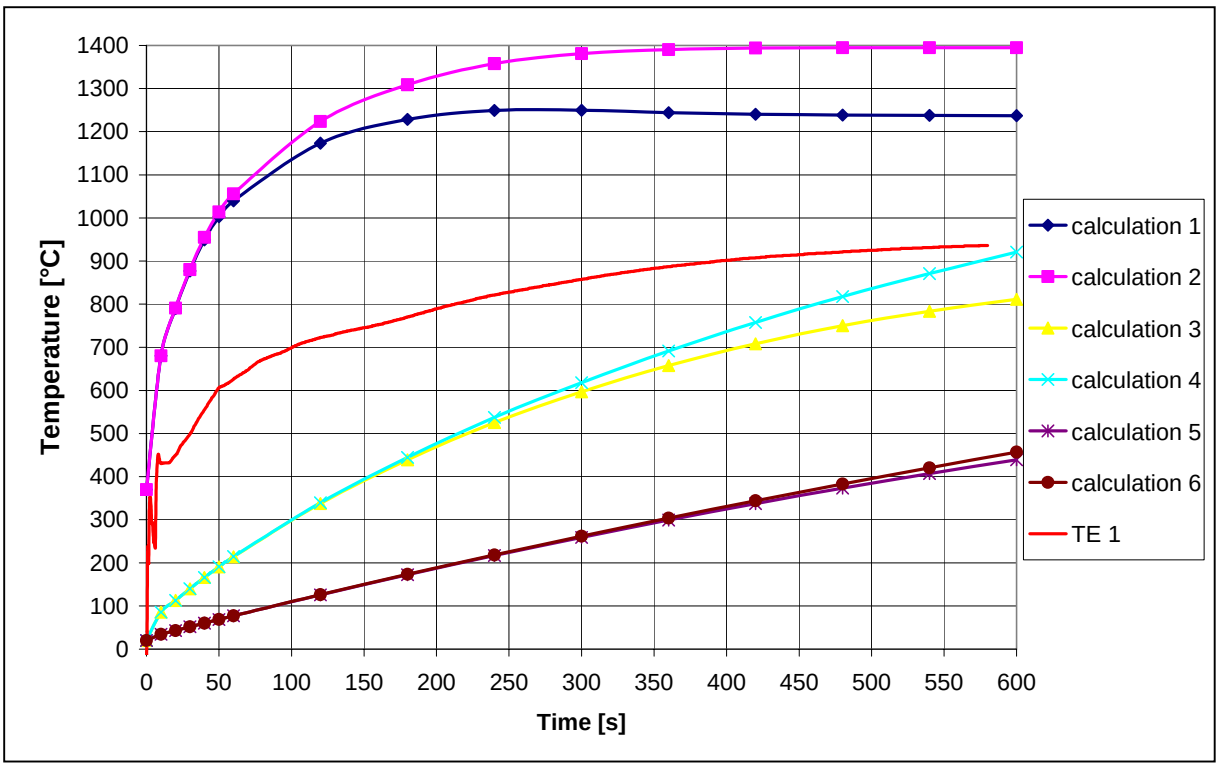

Figure 40: Temperature at the top of the steel plate in the experiment and in the calculations for KAPOOL 12

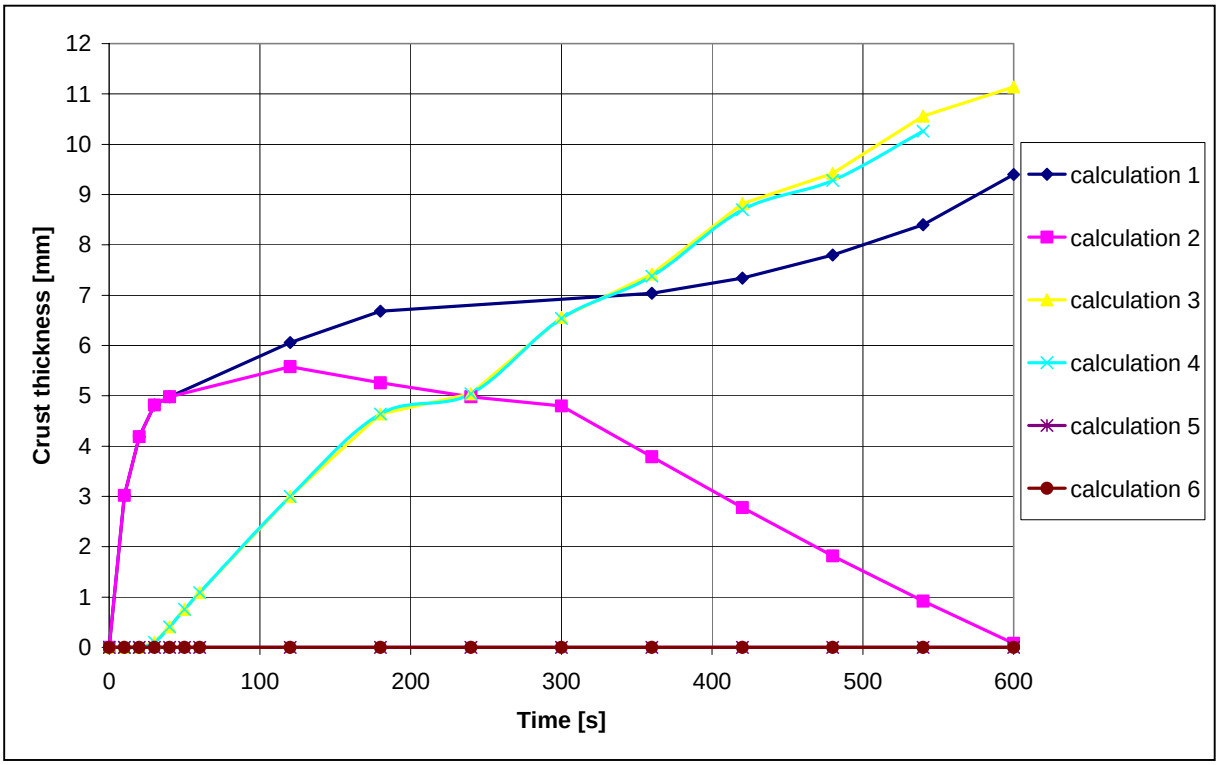

Figure 41: Crust thickness of the oxide melt at the contact surface to the steel plate in the different calculations for KAPOOL 12

Certainly, the 1-dimensional calculations do not account for lateral thermal heat losses to the environment, but anyhow, it can be concluded, that the oxide melt and the steel plate are not in good thermal contact during the experiment.
Therefore, more calculations have been performed, assuming a gap between the oxide melt and the steel plate. In calculation 3 and 4 there was a 1 mm gap between the oxide melt and the steel plate and the heat transfer over this gap was only due to radiation (no material was defined in this gap). In calculation 4 the bottom of the steel plate was insulated. For this reason there was no heat transfer to the environment due to radiation. The temperature evolution in these two calculations is identical up to about 200 s and after that the temperature in calculation 4 arises above the temperature in calculation 3. After 600 s, the temperature in calculation 3 is about 800 °C and in calculation 4 about 920 °C. The crust thickness evolution is identical to about 400 s and then the crust thickness in calculation 3 arises slightly more than in calculation 4. The end values for the crust thickness after 540 s are 10.2 mm for calculation 3 and 10.5 mm for calculation 4.
In calculation 5 and 6 the 1 mm gap between the oxide melt and the steel plate was defined as a material region filled with air. In these calculations the heat transfer from the oxide melt to the steel plate is only due to heat conduction. In calculation 6 the bottom of the steel plate was again insulated. Here the temperature at the top of the steel plate rises very slowly and the temperature after 600 s is about 440 °C for calculation 5 and 460 °C for calculation 6. In both calculations no crusts are calculated with HEATING5.

5.3.3 Conclusions of the HEATING5 calculations for KAPOOL 11 and 12

The calculations with HEATING5, which have been performed for the experiments KAPOOL 11 and KAPOOL 12, show that it is nearly impossible to recalculate exactly the complex phenomena in these experiments. But the calculations give an indication that after the first direct contact of the oxide melt and the steel plate heat transfer is reduced due to crust formation in the oxide melt. This crust progressively looses the contact with the steel plate during the further course of the experiment, so that the interfacial heat transfer is reduced by the existence of local gaps between crust and steel surface, restricting heat transfer mainly to radiation.

6 Interaction of an oxide melt with an aluminium plate (KAPOOL 13 and 15-17)

In the previous experiments with high temperature oxide melts, melt-through of a steel plate could not be achieved. This is due to the relatively low overheat of the simulated corium melt, referred to the melting temperature of the steel, and due to the transient character of the experiments, as no decay heat is generated in the melt.
To overcome the problem with available experimental installations, a further test sequence was performed, which uses an aluminium plate with a melting temperature of 660 °C instead of steel.
The setup of the subsequent 4 tests and their test parameters were different. Therefore each test is described in detail in the following chapters. In all tests the same mass of about 190 kg thermite and 66 kg CaO has been used to produce 150 kg of oxide melt, with liquidus and solidus temperatures of 1500 °C and 1395 °C, respectively.

6.1 The experiment KAPOOL 13

6.1.1 Setup of KAPOOL 13

In KAPOOL 13 the dimensions of the test container were identical to KAPOOL 12, Figure 42. The container was lined with a high-temperature ceramic insulation (Sitalcast). The aluminium plate of a thickness of 20 mm was fixed at the bottom of the container. The total diameter of the plate was ∅ 240 mm and the contact surface of the aluminium plate with the oxide melt was ∅ 200 mm.

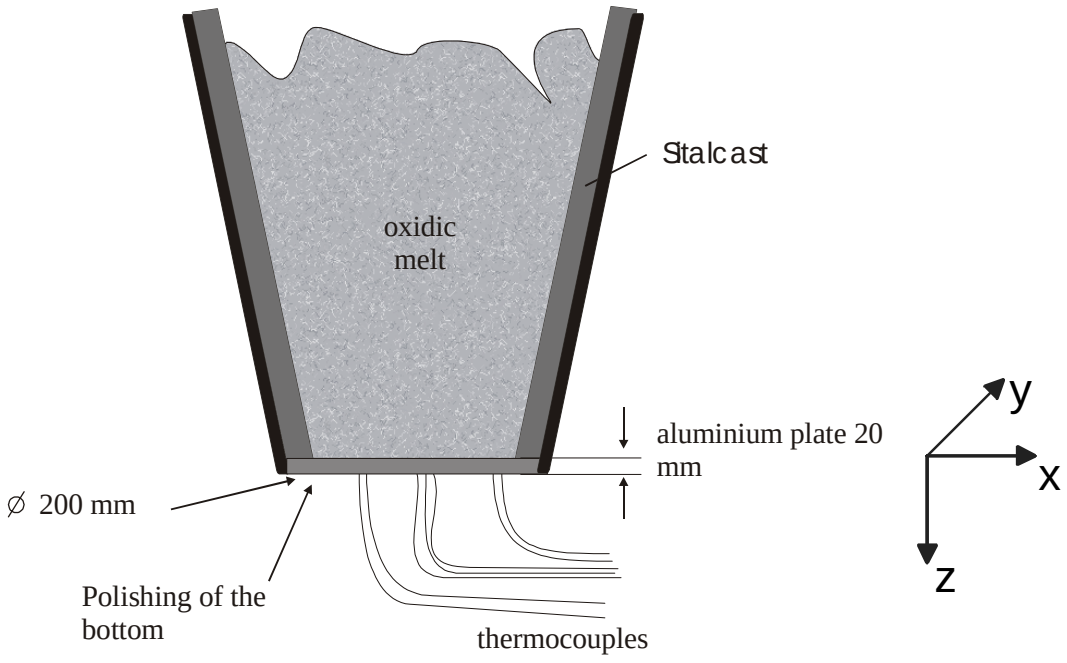

Figure 42: Setup of the test container in KAPOOL 13 and coordinate system

The bottom of the aluminium plate has been polished to reduce the downward heat transfer by radiation. The emissivity of a polished aluminium surface is low with ε=0.06 and therefore the heat losses due to radiation should be relatively low. In this experiment the aluminium plate was in good thermal contact with the outer steel structure of the container.

15 K-type thermocouples have been installed inside the aluminium plate at different vertical and horizontal positions. Five thermocouples were positioned at the top surface, five in the midplane (10 mm from the top surface) and five 18 mm below the top surface of the aluminium plate, Table 13.
Time 0 s is defined by the ignition of the thermite powder in the reaction crucible.

Table 13: Positions of NiCr-Ni thermocouples in the aluminium plate of KAPOOL 13

T/C #	Position x [mm]	Position y [mm]	Vertical position z [mm]
1	0	0	0
2	0	-50	0
3	-50	0	0
4	0	50	0
5	50	0	0
6	0	5	10
7	0	-55	10
8	-55	0	10
9	0	55	10
10	55	0	10
11	0	-5	18
12	0	-45	18
13	-45	0	18
14	0	45	18
15	45	0	18

6.1.2 Experimental Results of KAPOOL 13

6.1.2.1 Mass measurements in KAPOOL 13

The release of the melt from the reaction crucible started about 34 s after ignition. After separation of the metallic part of the thermite melt, only the oxidic part of the melt was transferred into the KAPOOL test container. Figure 43 shows the transient mass loss of the reaction crucible and the transient mass flow of oxide melt into the test container. The measured mass of the reaction crucible is rising during the thermite reaction due to a partial malfunction of the weighing system. Therefore this measurement gives only qualitative information. The weighing cells of the test container detect the first arrival of oxide melt 54.4 s after ignition and 29 s later 92 kg of oxide melt were gathered. During the test about 15 kg of oxide melt were ejected from the test container due to the vigorous agitation of the pool during the insertion of the W-Re thermocouples into the melt pool.

6.1.2.2 Oxide melt temperatures in KAPOOL 13

Nine temperature measurements of the melt have been performed, Figure 44. The temperature was 1850 °C in the beginning and dropped to about 1530 °C at 150 s after ignition, which is near the liquidus temperature of the melt. The last two measurements seem to be to low. The reason for this could be that the melt is near the liquidus temperature and therefore the oxide melt formed a crust at the tip of the thermocouple and the accuracy of the measurement decreases.

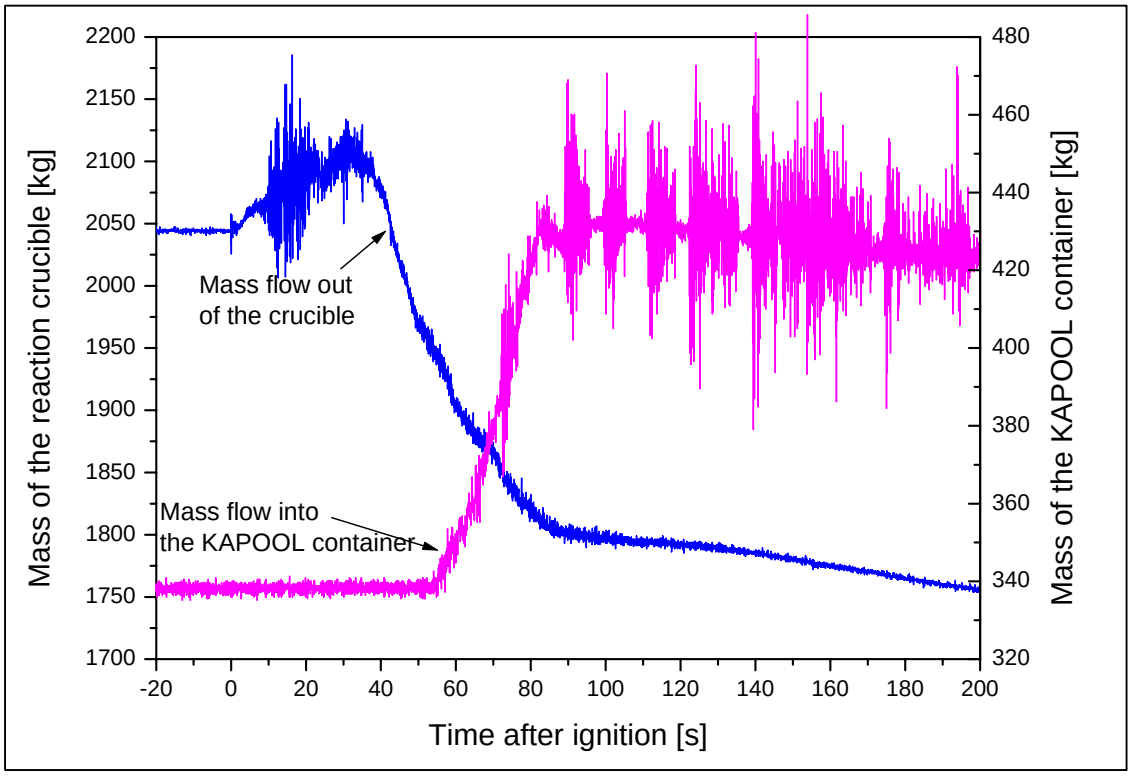

Figure 43: Mass of the reaction crucible and of the test container in KAPOOL 13

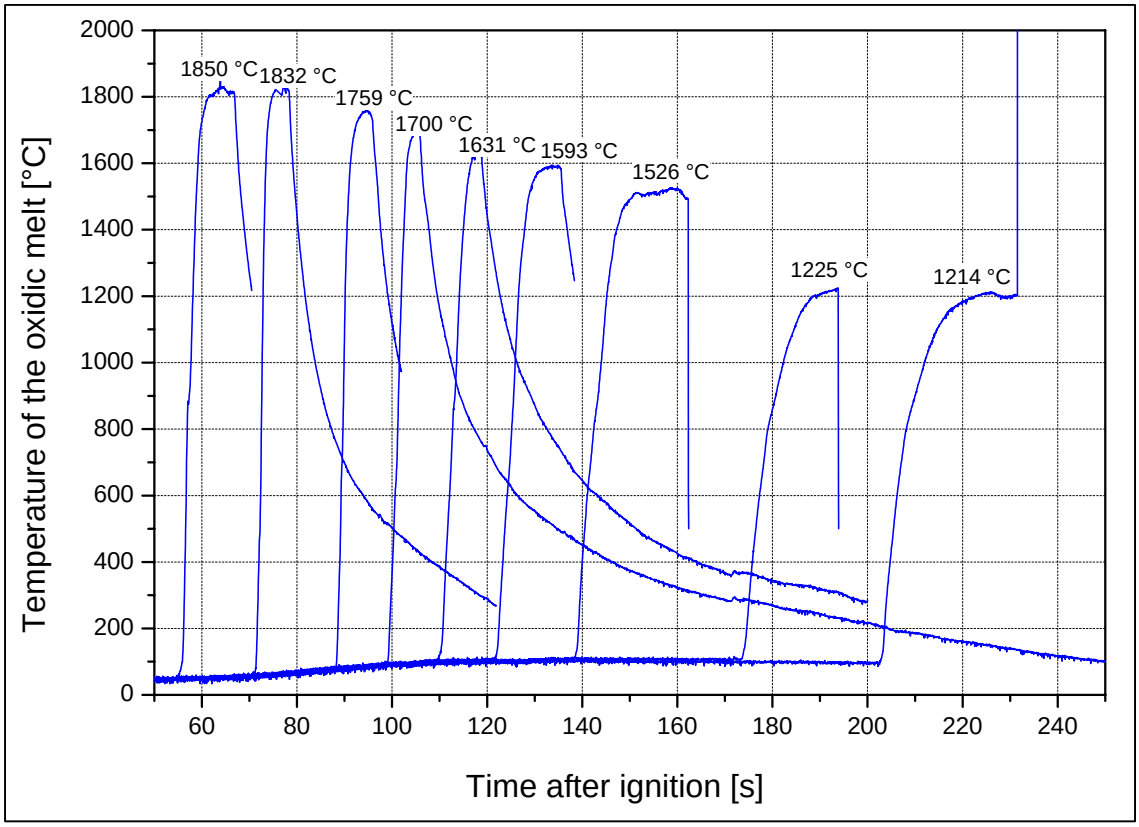

Figure 44: Measured temperature of the oxide melt in KAPOOL 13

6.1.2.3 Temperature readings of NiCr-Ni thermocouples in the aluminium plate

The temperature recordings in the aluminium plate showed that within 100 s after first contact of the oxide melt with the aluminium plate a maximum temperature of about 540 °C has been recorded at the top thermocouple, Figure 45. The aluminium melting temperature of about 660 °C has however not been reached and the plate was not penetrated. The temperatures at different vertical positions in the plate are very close together due to the high thermal conductivity of the aluminium plate (220 W/mK) and the low downward heat losses.

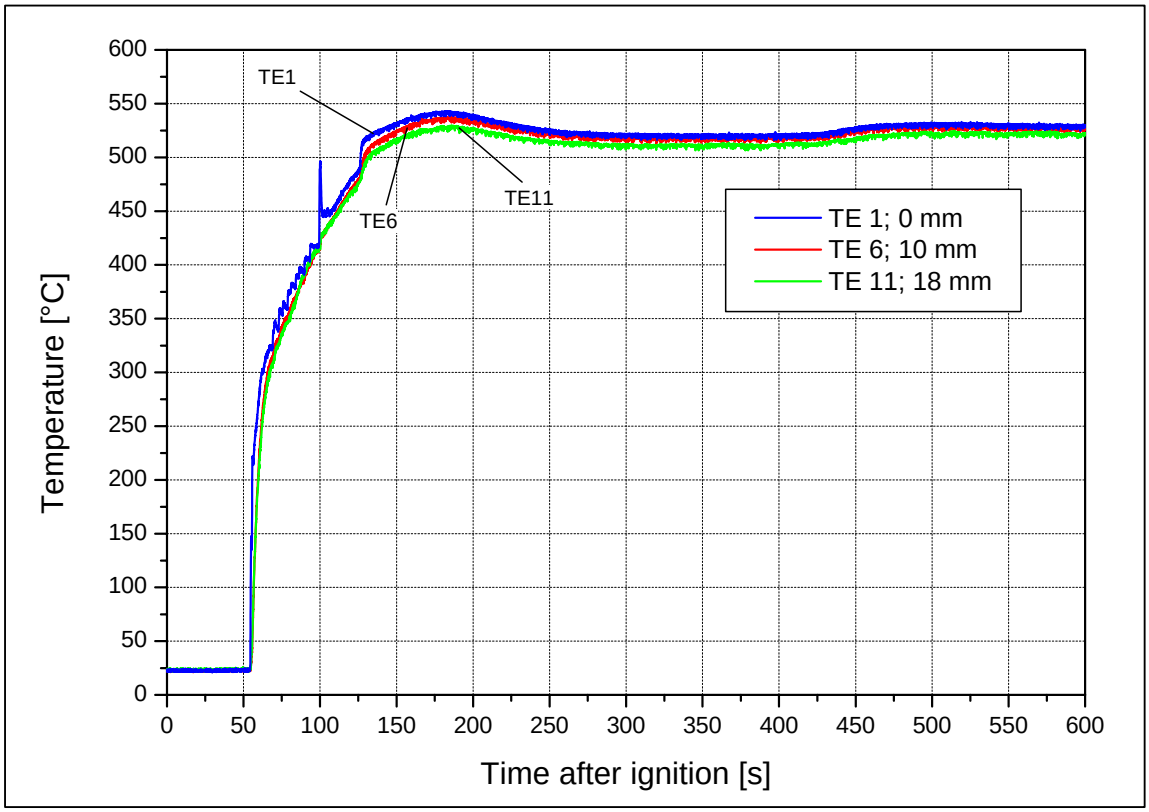

Figure 45: Transient temperature measurements in the center of the aluminium plate in KAPOOL 13

6.1.3 Post test examinations in KAPOOL 13

As in the tests KAPOOL 11 and 12 it is possible to calculate an initial contact temperature between the aluminium plate and the oxide melt. The material properties for the oxide melt are the same as in KAPOOL 11 and 12, but the material properties of the aluminium plate are different from the steel plate, s. Table 14. The initial oxide melt temperature is about 1900 °C.

Due to the higher thermal conductivity and the higher specific heat of aluminium in comparison to steel, the thermal penetration coefficient b is also higher (equations s. chapter 5.1.3). This higher value leads to a lower initial contact temperature of aluminium with the oxide melt as in KAPOOL 11 and 12 for a steel plate. The calculated initial contact temperature is in the range of 320 °C and is therefore significantly lower than the melting temperature of aluminium.

This low initial contact temperature indicates the formation of a solid oxide crust at the very beginning of the test. The thermal contact between the crust and the plate

may not be ideal, so thermal resistances must be assumed when modelling the problem.

Table 14: Material properties and calculation result

	Aluminium plate	**Oxide melt**
λ [W/mK]	220	~5,4
ρ [kg/m^3]	2702	2917
c_p [J/kgK]	1047	1400
T_1 [°C]	20	-
T_2 [°C]	-	1900
a [m^2/s]	7.78*10^{-5}	1.32*10^{-6}
b [Ws$^{1/2}$/Km^2]	24948	4696
T_i [°C]	**318**	

In Figure 46 the contact surfaces of the aluminium plate and the oxide melt after the test are shown. The aluminium plate shows no indication of an ablation by the oxide melt. The oxide crust is rough compared to the aluminium surface, which means that the thermal contact was not intimate. Heat transfer was therefore partly conductive, partly by radiation.

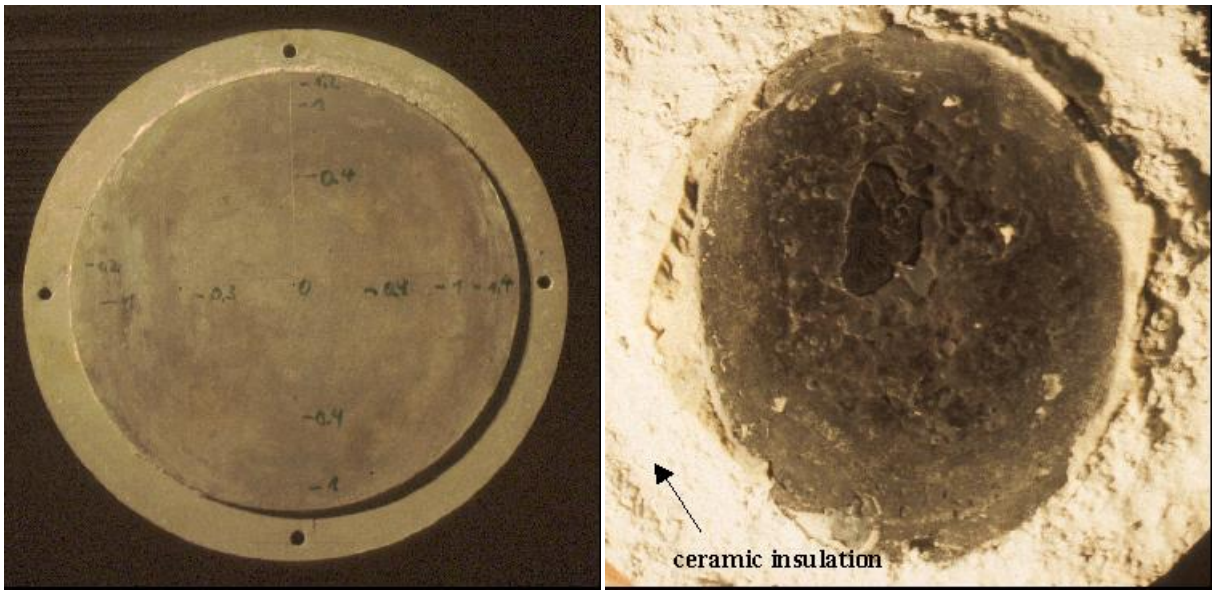

Figure 46: Contact surface between the aluminium plate (left) and the oxide melt (right)

Post-test surface profiles have been measured, they show different vaultings for the oxide crust and the aluminium plate, the crust having a larger vaulting than the plate, Figure 47. Figure 47 shows also a gap of minimum 1.5 mm between the aluminium plate and the oxide melt after the test. It is not clear, at which time this gap was formed and if this gap already existed during the test.
But nevertheless, due the the very uneven surface of the oxide melt, it can be concluded that gaps between the oxide crust and the aluminium plate existed during the test.

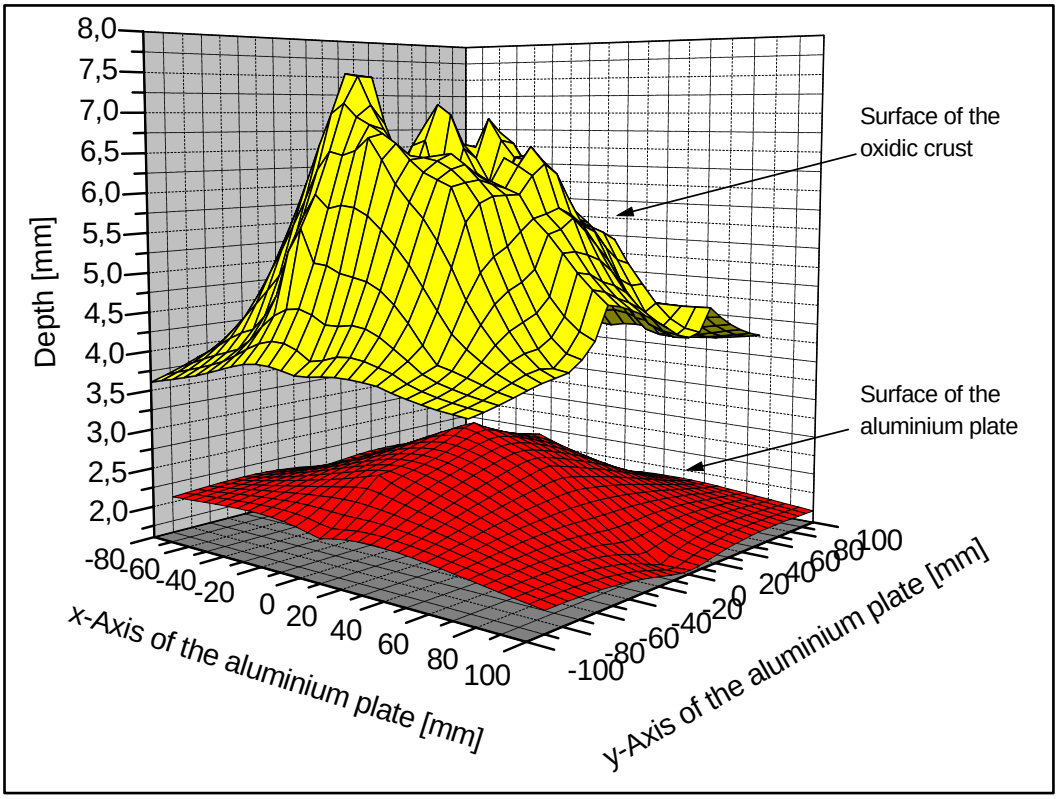

Figure 47: Surface profile of the melt and the aluminium plate at the contact surface for the test KAPOOL 13

In addition to the above described phenomena of crust and gap formation, in this test the lateral heat losses from the aluminium plate to the outer steel structures of the test container were relatively large. This could also be a reason for the vaulting of the aluminium plate, subsequent gap formation and hence high thermal resistances.
In summary there were two parallel effects, which may have contributed to the gap formation of the melt and the non-melting of the aluminium plate. But in conclusion, the formation of gaps was believed to be the main reason that the aluminium plate was not penetrated by the oxide melt.

6.1.4 Calculations of the KAPOOL 13 experiment with HEATING5

For the experiment KAPOOL 13 only three different 1-dimensional HEATING5 calculations have been performed. In the first calculation (calculation 1), the oxide melt is in direct contact with the aluminium plate. In the second (calculation 2) and the third calculation (calculation 3) a gap was modelled between the oxide melt and the steel plate. In the second calculation this gap was modelled without a material (heat transfer by radiation only) and in the third calculation this gap was modelled with the material air (heat transfer by conduction only). The material properties of the oxide melt and the aluminium plate are summarised in Table 15.

Table 15: Material properties for the HEATING5 calculations in KAPOOL 13

	oxide melt	**aluminium plate**	**air**
initial temperature T_0	1900 °C	20 °C	
solidus temperature T_s	1395 °C	660 °C	
heat conductivity λ	5.4 W/mK	220 W/mK	0,026 W/mK
density ρ	2917 kg/m^3	2702 kg/m^3	s. Table 9
specific heat c_p	1400 J/kgK	1047 J/kgK	1005 J/kgK
emissivity ε	0.9	0.06	
latent heat	1068000 J/kg	397000 J/kg	
height	400 mm	20 mm	1 mm

6.1.4.1 Modelling of the calculations

The modelling of the calculations with the oxide melt in direct contact with the aluminium plate includes 2 regions, left part of Figure 48. The aluminium plate is subdivided into 20 grid lines with a constant distance of 1 mm between each grid line. The oxide melt was subdivided in a grid with different distances between the grid lines. Near the contact surface between the oxide melt and the steel plate a fine 0.5 mm grid with 20 nodes was modelled. Above, 25 nodes with a distance of 2 mm and then 34 nodes with a distance of 10 mm were modelled. The whole modelling consists of 100 nodes.

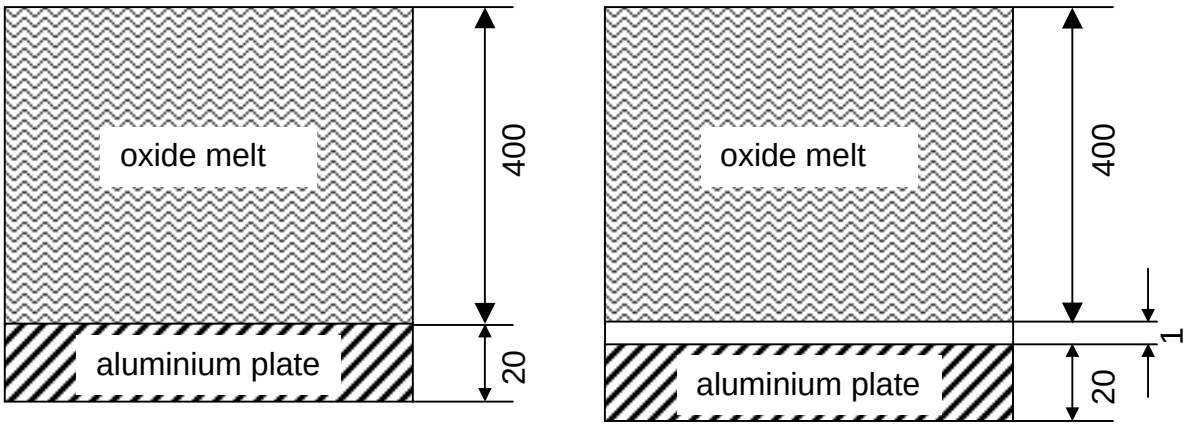

Figure 48: Modelling of the calculations of the KAPOOL 13 experiment

For the calculations with a gap between the oxide melt and the steel plate 2 additional nodes for this gap have been modelled (right part of Figure 48).

6.1.4.2 Results of the calculations

In Figure 49 the temperature at the top of the aluminium plate for the different calculations and for the thermocouple 1 from the experiment is shown. The time 0 s in this figure relates to the arrival of melt in the test container, which is about 55 s after ignition of the melt.

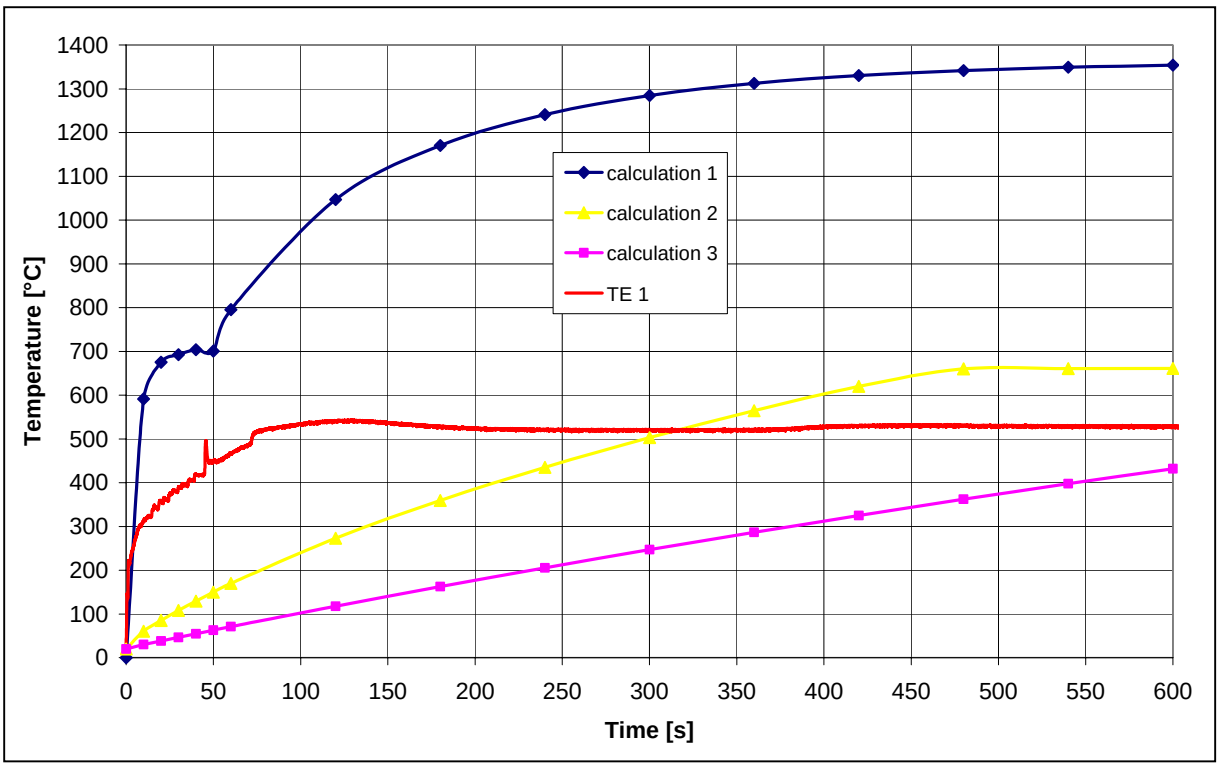

Figure 49: Temperature at the top of the aluminium plate in the experiment and in the calculations for KAPOOL 13

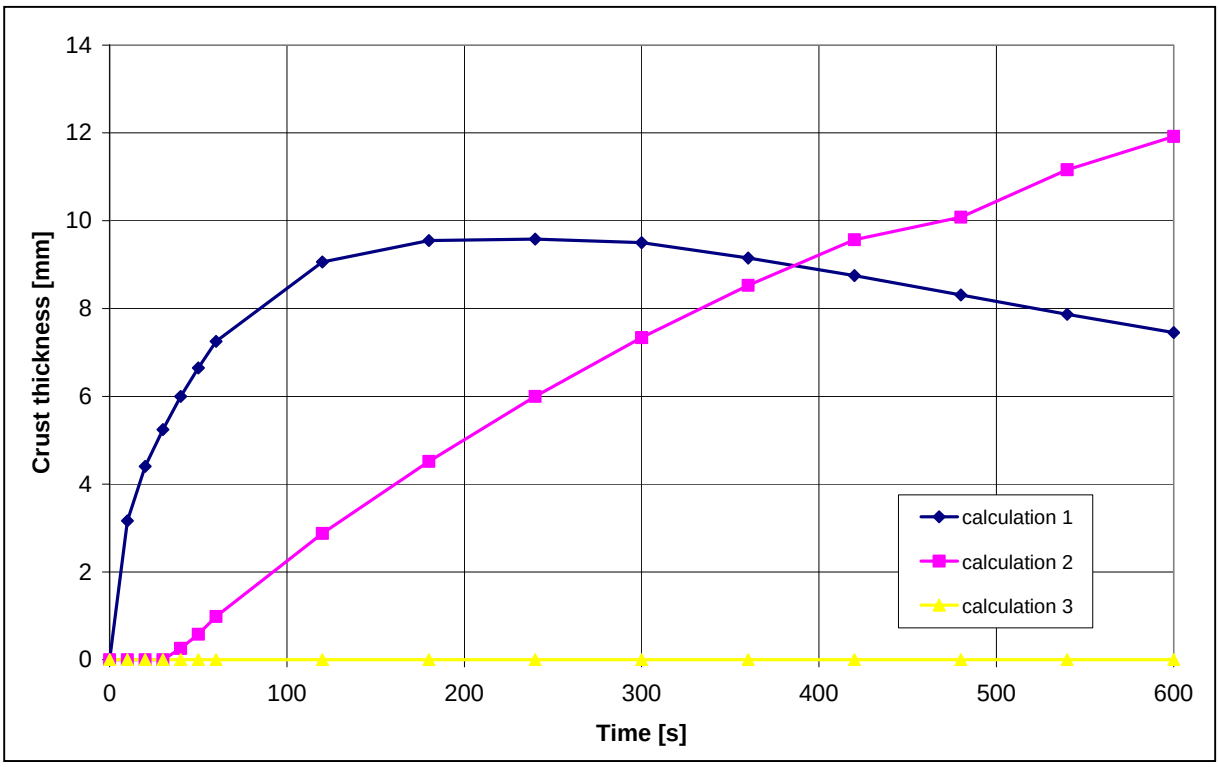

Figure 50: Crust thickness of the oxide melt at the contact surface to the aluminium plate in the different calculations for KAPOOL 13

The thermocouple 1 in the experiment shows a steep temperature increase to about 300 °C within 10 s. At this time there is a break in the temperature increase and the temperature rises much slower to about 540 °C after 100 s. In calculation 1 with the oxide melt and the aluminium plate in direct contact, the temperature increases very fast to about 600 s within 10 s. After exceeding the melting temperature of 660 °C, there is a short temperature plateau at about 700 °C for about 30 s. The aluminium plate is completely melted after about 45 s. In the calculation, the temperature at the surface of the aluminium plate rises further to about 1350 °C after 600 s.
In comparison, the temperature curve of calculation 1 and the temperature curve of the thermocouple of the experiment are identical up to about 8 s. This indicates that up to this time, the oxide melt and the aluminium plate were in good thermal contact.
The temperature in calculation 2 with a gap of 1 mm between the oxide melt and the aluminium plate (only radiation over the gap) increases slower as in calculation 1 and also as the thermocouple 1 from the experiment. But after 300 s the temperature increases above the temperature in the experiment and after about 480 s the melting temperature of aluminium with 660 °C is reached. The temperature in calculation 3 with a gap of 1 mm (air) between the oxide melt and the aluminium plate (heat conduction over the gap) increases slower as in calculation 2 and therefore much slower as in calculation 1 and as in the experiment. After 600 s a temperature of about 430 °C is reached.
In Figure 50 the calculated crust thicknesses of the oxide melt at the contact surface to the aluminium plate are plotted. In calculation 1 the crust thickness rises to about 6 mm after 40 s. At this time, the aluminium plate is nearly completely melted and would fail.
In calculation 2 the crust starts to grow after 30 s and then the thickness of the crust increases continuously over the whole calculation time. The crust thickness is about 12 mm after 600 s. In calculation 3 no crust is calculated over the total calculation time.

6.1.4.3 Conclusions from the HEATING5 calculations for KAPOOL 13

The calculations with the HEATING5 code for the experiment KAPOOL 13 approve the observations, which have been made during the analysis of the experiment. It can be seen, that up to about 8 s, the thermocouple 1 in the experiment shows the identical temperature increase as in the calculation 1 with an ideal contact between the oxide melt and the steel plate. At this time a crust of about 3 mm is calculated. After this time, the temperature in the experiment increases slower as in the calculation and from this it can be concluded, that the crust of the oxide melt loses partially the contact to the aluminium plate and a gap is formed. The heat transfer from the oxide melt to the aluminium plate is then partly by conduction and partly by radiation, so that the reduced heat transfer is not sufficient to melt the aluminium plate. In addition, a substantial heat transfer from the aluminium plate to the conical steel container may have reduced the temperature increase.

6.2 The experiment KAPOOL 15

6.2.1 Setup of KAPOOL 15

Compared to KAPOOL 13, several experimental parameters have been changed to conduct the test KAPOOL 15. The container had a cylindrical shape instead of a conical shape, Figure 51.

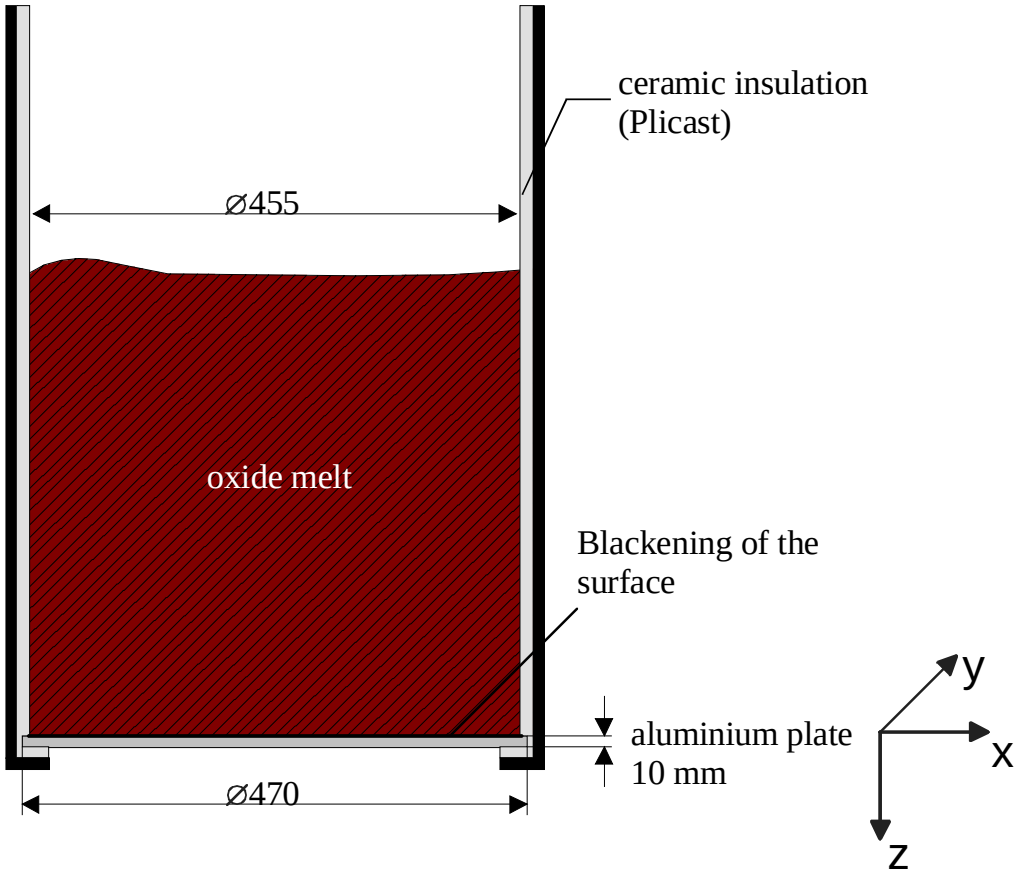

Figure 51: Setup of the test container in KAPOOL 15 and coordinate system

The aluminium plate had a thickness of 10 mm and a total diameter of ∅ 470 mm. The contact surface of the aluminium plate with the oxide melt was ∅ 455 mm. In this test the aluminium plate had no contact to the outer steel structures due to ceramic insulation rings around the plate and so lateral heat losses were widely eliminated. The top surface of the aluminium plate has been blackened with a high temperature coating to increase the heat transfer by radiation across the gaps that could exist between the oxide crust and the plate. The polishing of the bottom of the aluminium plate was abandoned, because the difference between the emissivity of polished and unpolished aluminium surfaces is relatively small (ε = 0.04 for polished aluminium and ε =0.07 for unpolished aluminium).
30 K-type thermocouples have been installed inside the aluminium plate at different vertical and horizontal positions, Table 16. Four thermocouples were positioned 3 mm above the top surface, 13 at the top surface and 13 thermocouples 8 mm below the top surface of the aluminium plate.
Time 0 s is defined by the ignition of the thermite powder in the reaction crucible.

Table 16: Positions of NiCr-Ni thermocouples in the aluminium plate of KAPOOL 15

T/C #	Position x [mm]	Position y [mm]	Vertical position z [mm]
1	0	0	0
2	56,25		0
3	112.5	0	0
4	168.75	0	0
5	0	56.25	0
6	0	112.5	0
7	0	168.75	0
8	-56.25	0	0
9	-112.5	0	0
10	-168.75	0	0
11	0	-56.25	0
12	0	-112.5	0
13	0	-168.75	0
14	0	0	-8
15	56.25	0	-8
16	112.5	0	-8
17	168.75	0	-8
18	0	56.25	-8
19	0	112.5	-8
20	0	168.75	-8
21	-56.25	0	-8
22	-112.5	0	-8
23	-168.75	0	-8
24	0	-56.25	-8
25	0	-112.5	-8
26	0	-168.75	-8
27	0	0	+3
28	112.5	0	+3
29	-56.25	-97.43	+3
30	-56.25	97.43	+3

6.2.2 Experimental Results of KAPOOL 15

6.2.2.1 Mass measurements in KAPOOL 15

The release of the melt from the reaction crucible started about 39 s after ignition. Figure 52 shows the transient mass loss of the reaction crucible and the transient mass flow of oxide melt into the test container. The pouring of oxide melt into the test container started 60 s after the ignition. The melt jet from the spout hit first the cylindrical wall of the test container, flowed down and reached the aluminium plate on one side. 10 s after the beginning of pouring a first thin melt jet was detected under the aluminium plate. At this time the melt height in the container was about 13 cm and about 60 kg of melt were gathered in the container. The total pouring time of the oxide melt into the test container was 30 s and in total about 150 kg of oxide melt flowed into the container.

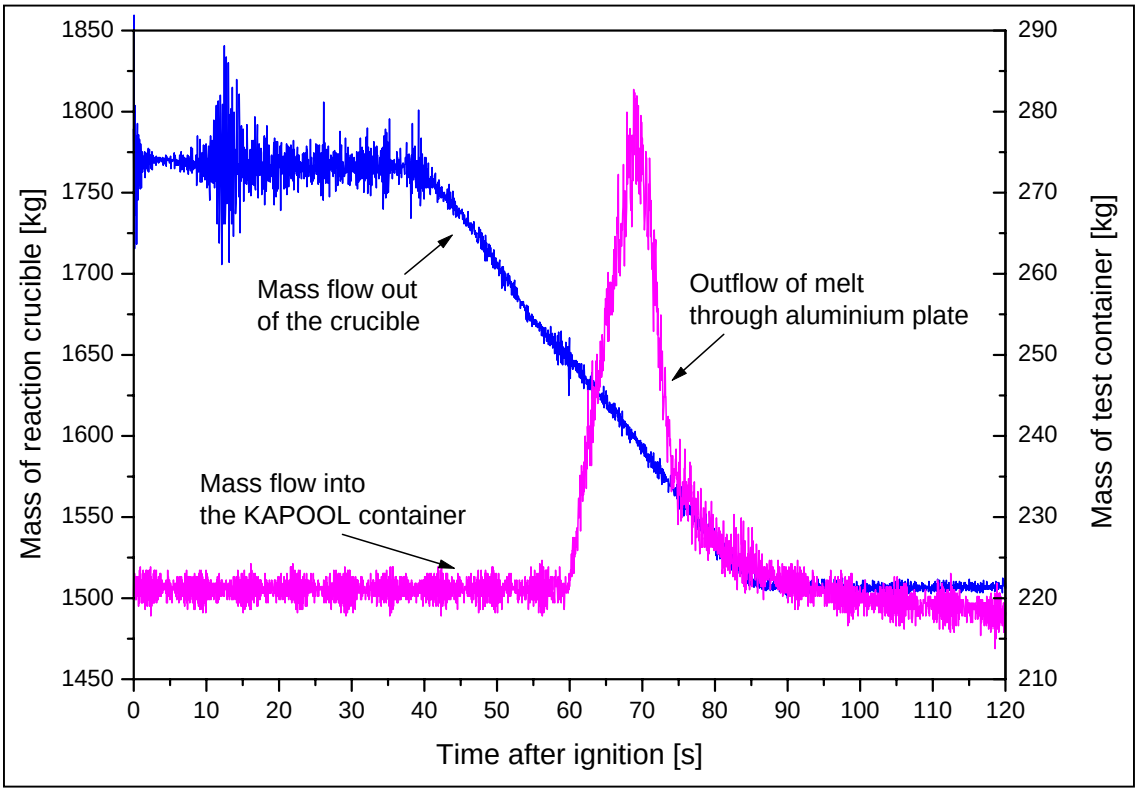

Figure 52: Mass of the reaction crucible and of the test container in KAPOOL 15

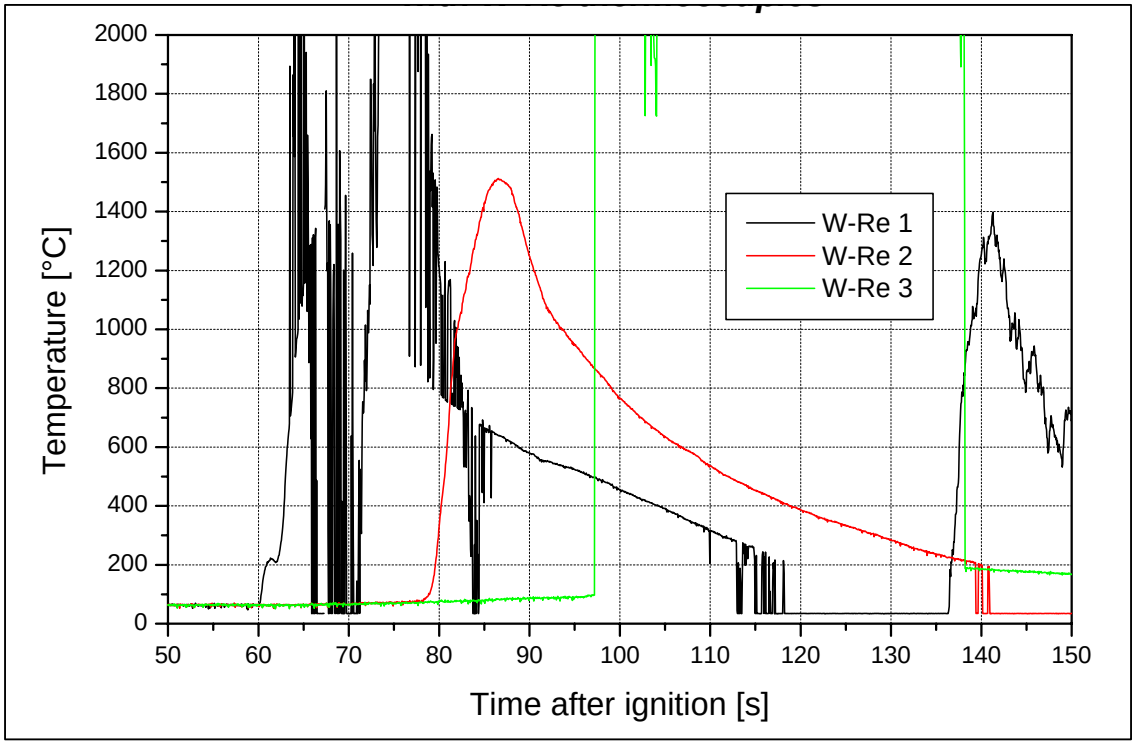

Figure 53: Measured temperature of the oxide melt in KAPOOL 15

6.2.2.2 Oxide melt temperatures in KAPOOL 15

3 W-Re thermocouples have been used to measure the temperature of the oxide melt, Figure 53. The first thermocouple was immediately destroyed after contact with the melt, which was flowing into the KAPOOL container. The second thermocouple was immersed 75 s after ignition into the test container, but at this time the aluminium plate was already destroyed and the melt was flowing out of the test container. Therefore the thermocouple was not immersed into an oxide melt pool and the melt was only flowing along the thermocouple. The measured temperature was about 1500 °C, but this value is probably not the correct melt temperature, which should have been higher. The third thermocouple was immersed about 97 s after ignition but at this time the melt pouring was already finished.
In this test there was no correct temperature measurement of the oxide melt, but it is assumed, that the initial melt temperature is comparable to the earlier experiments KAPOOL 12 and 13, which is close to 1900 °C.

6.2.2.3 Temperature readings of NiCr-Ni thermocouples in the aluminium plate

The thermocouples showed all a very similar behaviour. The temperature was rising up to about 660 °C and then the thermocouples were destroyed at slightly different times, Figure 54. From the failure times of the thermocouples it was possible to determine, that the erosion of the aluminium plate started where the melt first contacted the plate, and then proceeded into the direction of the melt flow, Figure 55.

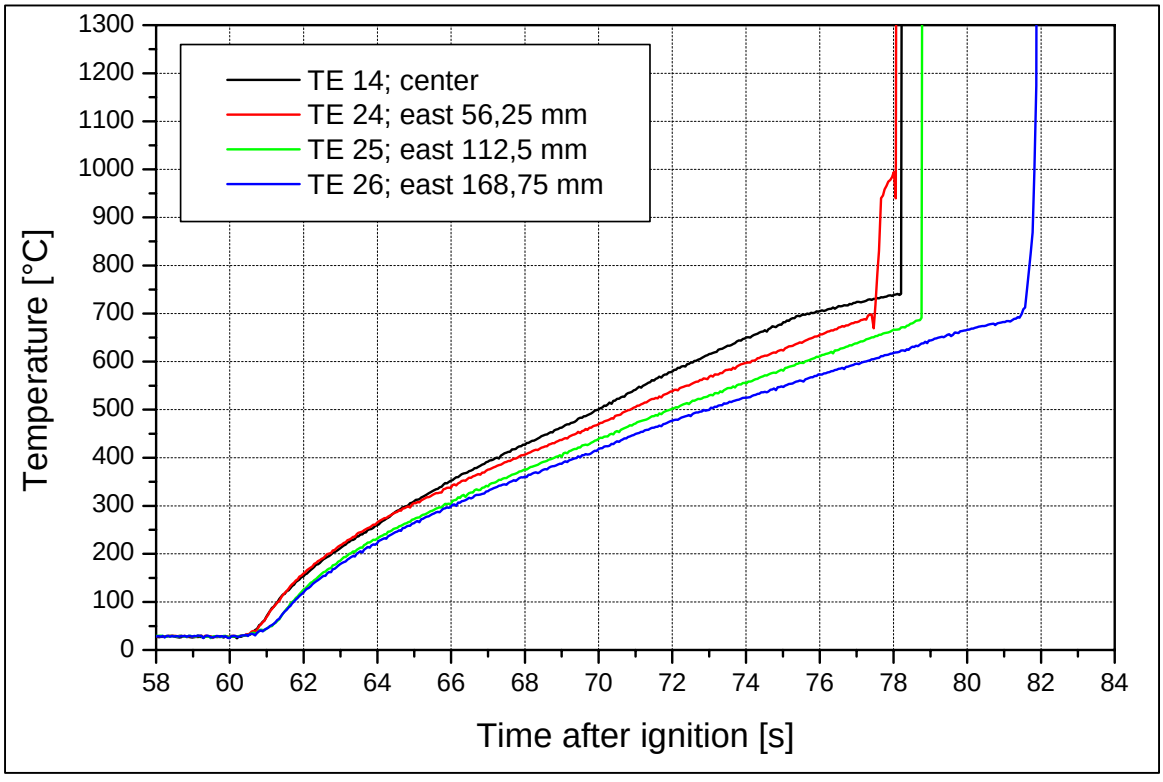

Figure 54: Transient temperature measurement 8 mm below the top surface at different horizontal positions

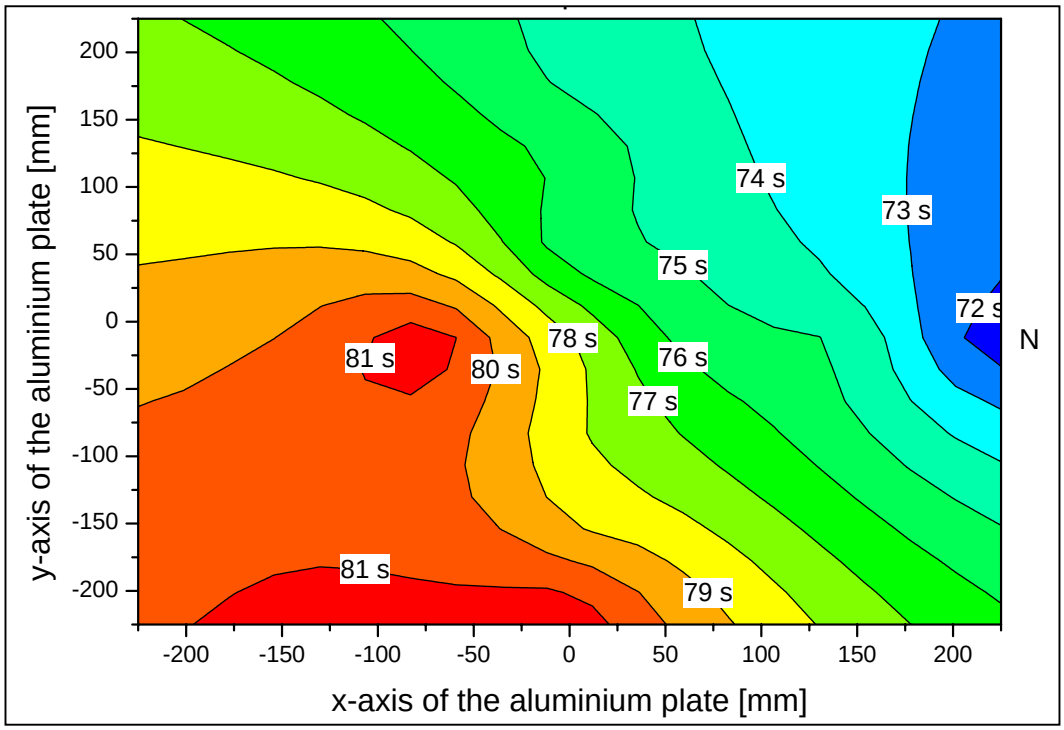

Figure 55: Failure time of the thermocouples 8 mm below the top surface of the aluminium plate in KAPOOL 15

6.2.3 Post test examinations in KAPOOL 15

In Figure 56 some photos of the video observation of the aluminium plate are shown. In the first photo (top left) the aluminium plate before the test is presented. In the following photos the failure of the aluminium plate and the outflow of the oxide melt from the test container is shown. The oxide melt penetrated the aluminium plate at that side, where the melt jet from the spout hit first the surface of the aluminium plate. At the beginning the melt jet was relatively compact due to a small outflow opening in the aluminium plate. During the outflow of the oxide melt, the hole in the aluminium plate increased. In the last photo (down right) the total oxide melt has been released from the test container, but the aluminium plate melted further due to a high heat transfer by radiation from the underlying oxide melt. The melt filaments, which are shown on the photo, are from the molten aluminium plate.
In Figure 57 two photos of the test container after the experiment are shown. The released oxide melt is collected at the bottom below the test container. On top of the melt there is some aluminium, which was melted after the release of the oxide melt.
In Figure 58 the bottom of the test container after the test is shown. The aluminium plate is almost completely molten, but there exists an oxide crust which is anchored at the sidewalls of the test container. This oxide crust was situated above the aluminium plate. The crust has a thickness of about 5 to 6 mm and is bent downwards. Furthermore, the oxide crust is covered with a thin aluminium layer on the lower side.
With these observations, it is now possible to reconstruct the failure mode of the aluminium plate. The oxide melt, which was flowing into the test container, formed an oxide crust at the contact surface to the aluminium plate. The aluminium plate heated up and started to melt. The aluminium plate and the overlying oxide crust failed and the melt was released from the test container.

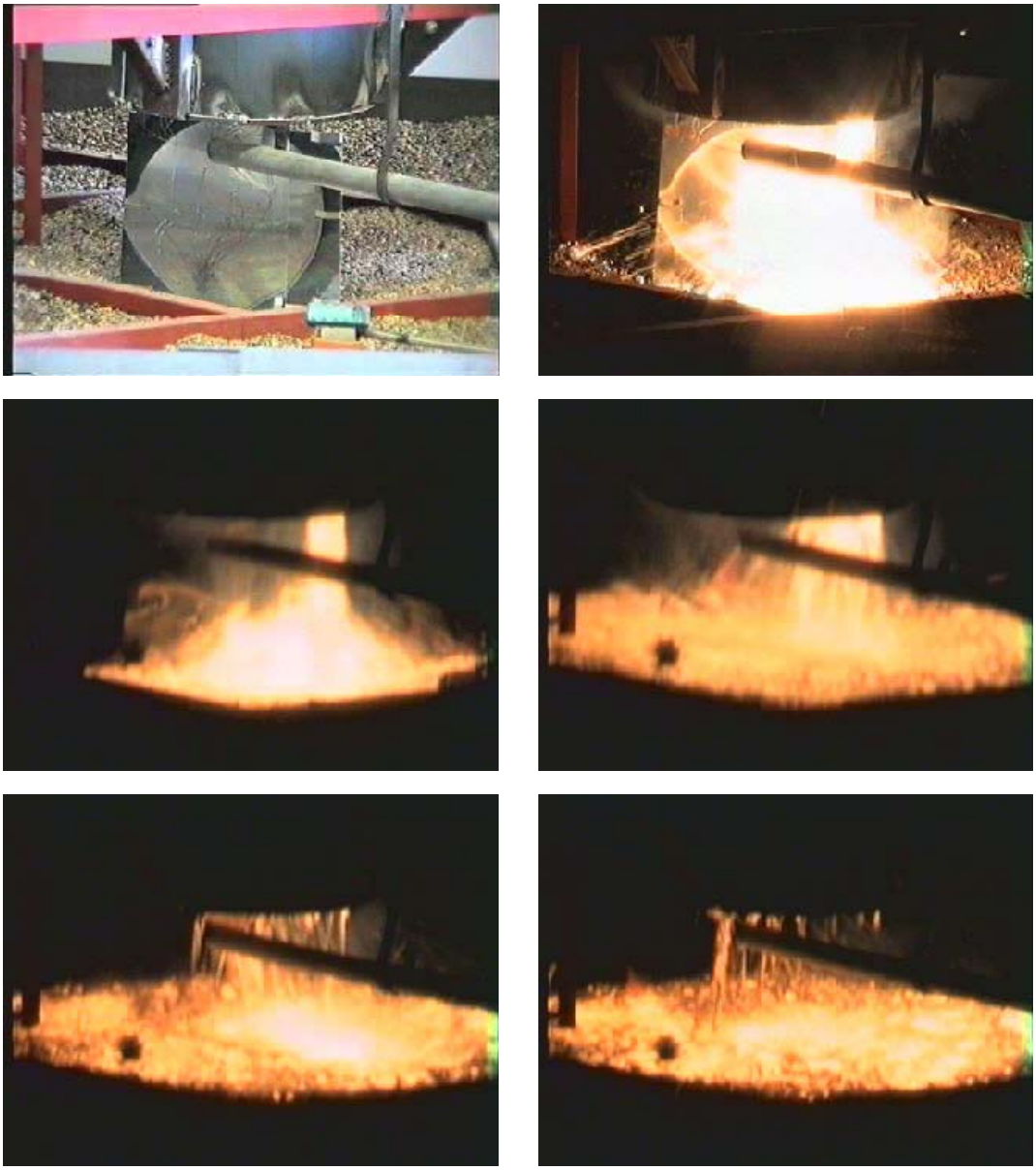

Figure 56: Photos from the video observation of the aluminium plate in KAPOOL 15

The aluminium plate melted almost completely, but parts of the oxide crust near the wall remained stable and determined the opening for the outflow.
In Figure 59 the bottom of the KAPOOL container is shown as a schematic drawing. In this drawing the residual aluminium plate and the overlying oxide crust is presented. The final size of the outflow hole is given by the oxide crust and is about 830 cm^2, which is about 50 % of the original surface (1626 cm^2). The hole in the aluminium plate is about 1369 cm^2 and is 84 % of the original surface.

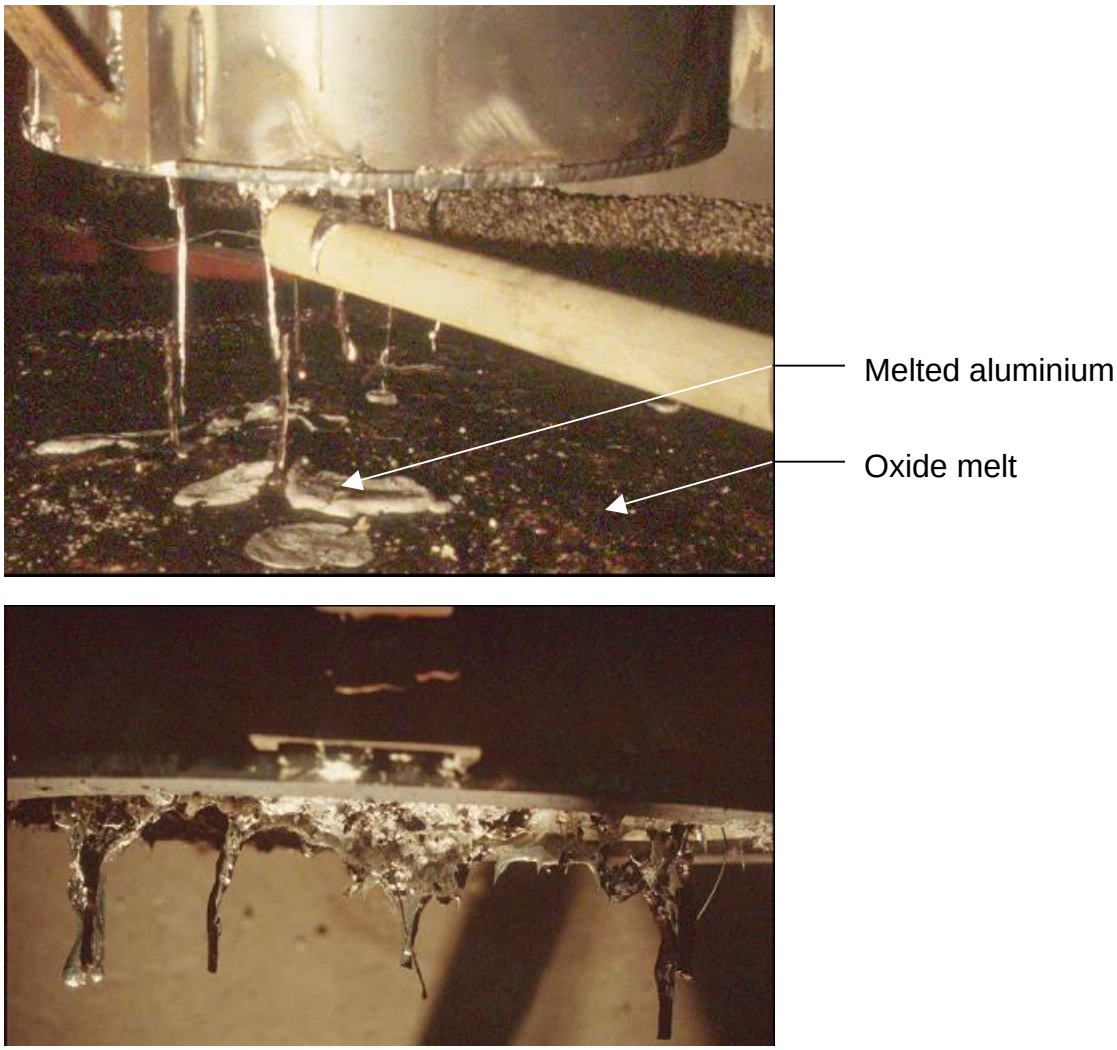

Figure 57: Photos of the test container after the test in KAPOOL 15

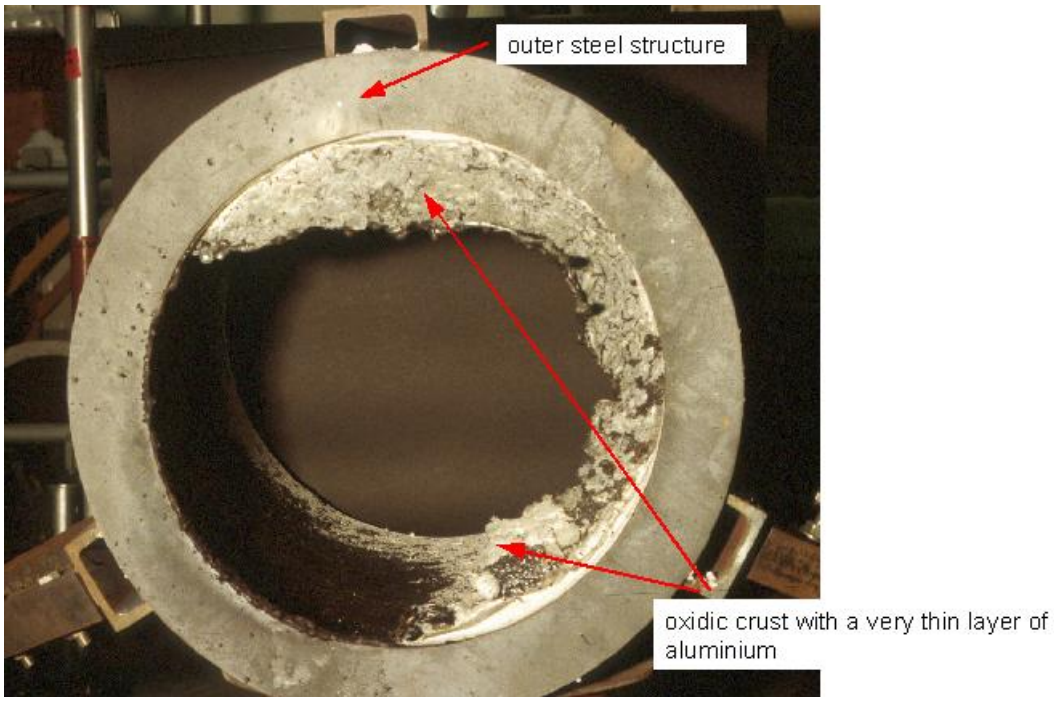

Figure 58: The bottom of the test container after the test in KAPOOL 15

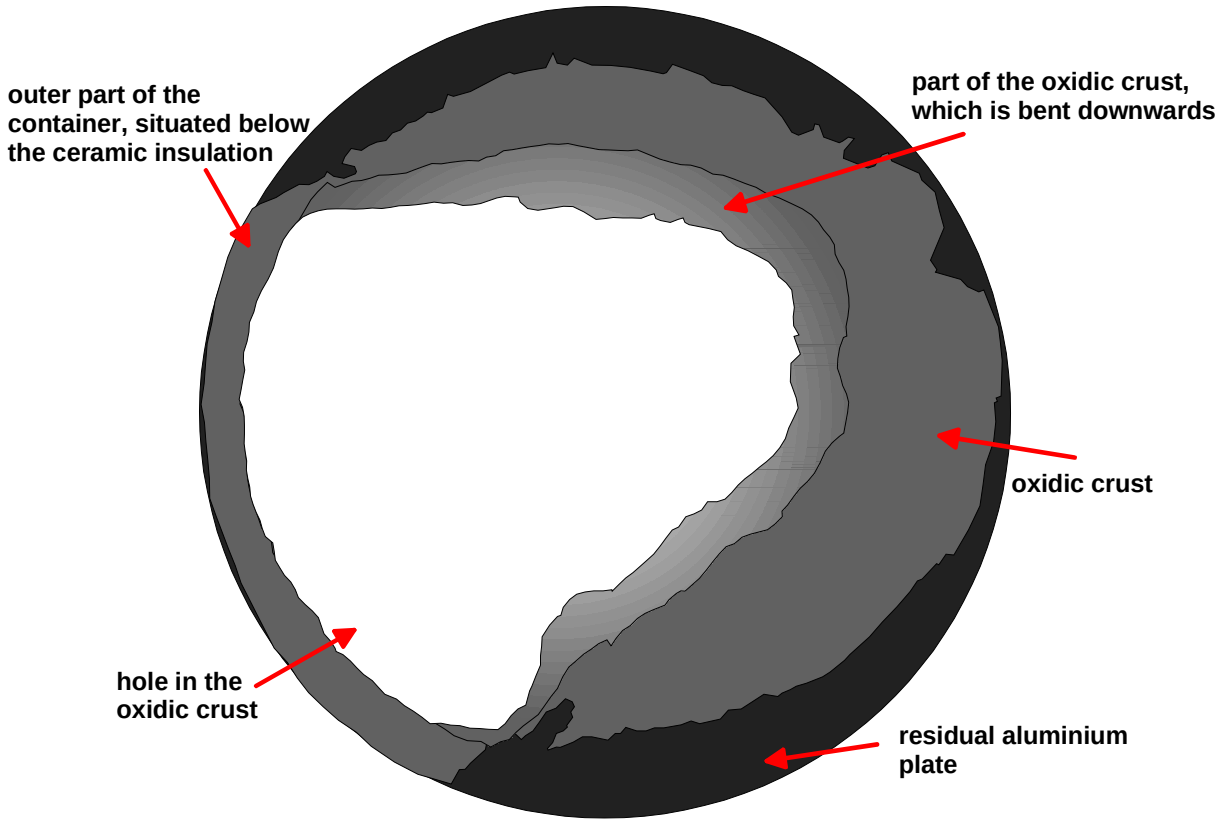

Figure 59: Schematic drawing of the bottom of the KAPOOL 15 container after the test

6.2.4 Calculations of the KAPOOL 15 experiment with HEATING5

For the test KAPOOL 15 two 1-dimensional calculations with HEATING5 have been performed. In the first calculation (calculation 1), the oxide melt is in direct contact with the aluminium plate and in the second calculation (calculation 2) a gap was modelled between the oxide melt and the aluminium plate, which limits heat transfer to radiation. The material properties, which have been used in these two calculations are summarised in Table 17. The emissivity of the bottom of the aluminium plate is 0.06 and in the case of calculations with a gap the emissivity of the upper surface of the aluminium plate is 0.3.

6.2.4.1 Modelling of the calculations

The modelling of the calculations with the oxide melt in direct contact with the aluminium plate includes 2 regions, left part of Figure 60. The aluminium plate has been subdivided into 10 grid lines with a constant distance of 1 mm between each grid line. The oxide melt was subdivided in a grid with different distances between the grid lines. Near the contact surface between the oxide melt and the aluminium plate 10 nodes with a distance of 1 mm was modelled. Above, 4 nodes with a distance of 20 mm and then 20 nodes with a distance of 10 mm were modelled. At the top of the melt, 2 nodes with a distance of 20 and 6 mm were modelled. For the calculation with a gap between the oxide melt and the aluminium plate, 1 additional node for this gap has been modelled.

Table 17: Material properties for the HEATING-5 calculations in KAPOOL 16

	oxide melt	**aluminium plate**	**air**
initial temperature T_0	1800 °C	20 °C	
solidus temperature T_s	1450 °C	660 °C	
heat conductivity λ	5.4 W/mK	220 W/mK	0,026 W/mK
density ρ	2917 kg/m^3	2702 kg/m^3	s. Table 9
specific heat c_p	1400 J/kgK	1047 J/kgK	1005 J/kgK
emissivity ε	0.9	0.06/0.3	
latent heat	1068000 J/kg	397000 J/kg	
height	316 mm	10 mm	1 mm

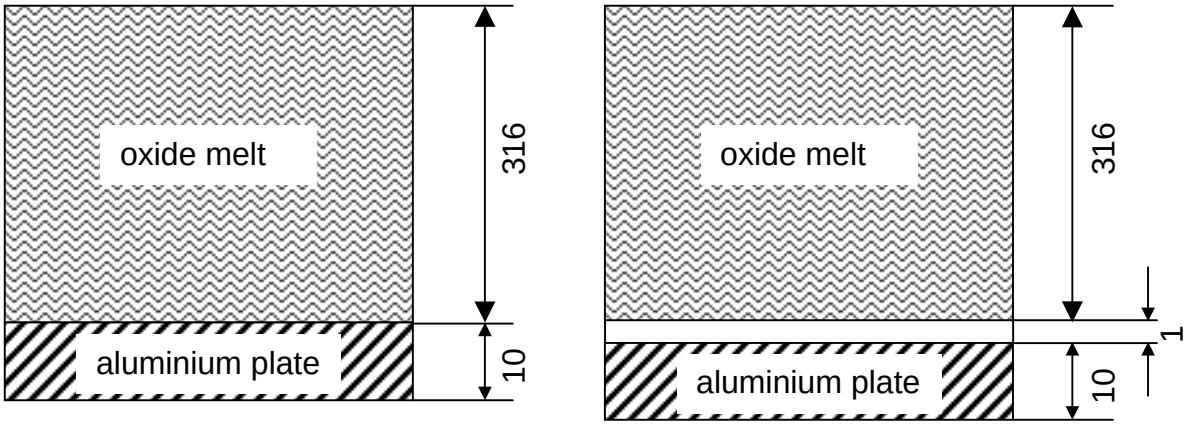

Figure 60: Modelling of the calculations of the KAPOOL 15 experiment

6.2.4.2 Results of the calculations

In Figure 61 the temperature 8 mm below the top surface of the aluminium plate for the two calculations and for the thermocouples 14 and 17 from the experiment is shown. The time 0 s in this figure relates to the arrival of melt in the test container, which is about 60 s after ignition. The thermocouples 17 in the center of the aluminium plate shows a continuous increase to about 660 °C and then the thermocouple is destroyed after about 10 s due to the melting of the plate and the release of melt out of the test container. In calculation 1 the temperature increases faster than the temperature of thermocouple 14 and shows a longer plateau temperature at 660 °C before the temperature increases again after about 10 s, which means that the aluminium plate is completely molten. The failure time of the thermocouple 14 agrees well with the time in the calculation 1, at which the aluminium plate is molten. But the thermocouples at the outer regions of the aluminium plate increased slower than the thermocouple in the center. This can be due to heat losses to the environment, but also due to crust and gap formation of the oxide crust and therefore due to a reduced heat transfer. In calculation1 a crust thickness of about 3 mm after 10 s is calculated.
The temperature in calculation 2 increases much slower than in calculation 1 and also than the thermocouples in the experiment. This indicates that the oxide crust did

not form a significant gap and therefore the heat transfer from the oxide crust to the aluminium plate was only slightly reduced. Additionally, due to the high thermal conductivity of the aluminium, the heat is easily conducted from the contact surfaces to areas, where the contact is less efficient.

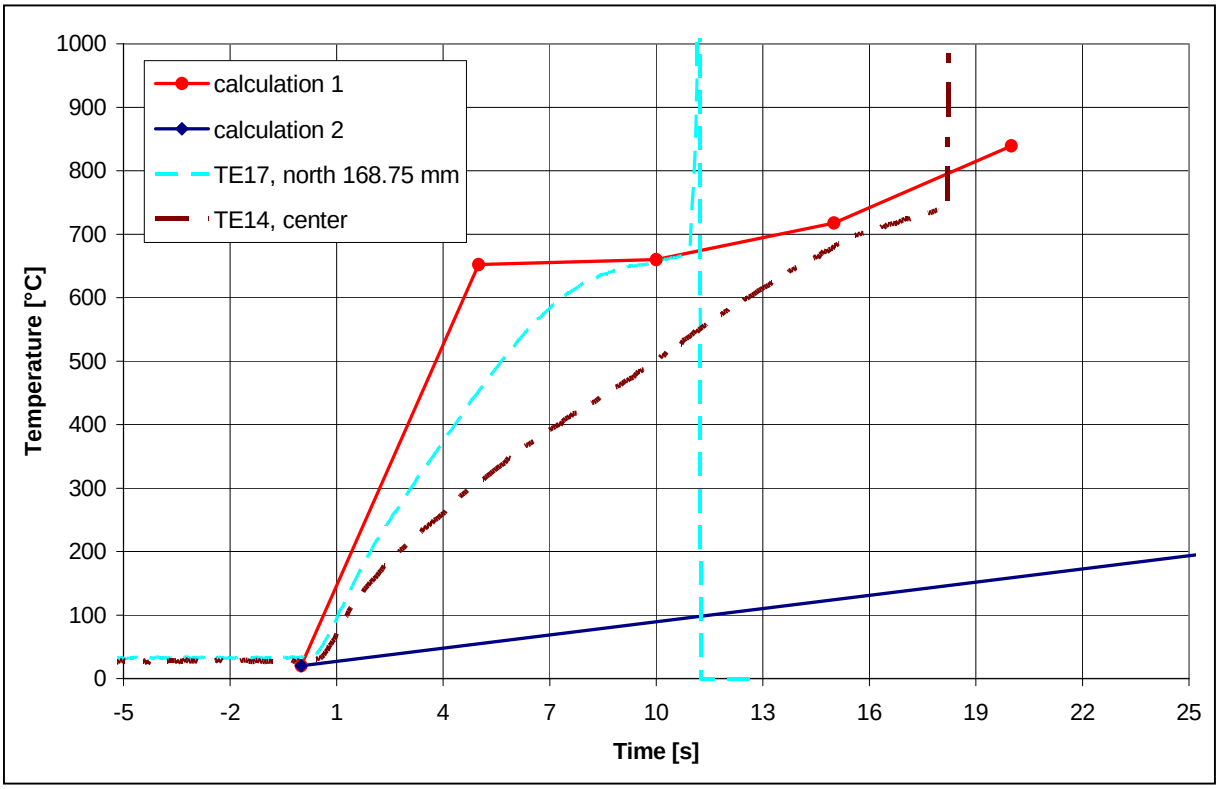

Figure 61: Temperature 8 mm below the top surface of the aluminium plate in the experiment and in the calculations for KAPOOL 15

6.3 The experiment KAPOOL 16

6.3.1 Setup of KAPOOL 16

To exclude an influence of the pouring process on the failure of the aluminium plate, as happened in KAPOOL 15, a further test, KAPOOL 16, has been conducted. This test was identical to KAPOOL 15 except for an additional 10 mm layer of borosilicate-glass concrete on top of the aluminium plate, Figure 62. This concrete layer simulates the condition, which would prevail at the end of the erosion of a thicker concrete layer.
The top surface of the aluminium plate was not blackened and the bottom was not polished. 25 K-type thermocouples have been installed inside the aluminium plate, all at the same vertical position (8 mm below the top surface), but at different horizontal positions, Table 18. 5 additional thermocouples in the concrete layer at 5 mm (that means 5 mm above the top surface of the aluminium plate) depth were installed to detect the erosion front in the concrete. The height of the concrete layer was chosen so that the estimated oxide melt/concrete interaction time is equal to the pouring time.
Time 0 s is defined by the ignition of the thermite powder in the reaction crucible.

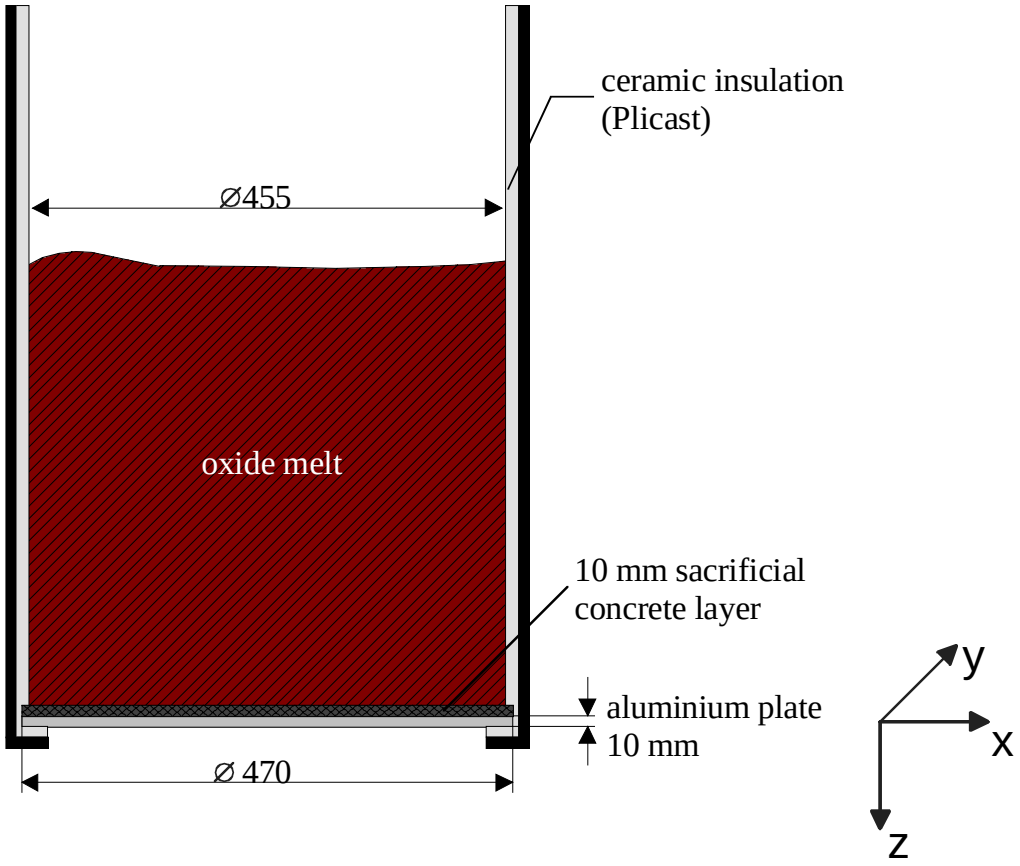

Figure 62: Setup of the test container in KAPOOL 16 and coordinate system

Table 18: Positions of NiCr-Ni thermocouples in the test container of KAPOOL 16

T/C #	Position x [mm]	Position y [mm]	Vertical position z [mm]
1	0	0	-8
2	50	0	-8
3	100	0	-8
4	150	0	-8
5	200	0	-8
6	70.7	70.7	-8
7	141.4	141.4	-8
8	0	50	-8
9	0	100	-8
10	0	150	-8
11	0	200	-8
12	-70.7	70.7	-8
13	-141.4	141.4	-8
14	-50	0	-8
15	-100	0	-8
16	-150	0	-8
17	-200	0	-8
18	-70.7	-70.7	-8
19	-141.4	-141.4	-8
20	0	-50	-8
21	0	-100	-8
22	0	-150	-8
23	0	-200	-8
24	70.7	-70.7	-8
25	141.4	-141.4	-8
26	0	0	+5
27	141.4	141.4	+5
28	-141.4	141.4	+5
29	-141.4	-141.4	+5
30	141.4	-141.4	+5

6.3.2 Experimental Results of KAPOOL 16

6.3.2.1 Mass measurements in KAPOOL 16

The release of the melt from the reaction crucible started about 46 s after ignition. Figure 63 shows the transient mass loss of the reaction crucible and the transient mass flow of oxide melt into the test container. The pouring of oxide melt into the test container started 66 s after ignition and was ended 100 s after ignition. 150 kg of oxide melt were gathered in the test container. The increased scattering of the mass of the test container is due to melt agitation from concrete erosion. The aluminium plate failed 110 s after ignition and the melt was released from the container within 2.5 s. This value agrees with the calculated 2.9 s using Toricelli's law[1] assuming an opening of 237 cm^2 (see chapter 6.3.3) which is constant in time.

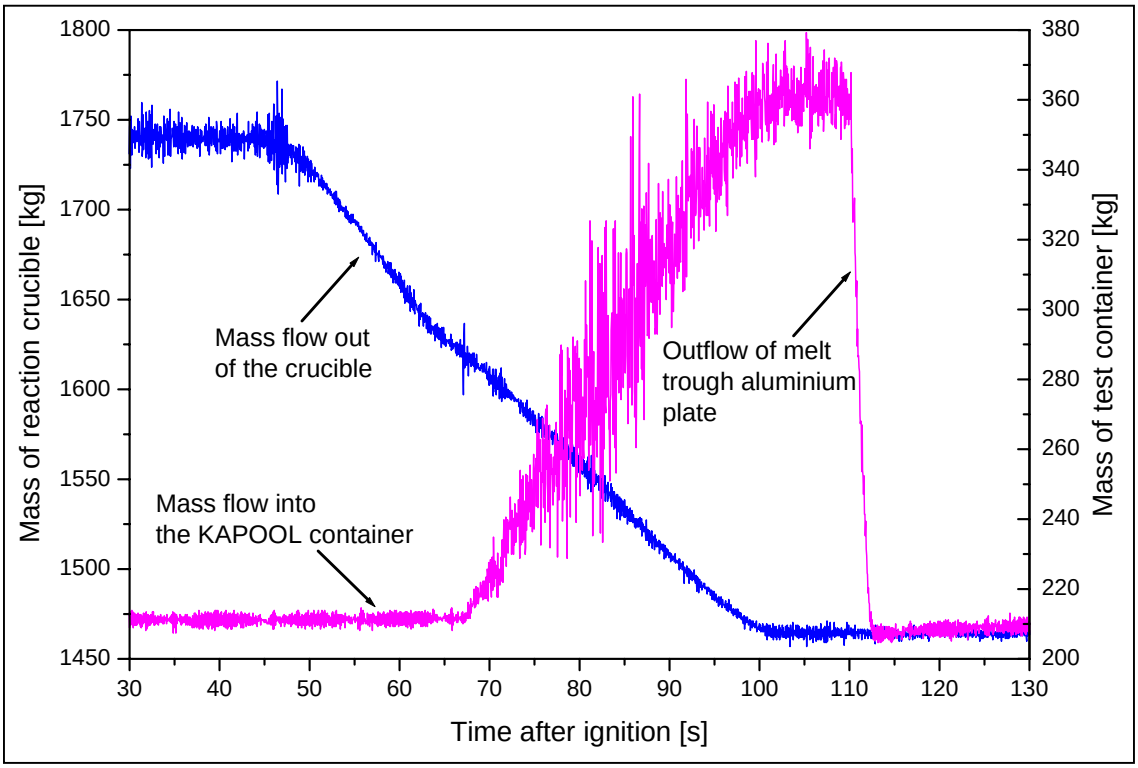

Figure 63: Mass of the reaction crucible and of the test container in KAPOOL 16

6.3.2.2 Oxide melt temperature in KAPOOL 16

4 W-Re thermocouples have been used to measure the oxide melt temperature, Figure 64. The initial melt temperature was 1880 °C and fell to 1800 °C within 40 s. The fourth thermocouple, which was immersed about 115 s after ignition into the test container, did not measure a melt temperature, because all melt was already released from the container. The measured value was only due to radiation.

[1] The time for complete gravity driven melt release is [14]:

$$t = \frac{A_0}{A_1} \cdot \frac{2}{\mu} \cdot \sqrt{\frac{h}{2 \cdot g}} \qquad \text{with}$$

A_0/A_1: Ratio of bottom surface to flow area
μ: contraction of the jet, 0.61 – 0.65
h: initial height of the melt
g: acceleration by gravity

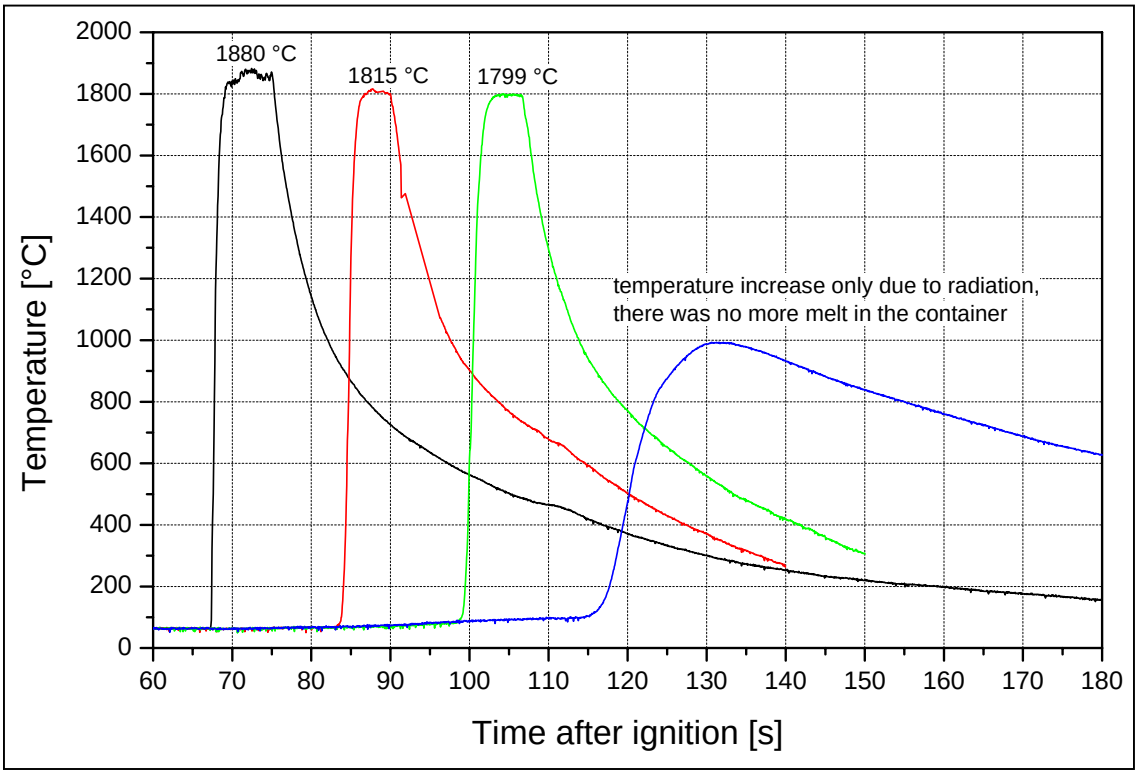

Figure 64: Measured temperature of the oxide melt in KAPOOL 16

6.3.2.3 Temperature readings of NiCr-Ni thermocouples in the test container

The thermocouples in the sacrificial concrete layer started to rise 4 s after start of the oxide melt pouring into the test container, Figure 65. The thermocouples show a temperature plateau at 100 °C over 3 to 4 s typical, which is due to the evaporating water in the concrete. Then the thermocouples were destroyed between 78 and 80 s after ignition, i.e. 11 to 13 s after start of melt pouring into the test container. This indicates that at this time half of the concrete layer was eroded.

From the data of the thermocouples in the concrete a concrete erosion rate of about 0.37 mm/s for the first 5 mm concrete could be calculated. Assuming that the concrete erosion rate for the second 5 mm concrete is lower than the erosion rate for the first 5 mm (~ 0.25 mm/s), the melt needs about further 20 s to erode the second 5 mm of concrete. So the concrete erosion was finished 100 s after ignition and this value agrees very well with the end of melt pouring.

The temperature in the aluminium plate started to rise when the concrete erosion preceded halfway, at about 80 s, Figure 66. Towards the end of melt pouring the maximum temperature in the plate was close to 600 °C. The temperature rise in the plate was rather homogeneous over the whole area except for the outer region of the aluminium plate, where the temperature rose more slowly. A temperature plateau of about 660 °C (which is the melting temperature of aluminium) was recorded for about 10 s from 100 to 110 s after ignition. At 110 s after ignition the outflow of oxide melt through the aluminium plate started simultaneously over a large area.

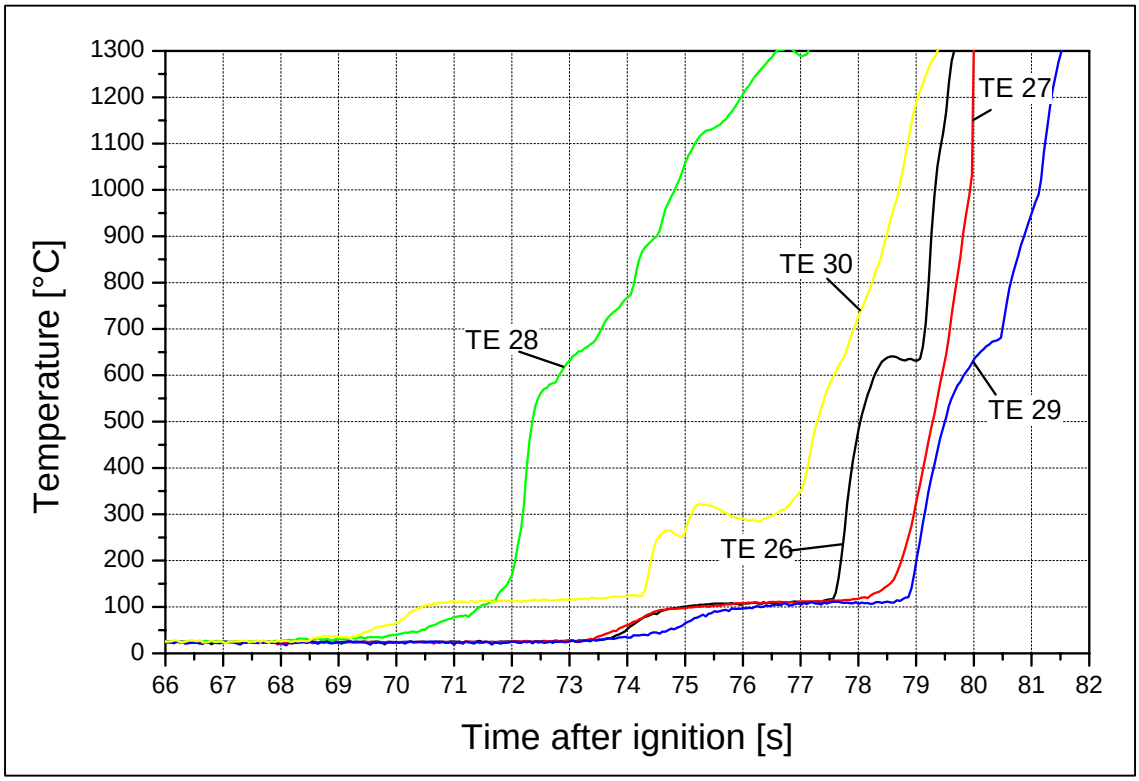

Figure 65: Transient temperatures in the sacrificial concrete in KAPOOL 16

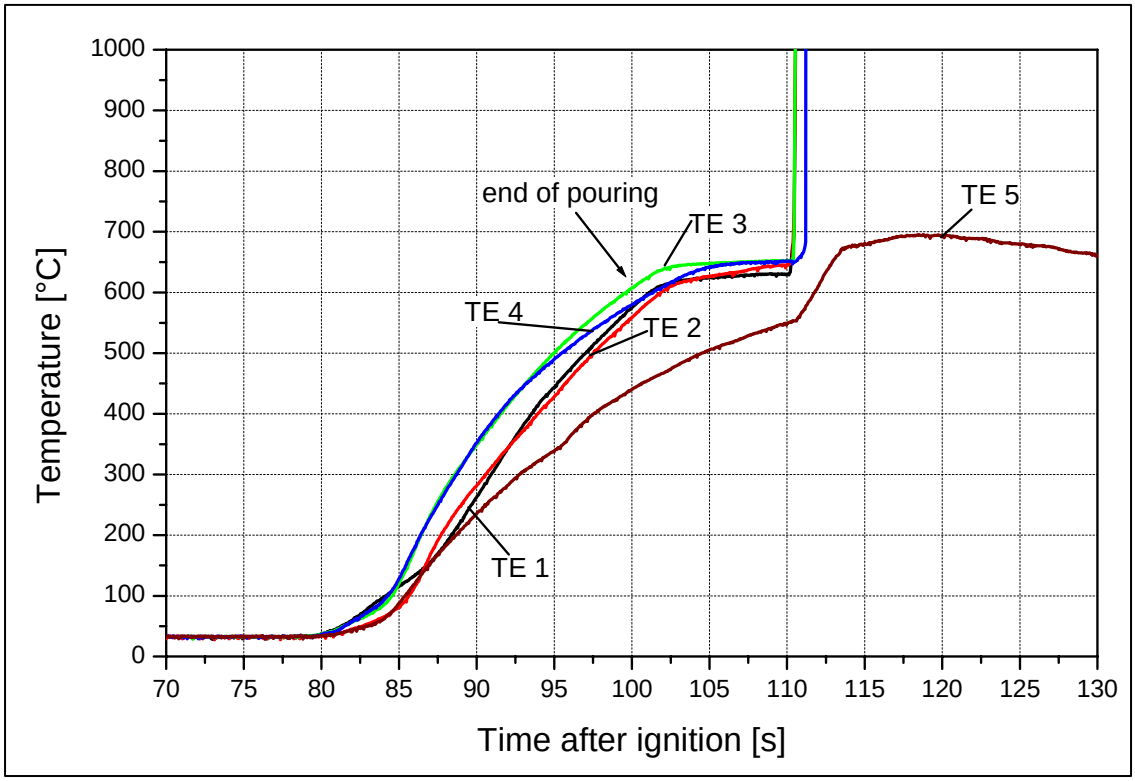

Figure 66: Transient temperatures 8 mm below the top surface of the aluminium plate in KAPOOL 16

6.3.3 Post test examinations in KAPOOL 16

In Figure 67 some photos of the video observation of the aluminium plate are shown. In the first photo, the view of the aluminium plate immediately before the melt penetrated the aluminium plate is given. In the next photos the outflow of the melt through the aluminium plate is presented. The outflow opening did not change in size during the outflow of the melt within 2.5 s.
Post test examination showed that a 3 cm wide region of the aluminium plate at the cylinder wall has no changes in structure. The rest is deformed plastically and bent downwards while the material in the center is completely melted and removed, Figure 68. The size of the outflow opening is given by an oxide crust, about 4 to 5 mm thick, and the area is 237 cm^2, which is 15 % of the original surface (1626 cm^2 of the aluminium plate is in contact with the melt). The oxide crust covers the residual aluminium plate and extends into the central voided area.
The size of the hole in the aluminium plate is 476 cm^2, which is about 30 % of the original surface.

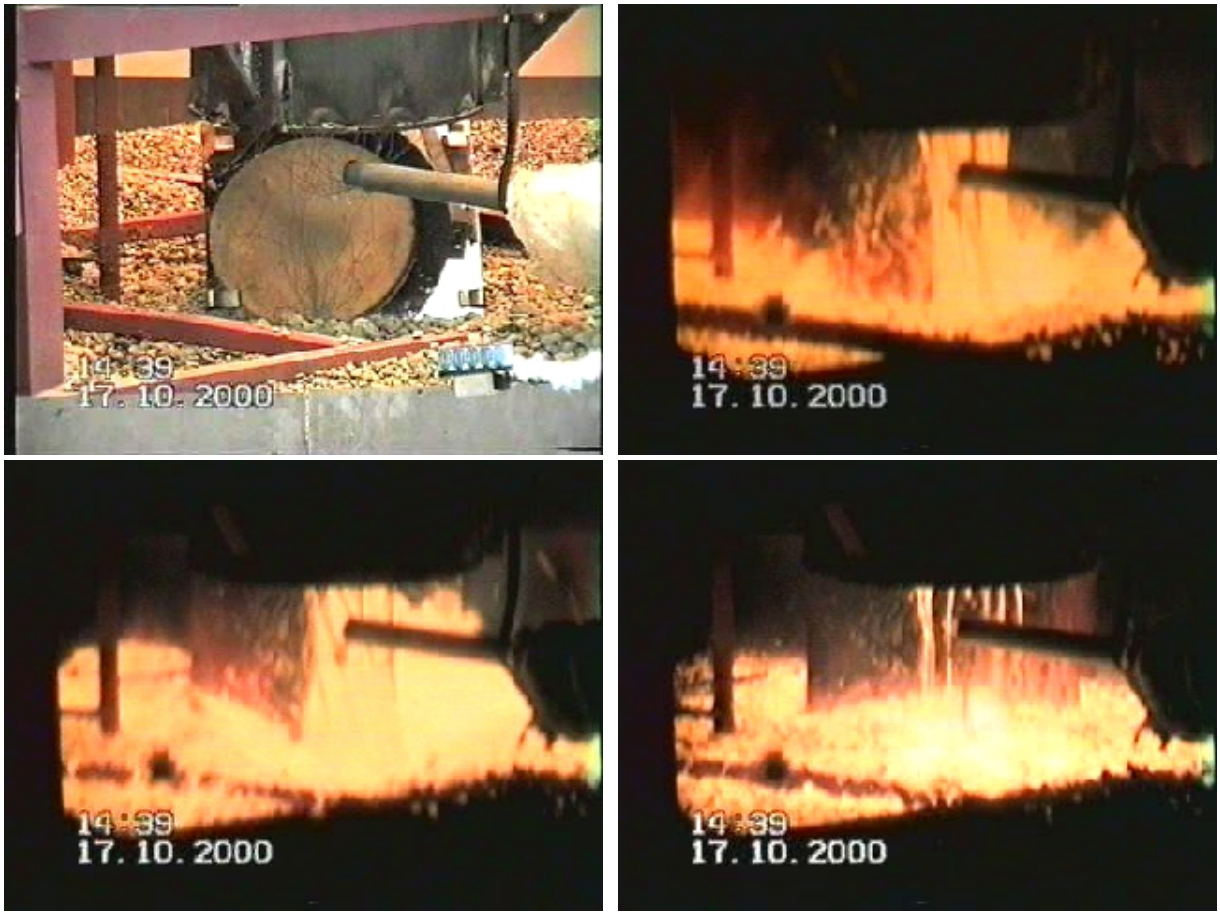

Figure 67: Photos from the video observation of the aluminium plate in KAPOOL 16

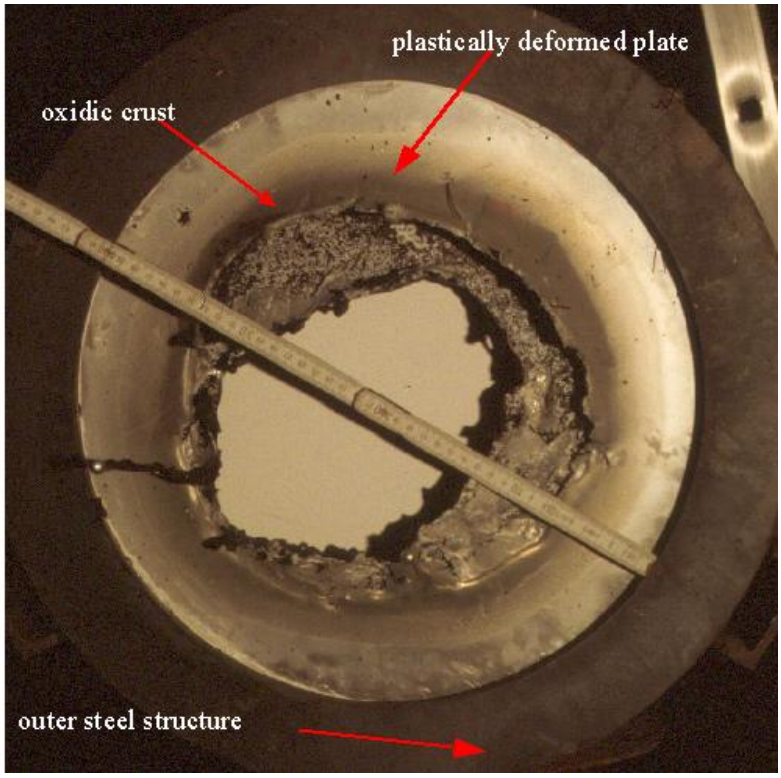

Figure 68: The bottom surface of the test container after the test in KAPOOL 16

6.4 The experiment KAPOOL 17

6.4.1 Setup of KAPOOL 17

In the last test KAPOOL 17, the same container could be used as in KAPOOL 16. The thickness of the aluminium plate was increased to 20 mm and the concrete layer was 15 mm except for a circle of ∅ 100 mm, Figure 69. In this eccentric circle the thickness of the concrete layer was only 10 mm. The depression in the concrete layer was chosen to simulate an inhomogeneous concrete erosion front.
The top surface of the aluminium plate was not blackened and the bottom was not polished. 27 K-type thermocouples have been installed inside the aluminium plate at different vertical and horizontal positions, Table 19. 4 thermocouples are installed at the upper surface of the plate, 13 thermocouples 10 mm below the upper surface and 10 thermocouples at the bottom of the plate. 4 thermocouples are installed 10 mm above the top surface of the plate in the sacrificial concrete layer and the last thermocouple at the upper surface of the sacrificial concrete layer, which is 15 mm above the aluminium plate.
Time 0 s is defined by the ignition of the thermite powder in the reaction crucible.

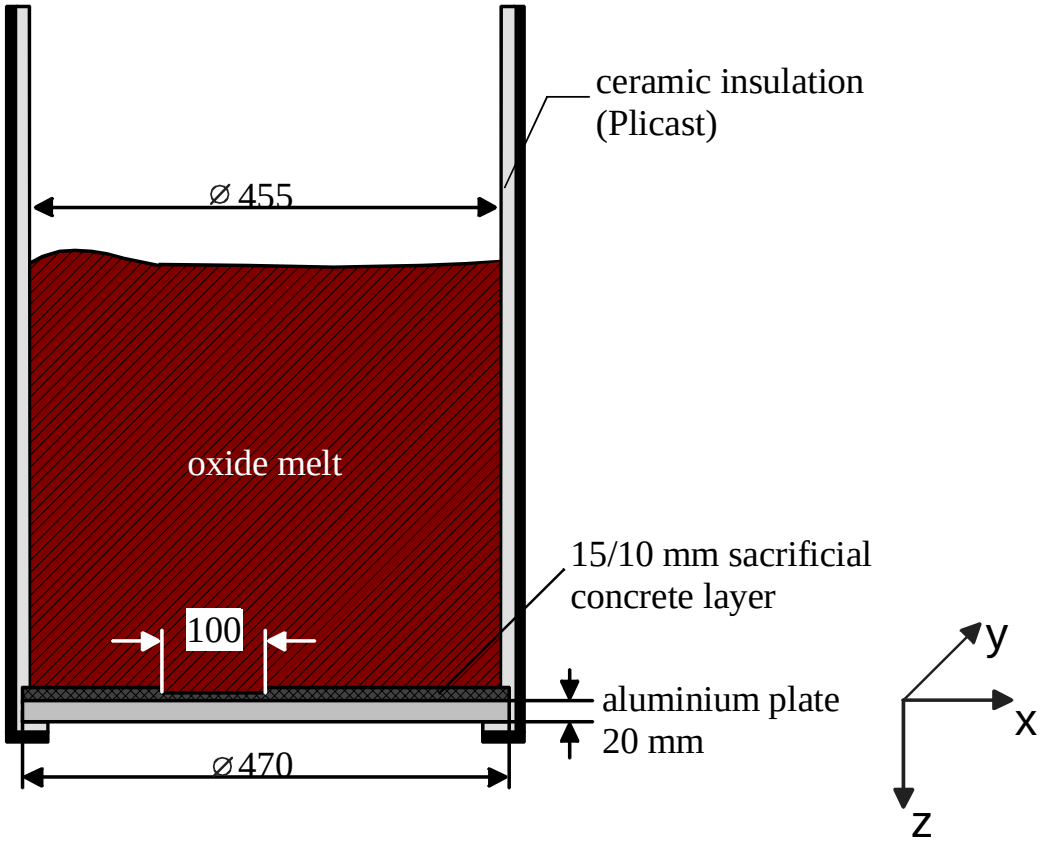

Figure 69: Setup of the test container in KAPOOL 17 and coordinate system

Table 19: Positions of NiCr-Ni thermocouples in the test container of KAPOOL 17

T/C #	Position x [mm]	Position y [mm]	Vertical position z [mm]
1	200	0	-10
2	200	0	-20
3	100	0	15
4	100	0	10
5	100	0	0
6	100	0	-20
7[2]	0	0	10
8[2]	0	0	0
9[2]	0	0	-10
10[2]	0	0	-20
11	0	100	-10
12	0	100	-20
13	0	200	-10
14	0	200	-20
15	0	-100	-10
16	0	-100	-20
17	0	-200	-10
18	0	-200	-20
19[1]	-50	0	10
20[1]	-50	0	0
21[1]	-50	0	-10
22[1]	-50	0	-20
23	-50	75	-10
24	-50	-75	-10
25[2]	-100	0	10
26[2]	-100	0	0
27[2]	-100	0	-10
28[2]	-100	0	-20
29	-100	100	-10
30	-100	-100	-10
31	-200	0	-10
32	-200	0	-20

[1]situated at different vertical positions in the center of the step in the concrete
[2]situated at different vertical positions at the rim of the step in the concrete

6.4.2 Experimental Results of KAPOOL 17

6.4.2.1 Mass measurements in KAPOOL 17

The release of the melt from the reaction crucible started about 22 s after ignition. Figure 70 shows the transient mass loss of the reaction crucible and the transient mass flow of oxide melt into the test container. The pouring of oxide melt into the test container started 42 s after ignition and was ended 31 s later at 73 s after ignition. 150 kg of oxide melt were gathered in the test container corresponding to a melt height of about 47 cm including the sacrificial concrete layer. 263 s after ignition the aluminium plate failed simultaneously over a large area and 150 kg oxide melt were discharged within 4 s.

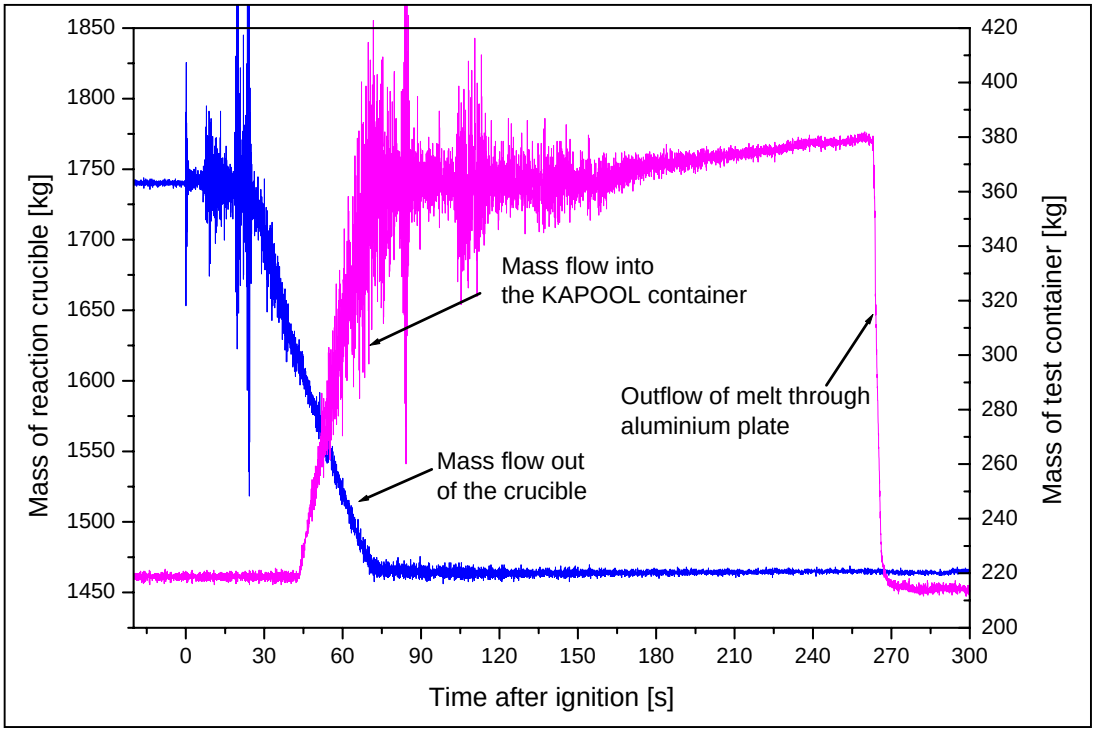

Figure 70: Mass of the reaction crucible and of the test container in KAPOOL 17

6.4.2.2 Oxide melt temperature in KAPOOL 17

4 W-Re thermocouples have been used to measure the oxide melt temperature, Figure 71. The initial melt temperature was 1870 °C and decreased steadily to about 1700 °C at 120 s after ignition.

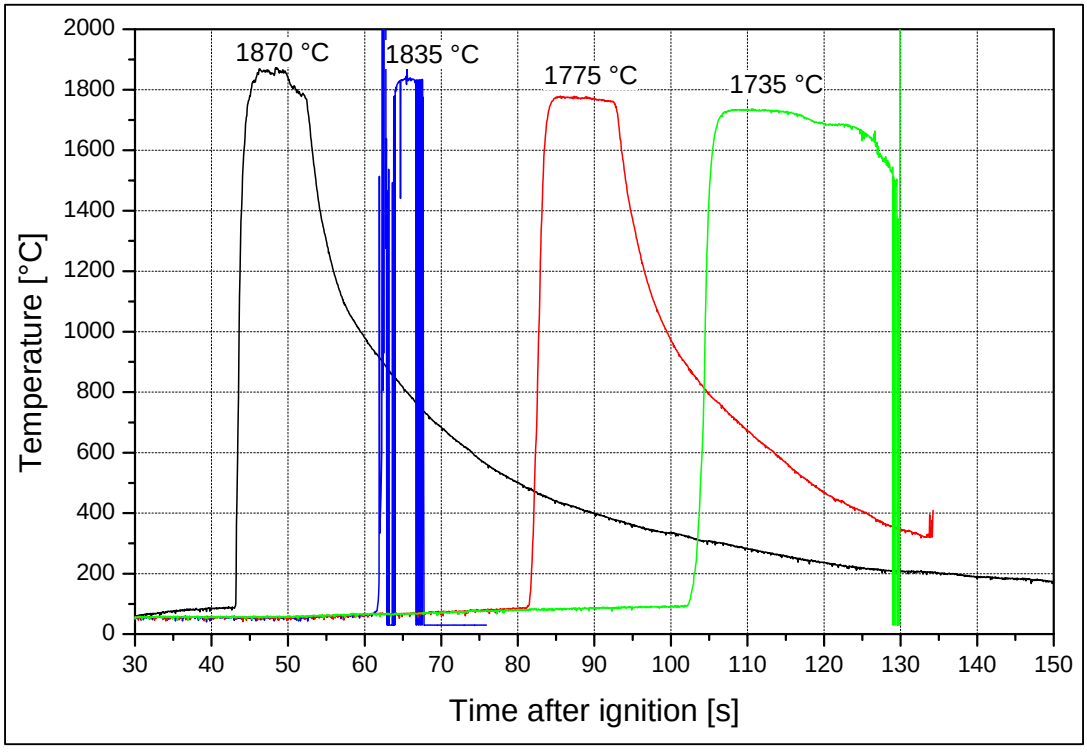

Figure 71: Measured temperature of the oxide melt in KAPOOL 17

6.4.2.3 Temperature readings of NiCr-Ni thermocouples in the test container

The thermocouples in the sacrificial concrete started to rise at different times because they are embedded at different vertical positions, Figure 72. The thermocouple 3 started to rise first because it was situated at the upper surface of the concrete. The thermocouples 7 and 19 started to rise afterwards; thermocouple 7 was situated at the rim and thermocouple 19 was situated in the center of the step in the concrete. At last the thermocouples 25 and 4, which were 5 mm below the upper surface of the 15 mm concrete layer, started to rise. They show also a temperature plateau at about 100 °C like in KAPOOL 16. From these thermocouples, an initial concrete erosion of about 0.35 mm/s was determined for the first 5 mm concrete. Similar erosion rates through iron melts have been measured for the identical concrete at the same melt temperatures [5]. The estimated time for the total concrete erosion was about 60 s and so the concrete erosion would be finished about 100 s after ignition. 20 s earlier the temperature readings of the K-type thermocouples 10 mm below the top surface of the aluminium plate started to rise, Figure 73. Thermocouple 9, 21 and 27, which are located under the thinner concrete layer, show a faster temperature rise and reach the melting temperature of the aluminium plate at 170 to 190 s. For the thermocouples 1 and 31 at the radius 200 mm, close to the rim of the plate, the melting temperature was either reached later in time or not at all. Failure of the thermocouples at about 263 s indicates the start of outflow of the melt.

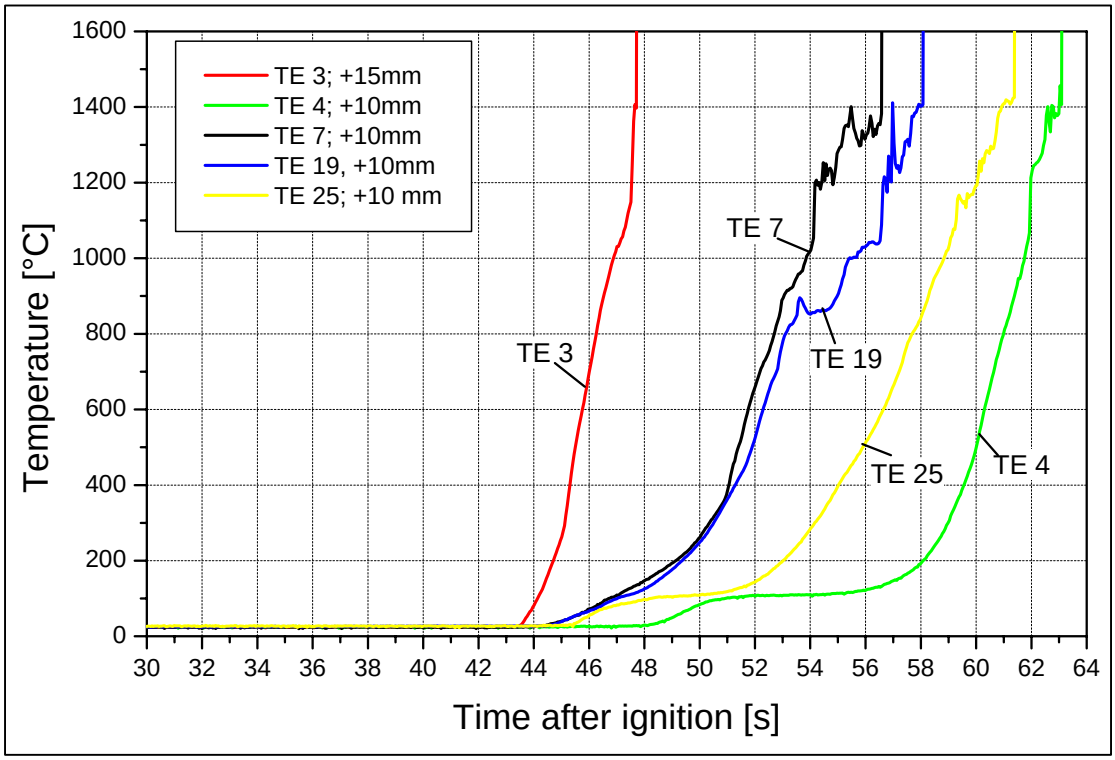

Figure 72: Transient temperatures at different positions in the sacrificial concrete layer in KAPOOL 17

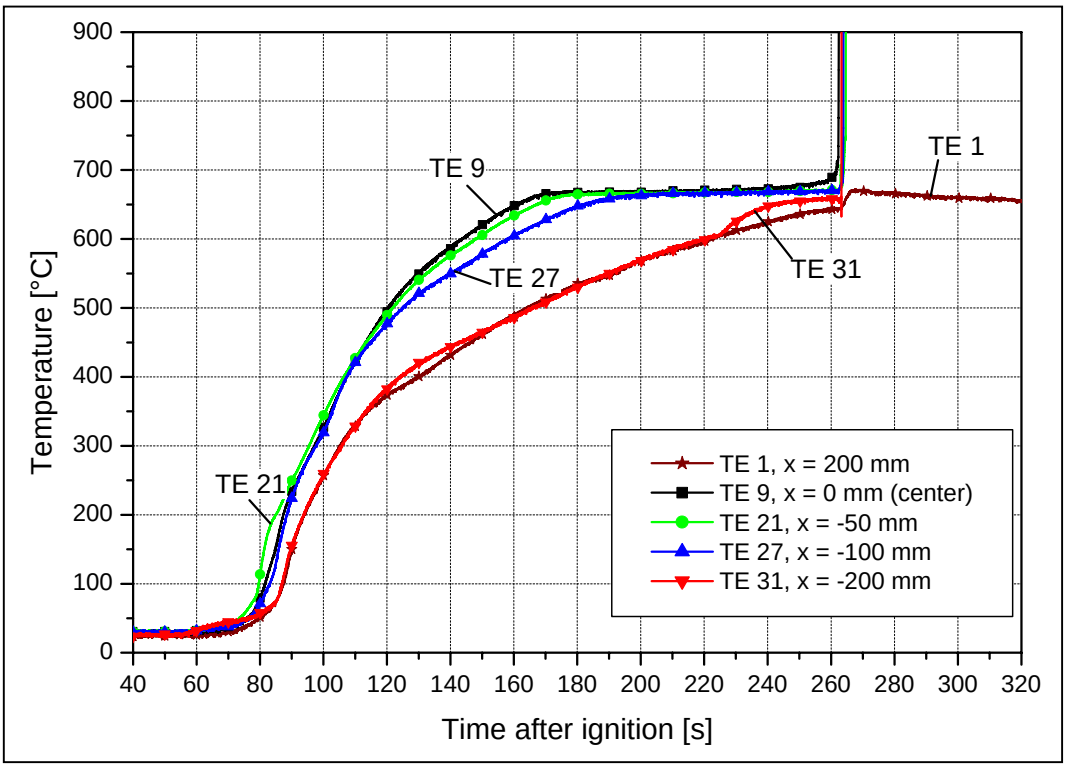

Figure 73: Transient temperatures 10 mm below the upper surface of the aluminium plate in KAPOOL 17

From the readings of all thermocouples it was possible to detect that the plate failed in the region where the thickness of the concrete was only 10 mm. In this test the oxide melt has been in contact with the aluminium for about 160 s after the end of concrete erosion. During this rather long period there is a high probability that an oxide crust existed on top of the plate. The crust thickness can be estimated using HEATING5 calculations as performed e.g. in chapter 6.2.4. If one assumes that a gap exists between the crust and the aluminium plate and heat transfer over the gap is only by radiation, a crust thickness of 2.5 mm is calculated. In the case of a perfect thermal contact the thickness of the crust is 6 mm.

6.4.3 Post test examinations in KAPOOL 17

In Figure 74 the test container after the end of the experiment is shown. The icicle like material is pendant mass of aluminium which relocated and solidified after outflow of the oxide was completed. It is detected, that the aluminium plate failed in the region, where the step in the concrete was located. Furthermore, the video observation of the aluminium plate during the test showed that the aluminium plate at the failure location melted down first, immediately followed by the outflow of the oxide melt. As registered by the mass loss in Figure 70, the outflow can be characterised as one single event. In Figure 75 the bottom of the test container after the test is shown. In the outer region of the test container the residual aluminium plate is visible. An oxide crust is visible in the inner region, overlying the residual aluminium plate. The bottom of this oxide crust is covered with a thin aluminium layer. More detailed examination showed that there are two oxide crust layers overlying the aluminium plate. The first crust was formed in contact with the aluminium plate, while the second crust was a floating crust from the top of the oxide melt pool, sinking to the bottom when the melt was released. The hole for the outflow is again limited by the oxide crust, like in KAPOOL 16, but is not detectable due to the welding with the sec-

ond oxide crust. The average size of the outflow hole can however be estimated with the help of Torricelli's law (see footnote on page 66). With the melt release time of about 4 s and a melt mass of 150 kg, the size of the outflow hole in the oxide crust is about 172 cm^2, which is about 11 % of the original surface (1626 cm^2), and corresponds to 148 mm diameter. The measured size of the hole in the aluminium plate is 824 cm^2, which is 51 % of the original surface (1626 cm^2), Figure 75.

Figure 74: Photo of the test container after the test in KAPOOL 17

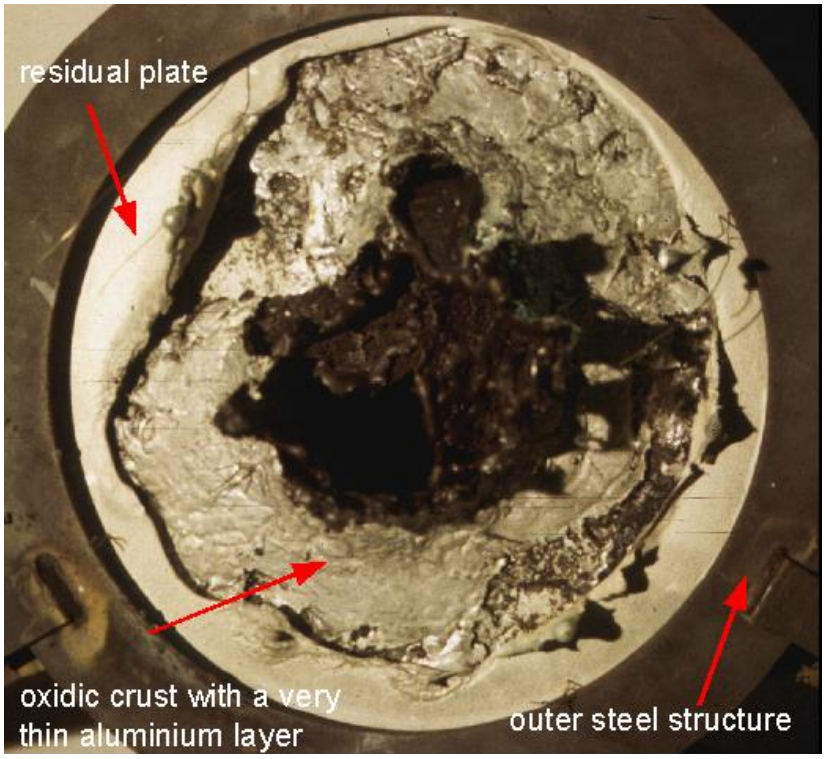

Figure 75: The bottom surface of the aluminium plate after the test in KAPOOL 17

7 Summary and conclusions

The KAPOOL experiments investigated the processes of melt-through of a metal plate by a simulated corium melt, as it might occur in special reactor cavities. Especially, the erosion of sacrificial concrete [6], the melt-through of the metal plate and the melt release were examined. The experiments were performed with high temperature melts without simulation of the nuclear decay heat, so that heat-up and possible failure of the plate are limited by the initial overheat of the melt.
In Table 20 the main parameters and results of all tests, which were presented in this report, are summarised.

Table 20: Summary of the main parameters and results of the KAPOOL experiments

	KAPOOL 9	**KAPOOL 11**	**KAPOOL 12**	**KAPOOL 13**
Metal plate	steel	steel	steel	aluminium
Thickness of metal plate	40 mm	25 mm	15 mm	20 mm
Melt type	Thermite + 8 wt% SiO_2	Thermite + 8 wt% SiO_2	Thermite + 35 wt% CaO	Thermite + 35 wt% CaO
Melt in contact with metal plate	iron	oxide	oxide	oxide
Melt mass	75 kg iron and 75 kg oxide	120 kg	135 kg	92 kg
Initial melt temperature	~ 2200 °C	1988 °C	1899 °C	1850 °C
Sacrificial concrete layer	yes	no	no	no
Failure of the melt gate	yes	no	no	no
	KAPOOL 15	**KAPOOL 16**	**KAPOOL 17**	
Melt gate	aluminium	aluminium	aluminium	
Thickness of melt gate	10 mm	10 mm	20 mm	
Melt type	Thermite + 35 wt% CaO	Thermite + 35 wt% CaO	Thermite + 35 wt% CaO	
Melt in contact with metal plate	oxide	oxide	oxide	
Melt mass	150 kg	150 kg	150 kg	
Initial melt temperature	~1880 °C	1880 °C	1870 °C	
Sacrificial concrete layer	no	yes	yes	
Failure of the melt gate	yes	yes	yes	

The main results of the experiments are:

- Iron melts in contact with a steel plate simulating the melt gate between the reactor cavity and the core catcher compartment lead to a fast melt-through of the plate.
- Oxide melts in contact with a steel or an aluminium plate lead to oxide crust formation in contact with the steel or aluminium and subsequent formation of gaps between the crust and the plate. These investigations could be reproduced by calculations with the HEATING5 code.
  - In the case of the steel plate no ablation of the plate by the oxide melt could be achieved.
  - Because of the lower melting temperature of aluminium, penetration of an aluminium plate was observed and investigated under various conditions, with and without a concrete layer covering the plate.

In a more general sense, important phenomena could be deduced from the experiments and from calculations with the HEATING5 code:

1. The contact of a high-temperature melt and a metal plate leads to a low initial contact temperature.
2. Due to this low initial contact temperature, an oxide crust is formed. This is a transient phenomenon and in the case of the existence of decay heat in the melt or when the energy content of the melt is sufficient, this crust would remelt.
3. The oxide crust on the surface of the metal plate can loose the contact to the metal plate and gaps are formed between the crust and the plate. This leads to a growing heat resistance between the oxide melt and the metal plate, which is an important factor for the occurrence and timing of the melt-through of the metal plate.
4. The properties of the metal plate are very important (melting temperature, thermal conductivity).
5. In most reactor cases, the melting temperature of the metal plate is lower than the melting temperature of the oxide crust. Therefore the metal plate fails first and then the stability of the oxide crust is important and has an influence on the size of the hole in the crust.

A drawback of the KAPOOL tests is the transient character: Volumetric heat production in the melt is not possible. In the case of real corium melts with decay heat a later thermal erosion of a melt gate made of steel would be expected in contrary to the outcomes of the tests KAPOOL 11 and 12.
From the results of the KAPOOL tests 15-17 it is advantageous to use aluminium as the material for the bottom of the reactor cavity if promotion of melt release is desired, as for this material the tests have proved a sufficient fast and large opening of the plate. A very important advantage of aluminium is its high thermal conductivity, which supports a fast opening of the gate over a large area. When using steel as material for the melt gate, further investigations deem necessary to study the opening of this gate by an oxide melt.
In a more general sense, the present KAPOOL experiments and their analysis give important insight into the behaviour of a melt in contact with a cold wall, a process that can occur in various sequences of a severe accident. Crust formation and crust stability are inherent problems, especially when an oxide melt contacts a colt metal structure. The formation of gaps between the crust and the wall, correlated with a substantial increase of the thermal contact resistance, are generic problems, and are found in all KAPOOL tests with oxide melts. One of main reasons for gap formation is

the elongation of the metal plate and shrinking of the oxide crust, when their temperatures come closer. Furthermore, the change of the temperature gradients, perpendicular to the surfaces of the wall and the crust, changes or provokes curvature of the surfaces, which is another reason for gap formation. These processes may have contributed to gap formation in the Three Mile Island accident after relocation of the large corium mass to the lower head, where a gap between the reactor pressure vessel and solidified melt was reported.

8 References

[1] Alsmeyer H., Tromm W., “The COMET Concept for Cooling Core Melts: Evaluation of the Experimental Studies”, Forschungszentrum Karlsruhe, FZKA 6186, EXV-CSC(99)-D036, Oktober 1999

[2] Alsmeyer H., Fieg G., Huber F., Tromm W., Werle H., Wittmaack R., “Studies on Core Melt Retention Concepts for the EPR” Proc. SFEN/KTG Conference on the EPR Project, Strasbourg, November 1995, p. 204

[3] Alsmeyer H., Fellmoser F., Fieg G., Huber F., Stegmaier U., Tromm W., Werle H., “Ex-Vessel Melt Behavior in the EPR“ Proc. SFEN/KTG Conference on the EPR Project, Cologne, October 1997, p. 161

[4] Fischer M., "Main Features of the EPR Melt Retention Concept", OECD Workshop on Ex-Vessel Debris Coolability, Karlsruhe, Germany, November 1999, p. 208

[5] Fellmoser F., Engel G., Fieg G., Massier H., Werle H., “Simulationsexperimente zum Verhalten von Kernschmelzen in der Reaktorgrube des EPR: KAPOOL 1-5“, FZKA 6212, Forschungszentrum Karlsruhe, May 1999

[6] Eppinger B., Fellmoser F., Fieg G., Massier H., Stern G., “Experiments on Concrete Erosion by a Corium Melt in the EPR Reactor Cavity: KAPOOL 6-8”, FZKA 6453, Forschungszentrum Karlsruhe, March 2000

[7] Engel G., Eppinger B., Fellmoser F., Fieg G., Messainguiral C., Massier H., Schmidt-Stiefel S., “KAPOOL Experiments to Simulate Molten Corium-Sacrificial Concrete Interaction and Gate Opening in the EPR Core Catcher Concept”, Proceedings of the OECD Workshop on Ex-Vessel Debris Bed Coolability, Karlsruhe, 15-18 November 1999, FZKA 6475, pp 66-75, May 2000

[8] Eppinger B., Fellmoser F., Fieg G., Tromm W., “KAPOOL Experiments to Simulate Molten Corium-Sacrificial Concrete Interaction”, Proceedings of ICONE-9, Nice, France, April 8-12, 2001, Vol.1, Track 7-207

[9] Turner W.D., Elrod D.C., Siman-Tov I.I., "HEATING5 - An IBM 360 Heat Conduction Program", ORNL/CSD/TM-15, Computer Sciences Division, Union Carbide Corporation, Nuclear Division, Oak Ridge, 1975

[10] J. L. Rempe, G. L. Thinnes, Chris M. Allison, "Light Water Reactor Lower Head Failure Analysis (Draft)", NUREG/CR-5642, Idaho National Engineering Laboratory, December 1990

[11] Schmidt-Stiefel S., private communication, 1999

[12] Slag Atlas, Edited by the Verein Deutscher Eisenhüttenleute, Verlag Stahleisen mbH, Düsseldorf, 1981

[13] Elsner N., "Grundlagen der technischen Thermodynamik", Band 2, Akademie Verlag GmbH, Berlin 1993

[14] Bohl W., "Technische Strömungslehre", Vogel Fachbuch, Kamprath Reihe, 1998

[15] Eppinger B., Fieg G., Massier H., Schütz W., Stegmaier U., "Simulationsexperimente zum Ausbreitungsverhalten von Kernschmelzen: KATS-8 bis KATS-17", FZKA 6589, Forschungszentrum Karlsruhe, März 2001

[16] VDI Wärmeatlas, Verein deutscher Ingenieure, Springer-Verlag, Berlin Heidelberg 2002

Appendix A

Determination of heat transfer coefficients during erosion of the steel plate in KAPOOL 9

From Figure 5 in chapter 4.2.2 it is possible to calculate erosion rates of the centre of the steel plate (a) during concrete erosion and (b) after the end of concrete erosion. For that purpose, the experimental data of the 1300 °C front are fitted by analytical curves. The time dependent, fitted erosion front of the steel plate up to the end of concrete erosion until about 25 s after ignition and after the end of concrete erosion are shown in Figure 76.

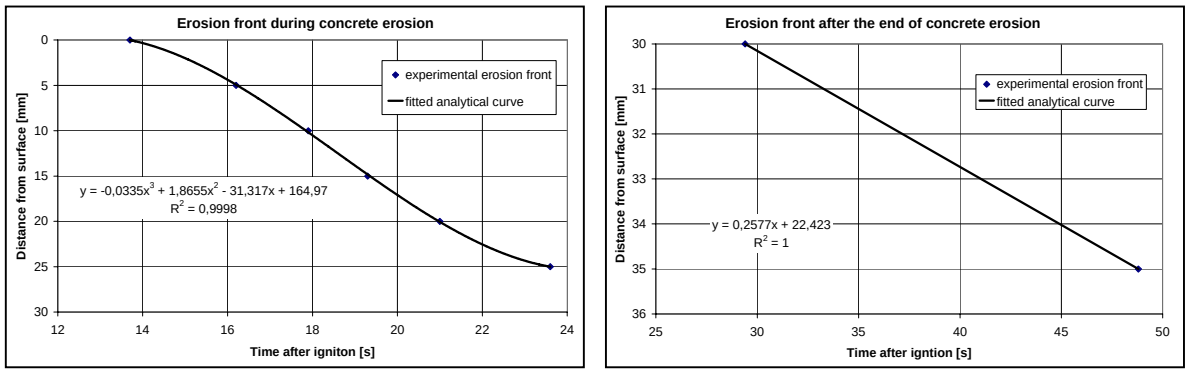

Figure 76: Erosion front with fitted analytical curves during (a) and after concrete erosion (b)

The erosion rates of the steel plate (mm/s) during and after the end of concrete erosion are determined by differentiation of these analytical curves, Figure 77. The maximum erosion rate is about 3.3 mm/s and occurs during the concrete erosion process. After the end of concrete erosion up to the time where the steel plate fails, a constant erosion rate of about 0.26 mm/s is reached.

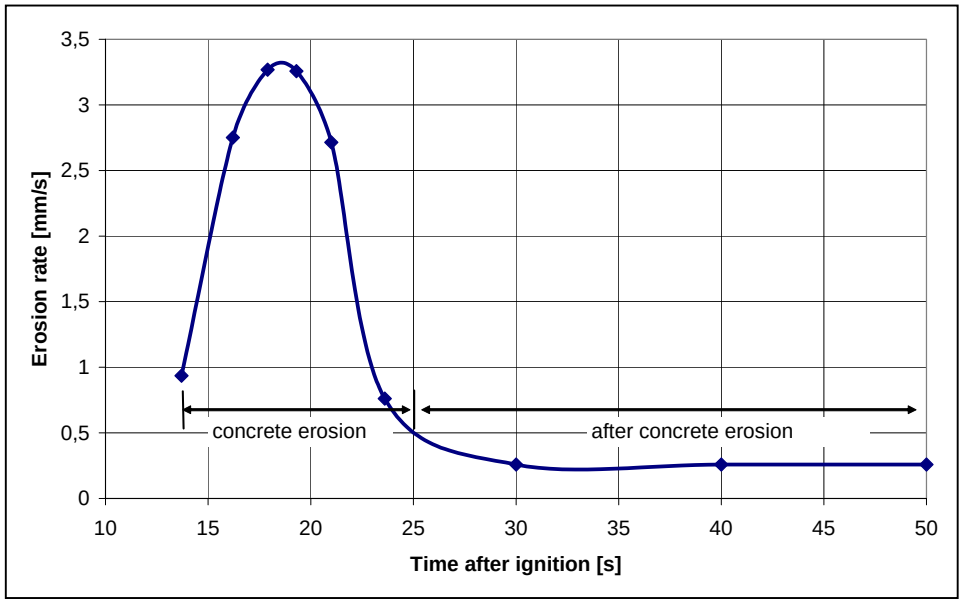

Figure 77: Erosion rates of the steel plate during and after concrete erosion

In a next step, the measured iron melt temperatures are also fitted by an analytical curve, Figure 78.

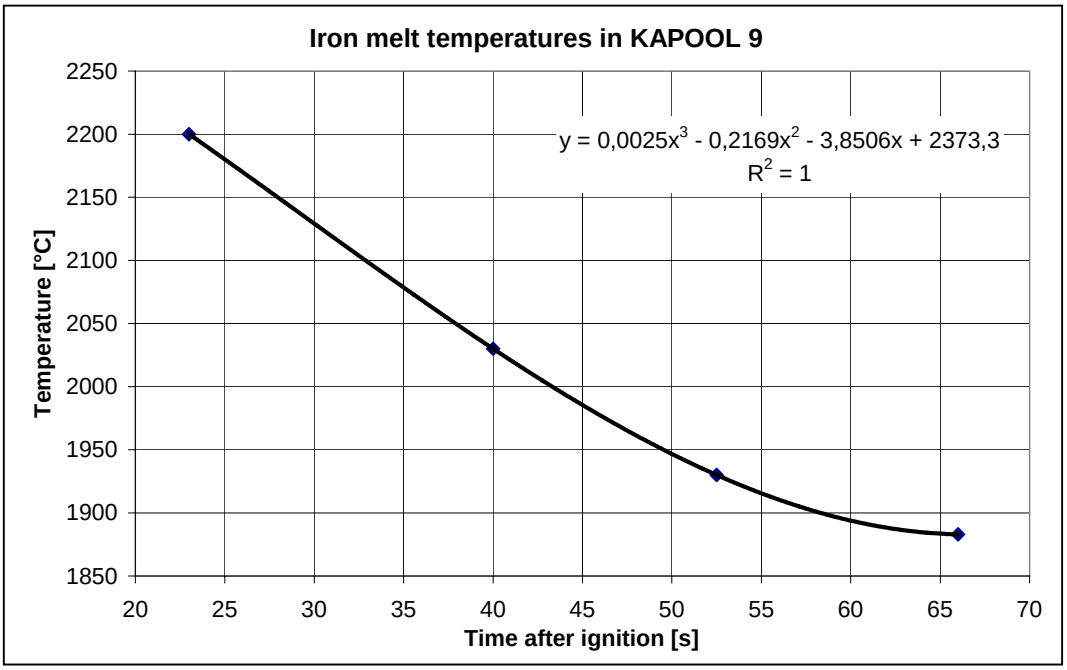

Figure 78: Iron melt temperatures with fitted analytical curve

Finally, the erosion rate of the steel plate is plotted as a function of the corresponding iron pool temperature, Figure 79.

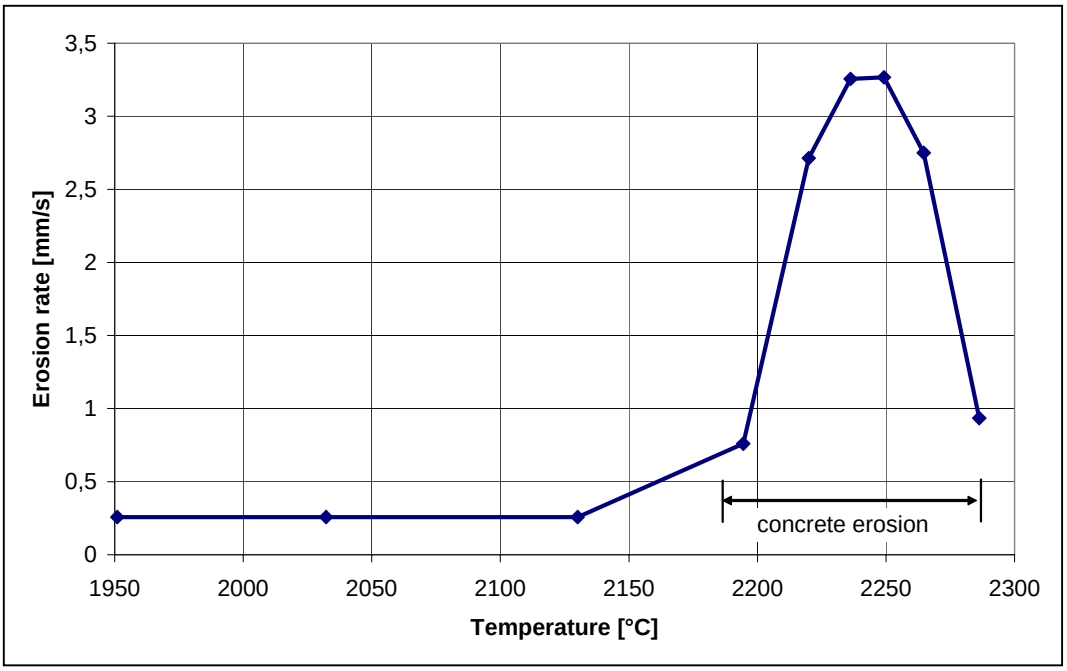

Figure 79: Erosion rates of the steel plate as a function of the iron melt temperature

The maximum erosion rate of the steel plate of about 3.3 mm/s at about 2230 °C is higher than the erosion rate of concrete, which was 0.8 to 1 mm/s at similar temperatures in earlier KAPOOL experiments [8].

After these calculations, heat transfer coefficients α can be determined by the following equations:

$$q = \Delta h \cdot \rho \cdot v$$

$$\alpha = \frac{q}{\Delta T} \quad \text{with}$$

Δh : Rate of change of enthalpy (latent heat + sensible heat)
ρ : Density of the steel plate
v : Erosion rates of the steel plate
ΔT : Temperature difference between iron melt and steel plate

In Figure 80 the derived heat transfer coefficients as a function of the temperature of the iron melt and as a function of the time are plotted.

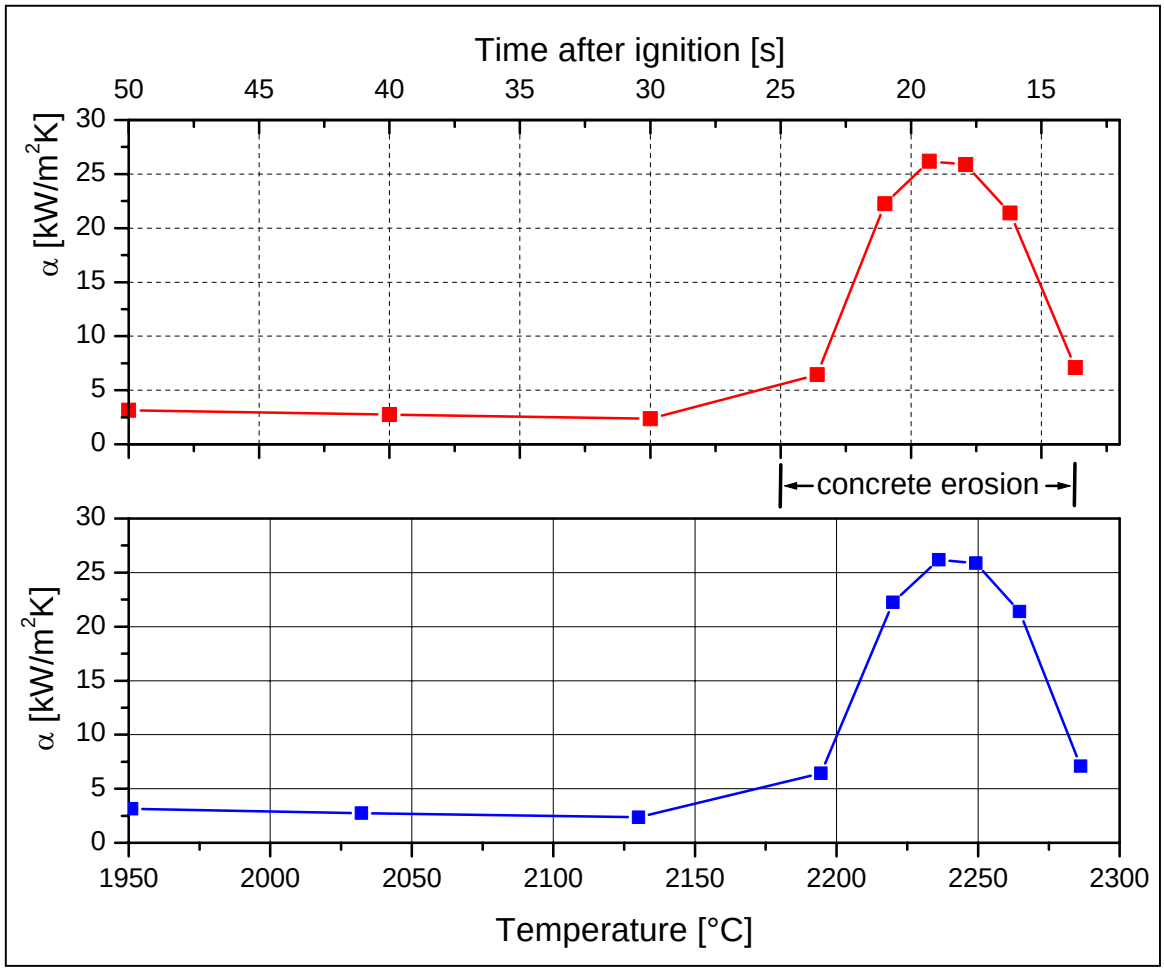

Figure 80: Heat transfer coefficients α as a function of the temperature and the time

The maximum heat transfer coefficient to the steel plate of about 25 kW/m^{2}K occurs during the concrete erosion phase about 17 s after ignition and corresponds to a melt temperature of about 2200 °C.
In comparison with heat transfer coefficients during normal concrete erosion of about 3 kW/m^{2}K [8], these values are more than a factor 8 higher.

The difference may be explained by the following effects:
In the case of normal concrete erosion, there is always a release of gas bubbles, which can form a partial or closed gas film on the concrete surface, which impedes the heat transfer.
In KAPOOL 9, where the concrete erosion process takes place simultaneously to the melting of the free steel plate in the center, the gas bubbles lead to strong convection, which transports always hot melt to the melting steel interface.
These two opposite effects seem to be the reason for the higher heat transfer coefficients of the steel plate erosion during the concrete erosion phase.
After the end of the concrete erosion phase, the heat transfer coefficient to the steel plate reduces by a factor of 10.